Universidade do Minho
U.PORTO
Universidade de Aveiro
Departamento de
Eletrónica, Telecomunicações e Informática
2013

Darlene Maciel
Neves

Channel Estimation and Parameters Acquisition Systems Employing Cooperative Diversity

Universidade do Minho U.PORTO Universidade de Aveiro
2013
Departamento de Eletrónica, Telecomunicações e Informática

Darlene Maciel Neves

Channel Estimation and Parameters Acquisition Systems Employing Cooperative Diversity

Tese apresentada às Universidades de Minho, Aveiro e Porto para cumprimento dos requisitos necessários à obtenção do grau de Doutor em Engenharia Eletrotécnica e Telecomunicações no âmbito do programa doutoral MAP-Tele, realizada sob a orientação científica do Doutor Atílio Gameiro, Professor Associado do Departamento de Eletrónica, Telecomunicações e Informática da Universidade de Aveiro e co-orientação do Doutor Adão Silva, Professor Auxiliar do Departamento de Departamento de Eletrónica, Telecomunicações e Informática da Universidade de Aveiro

Apoio financeiro da Fundação para a Ciência e a Tecnologia – FCT através da bolsa SFRH / BD / 33445 / 2008 e do FSE no âmbito do Programa Operacional Potencial Humano (POPH) do QREN.

o júri / the jury

presidente / president

Prof. Doutor Fernando Manuel dos Santos Ramos
Professor Catedrático da Universidade de Aveiro

vogais / examiners committee

Prof. Doutor Atílio Manuel da Silva Gameiro
Professor Associado da Universidade de Aveiro (orientador)

Prof. Doutor Adão Paulo Soares Silva
Professor Auxiliar da Universidade de Aveiro (co-orientador)

Prof. Doutor Paulo Jorge Coelho Marques
Professor Adjunto do Instituto Politécnico Castelo Branco

Prof. Doutor Rui Miguel Henriques Dias Morgado Dinis
Professor Auxiliar com Agregação da Faculdade de Ciências e Tecnologia da Universidade Nova de Lisboa

Prof. Doutor Carlos Miguel Gaspar Nogueira Ribeiro
Professor Adjunto do Instituto Politécnico de Leiria

Prof. Doutor José Rodrigues Ferreira da Rocha
Professor Catedrático da Universidade de Aveiro

agradecimentos / acknowledgments

Being apart from my loved ones was the hardest thing that I have ever had to cope with. Thank God, I have not been alone.

I would like to express my gratitude to my advisers professor Atílio Gameiro and professor Adão Silva not only for giving me the opportunity to work with such an amazing research group, but also for the unconditional time and support.

I would like to thank all my colleagues and friends at University of Aveiro, MAP-Tele programme, and Instituto de Telecomunicações. Daniel Castanheira, Sara Teodoro, Andrea Moço, Daniel Castañeda and José Assunção without them the physical layer related meetings would not be the same. I am also very appreciated to Carlos Ribeiro for all the valuable discussions.

I also acknowledge Instituto de Telecomunicações and University of Aveiro for providing me great working conditions and Fundação para a Ciência e a Tecnologia for vital support and funding.

I also owe a deep amount of appreciation to my parents Nice and Sena, my sibling Denise and Samuel for all the warming affection coming from the other side of the Atlantic.

Jacklyn, if I had a shiny star for every time you brightened my day, everything out there would be dark. Thanks for all.

Palavras-chave

OFDM, estimação de canal, sub-portadoras pilotos, estimação iterativa, sistemas cooperativos

Resumo

Este trabalho tem por objetivo o estudo de novos esquemas de estimação de canal para sistemas de comunicação móvel das próximas gerações, para os quais técnicas cooperativa são consideradas.

Os sistemas cooperativos investigados neste trabalho estão projetados para fazerem uso de terminais adicionais a fim de retransmitir a informação recebida para o utilizador final. Desta forma, pode-se usurfruir de benefícios relacionados às comunicações cooperativas tais como o aumento do rendimento do sistema, fiabilidade e extra cobertura. Os cenários são basedos em sistemas OFDM que empregam estimadores de canal que fazem uso de sinais piloto e que originalmente foram projetados para ligações ponto a ponto.

Os estudos analíticos consideram dois protocolos de encaminhamento, nomeadamente, *Amplify-and-Forward* e *Equalise-and-Forward*, ambos para o caso *downlink*. As estatísticas dos canais em estudo mostram que tais canais ocasionam características específicas para as quais o filtro do estimador e a equalisação devem ser apropridamente projetados. Estas características requerem ajustes que são necessários no processo de estimação a fim de estimar os canais, refinar as estimativas iniciais através de processos iterativos e ainda obter outros parâmetros do sistema que são necessários na equalização.

O desempenho dos esquemas propostos são avaliados tendo em consideração especificações padronizadas e modelos de canal descritos na *International Telecommunication Union*.

Keywords OFDM, channel estimation, pilot subcarriers, iterative estimation, cooperative systems

Abstract This work investigates new channel estimation schemes for the forthcoming and future generation of cellular systems for which cooperative techniques are regarded.
The studied cooperative systems are designed to re-transmit the received information to the user terminal via the relay nodes, in order to make use of benefits such as high throughput, fairness in access and extra coverage. The cooperative scenarios rely on OFDM-based systems employing classical and pilot-based channel estimators, which were originally designed to point-to-point links.
The analytical studies consider two relaying protocols, namely, the Amplify-and-Forward and the Equalise-and-Forward, both for the downlink case. The relaying channels statistics show that such channels entail specific characteristics that comply to a proper filter and equalisation designs. Therefore, adjustments in the estimation process are needed in order to obtain the relay channel estimates, refine these initial estimates via iterative processing and obtain others system parameters that are required in the equalisation.
The system performance is evaluated considering standardised specifications and the International Telecommunication Union multipath channel models.

"The only thing that will redeem mankind is cooperation."
— Bertrand Russell

To my parents,
To Jacklyn.

Contents

Contents i

List of Acronyms v

List of Figures ix

List of Tables xiii

List of Symbols xv

1 Introduction 1
- 1.1 The Mobile Communications Journey . . . 1
- 1.2 Motivations and Goals . . . 7
- 1.3 Main Contributions and Dissemination . . . 8
- 1.4 Thesis Organisation . . . 9

2 Basic Principles of Wireless and Cooperative Communications 11
- 2.1 Wireless Medium . . . 11
  - 2.1.1 Propagation: Mechanisms and Effects . . . 11
  - 2.1.2 Channel Modelling . . . 13
  - 2.1.3 Channel Characterisation . . . 14
    - 2.1.3.1 Spectral Domain . . . 14
    - 2.1.3.2 Temporal Domain . . . 15
- 2.2 OFDM-based Systems . . . 17
- 2.3 Diversity in Wireless Communications . . . 19
- 2.4 Cooperative Communications . . . 21
  - 2.4.1 Cooperative Systems . . . 23
  - 2.4.2 Relaying Protocols . . . 24
  - 2.4.3 Relay-Assisted Approach Scenarios . . . 28

3 Channel Estimation in OFDM Systems 33
- 3.1 Introduction . . . 33
- 3.2 Pilot-Assisted OFDM-Based Systems . . . 33
- 3.3 Channel Estimation . . . 36
  - 3.3.1 Pilot Density and Pilot Patterns . . . 37
- 3.4 Classical Channel Estimators . . . 40
  - 3.4.1 Least Squares Estimator . . . 40

3.4.2 Minimum Mean Square Error . . . 41
3.4.3 Complexity Analysis . . . 43
3.4.3.1 LS Channel Estimation with FIR Interpolation Filter . . . 43
3.4.3.2 MMSE Channel Estimation . . . 44
3.4.4 Metrics of Assessment . . . 45
3.4.4.1 Bit Error Rate . . . 45
3.4.5 Mean Square Error - MSE . . . 48

4 Channel Estimation for AF Relay-Assisted OFDM-Based Systems 49
4.1 Introduction . . . 49
4.2 System Model . . . 50
4.2.1 Relay-Assisted Scenario . . . 51
4.2.2 Relay Channel Statistics . . . 53
4.3 Relay Channel Estimation . . . 58
4.4 Performance Assessment . . . 60
4.5 Conclusion . . . 67

5 Channel Estimation for EF Relay-Assisted OFDM-Based Systems 69
5.1 Introduction . . . 69
5.2 EF Relay-Assisted Scenario . . . 71
5.3 System Model . . . 72
5.4 EF Relay-Assisted System . . . 73
5.4.1 Phase I . . . 75
5.4.2 Phase II . . . 78
5.5 Parameters and Channel Estimates . . . 81
5.5.1 Computing the Variance of the Overall Noise . . . 81
5.5.2 Estimating the Equivalent Channel . . . 82
5.5.3 The Impact of Using $\alpha_k \Gamma_k$ as Pilot . . . 86
5.6 Performance Assessment . . . 92
5.6.1 System Parameters . . . 92
5.7 Conclusion . . . 96

6 A Data-Aided Channel Estimation Method for OFDM Relay-Assisted 97
6.1 Introduction . . . 97
6.2 EF Relay-Assisted System Model . . . 99
6.2.1 Phase I . . . 101
6.2.2 Phase II . . . 102
6.3 Improving the Relay Channel Estimates . . . 102
6.3.1 Proposed Pilot-Data Aided Channel Estimator Scheme . . . 103
6.3.1.1 The Data-based Channel Estimation . . . 104
6.3.2 Adjacent Virtual Pilot Subcarriers . . . 109
6.4 Performance Assessment . . . 111
6.4.1 System Parameters . . . 111
6.5 Conclusion . . . 118

7 Conclusions and Future Works **119**
7.1 Summary and Concluding Remarks 119
7.2 Directions for Future Works 121

References **123**

A Estimates Corrupted by Noise Terms with Different Variances **133**

B MSE Data-Aided Estimation and the Error Probability **137**

List of Acronyms

3GPP	3rd Generation Partnership Project	3
AF	Amplify-and-Forward	7
AMPS	Advanced Mobile Phone Service	1
AWGN	Additive White Gaussian Noise	41
BER	Bit Error Ratio	45
BS	Base Station	21
CDF	Cumulative Distribution Function	46
CEPT	European Conference of Postal and Telecommunications Administrations	2
CF	Compress-and-Forward	27
CFO	Channel Frequency Offset	50
CFR	Channel Frequency Response	14
CIR	Channel Impulse Response	13
CoMP	Coordinated MultiPoint	6
CP	Cyclic Prefix	18
CSI	Channel State Information	49
DF	Decode-and-Forward	7
DFT	Discrete Fourier Transform	35
EF	Equalise-and-Forward	10
EDGE	Enhanced Data Rates for GSM Evolution	2
ICIC	Intercell Interference Coordination	7
EM	Expectation Maximisation	97
ETSI	European Telecommunication Standards Institute	2
EV-DO	Evolution- Data Optimized	3
FD	Frequency Domain	19
FDMA	Frequency Division Multiple Access	1
FFT	Fast Fourier Transform	19
FT	Fourier Transform	14
GPS	Global Positioning System	2

GPRS	General Packet Radio Service	2
HSPA	High-Speed Packet Access	3
ICI	Inter-Carrier Interference	18
i.i.d	independent and identically distributed	52
IDFT	Inverse Discrete Fourier Transform	17
IEEE	Institute of Electrical and Electronics Engineers	3
IFFT	Inverse Fast Fourier Transform	17
IFT	Inverse Fourier Transform	14
ISI	Inter-Symbol Interference	18
ITU	International Telecommunication Union	3
LOS	Line-of-Sight	11
LS	Least Square	40
LTE	Long Term Evolution	3
LTE-A	LTE-Advanced	4
M2M	Machine-to-Machine	6
MRC	Maximum Ration Combining	19
MIMO	Multiple-Inputs and Multiple-Outputs	3
MISO	Multiple-Inputs and Single-Output	21
MMSE	Minimum Mean Square Error	41
MMS	Multimedia Messaging Service	2
MSE	Mean Square Error	48
MU-MIMO	Multi-user MIMO	6
NMT	Nordic Mobile Telephony	1
NTT	Nippon Telephone and Telegraph	1
OFDM	Orthogonal Frequency-Division Multiplexing	8
OFDMA	Orthogonal Frequency-Division Multiple Access	4
PDC	Pacific Digital Cellular	2
PDF	Probability Density Function	46
PDP	Power Delay Profile	14
PSD	Power Spectrum Density	16
QoS	Quality of Service	1
QPSK	Quadrature Phase-Shift Keying	46
RA	Relay Assisted	7
RMS	Root Mean Square	14
RN	Relay Node	7
SFBC	Space Frequency Block Code	7

SMS	Short Message Service	2
SISO	Single-Input and single-output	21
SNR	Signal-to-Noise Ratio	19
PSD	Power Spectrum Density	16
STBC	Space Time Block Code	7
SDR	Software Defined Radio	122
TACS	Total Access Communication System	1
TD	Time Domain	39
TDMA	Time Division Multiple Access	2
TIA	Telecommunications Industry Association	2
UMTS	Universal Mobile Telecommunication Services	2
UT	User Terminal	10
UTRA	Universal Terrestrial Radio Access	3
WAP	Wireless Application Protocol	2
WiMAX	Worldwide Interoperability for Microwave Access	3
WSSUS	Wide Sense Stationary Uncorrelated Scattering	16

List of Figures

1.1 Expected peak network performance capabilities. . . . 3
1.2 Global total traffic in mobile networks, 2007 − 2012, from *Traffic and Market Data Report, Ericsson, 2012.* . . . 5
1.3 Global mobile traffic: voice and data 2010−2018, from *Traffic and Market Data Report, Ericsson, 2012.* . . . 5

2.1 Reflection, refraction, diffraction and scattering propagations. . . . 12
2.2 Multipath, path-loss and shadowing effects. . . . 13
2.3 OFDM System. a) Transmitter. b) Receiver. . . . 18
2.4 Cooperative transmission. . . . 21
2.5 Point-to-point link. . . . 23
2.6 Two-hop link. . . . 23
2.7 Three-terminal relay link. . . . 24
2.8 Multiple relay scenario. . . . 24
2.9 Half-duplex relaying protocols. . . . 25
2.10 Block diagram of the cooperative link with the RN employing the AF protocol. 26
2.11 Block diagram of the cooperative link with the RN employing the DF protocol. 27
2.12 Block diagram of the cooperative link with the RN employing the CF protocol. 27
2.13 Block diagram of the cooperative link with the RN employing the EF protocol. 28
2.14 Traditional relaying. . . . 29
2.15 Diversity enhancement scenario. . . . 29
2.16 Coverage enlargement scenario. . . . 30
2.17 Fairness enhancement scenario. . . . 30
2.18 Cluster scenario. . . . 31

3.1 OFDM System. a) Pilot-aided OFDM-based transmitter. b) Pilot-aided OFDM-based receiver . . . 34
3.2 Time-Frequency OFDM frame with regular scattered pilot arrangement. . . . 37
3.3 a) Block-type arrangement b) Comb-type arrangement. . . . 39

4.1 AF relay-assisted scenario. . . . 51
4.2 AF relay-assisted scenario: Block diagram. . . . 52
4.3 PDF: Rayleigh and double Rayleigh distributions. . . . 54
4.4 PDP: ITU Pedestrian Model A - point-to-point link. . . . 56
4.5 PDP: ITU Pedestrian Model A - compound link. . . . 56
4.6 PDP: ITU Pedestrian Model B - point-to-point link. . . . 56
4.7 PDP: ITU Pedestrian Model B - compound link. . . . 57

4.8 MMSE channel estimation performance for AF relay channel with ITU Pedestrian model A. . . . 63
4.9 MMSE channel estimation performance for point-to-point link with ITU Pedestrian model A. . . . 63
4.10 LS channel estimation performance for AF relay channel with ITU Pedestrian model A. . . . 64
4.11 LS channel estimation performance for point-to-point link with ITU Pedestrian model A. . . . 64
4.12 MMSE channel estimation performance for AF relay channel with ITU Pedestrian model B. . . . 65
4.13 MMSE channel estimation performance for point-to-point link with ITU Pedestrian model B. . . . 65
4.14 LS channel estimation performance for AF relay channel with ITU Pedestrian model B. . . . 66
4.15 LS channel estimation performance for point-to-point link with ITU Pedestrian model B. . . . 66

5.1 EF relay-assisted scenario. . . . 71
5.2 Pilot Pattern. . . . 73
5.3 Symbols arrangement per antenna element. . . . 73
5.4 EF relay-assisted scenario: Block diagram. . . . 74
5.5 Combining processing related to both transmission phases. . . . 74
5.6 Symbols arrangement per antenna at the RN. . . . 83
5.7 Equidistant and equipowered pilots. . . . 83
5.8 Equidistant and non-equipowered pilots. . . . 84
5.9 Equispaced and non-equipowered pilots and the corresponding CIR. . . . 85
5.10 $\alpha_k \Gamma_k$ per subcarrier. . . . 85
5.11 MSE performance: Pilots with fluctuation in amplitude. . . . 87
5.12 MSE performance: pilots with non-unitary yet constant values. . . . 88
5.13 MSE performance: pilots with non-unitary yet constant values. . . . 89
5.14 Maximum element off-diagonal of $\mathbf{R}_{\hat{\vartheta}\hat{\vartheta}}$. . . . 91
5.15 System BER performance: Impact of using σ_{t}^2 and $\sigma_{k,\mathrm{t}}^2$. . . . 94
5.16 System BER performance: Perfect channel knowledge and channel estimates. . . . 94
5.17 Channel estimation MSE performance: RA Scheme $2 \times 1 \times 1$. . . . 95
5.18 Channel estimation MSE performance: RA Scheme $2 \times 2 \times 1$. . . . 95

6.1 EF RA scenario. . . . 99
6.2 EF RA system: Block diagram. . . . 100
6.3 Pilot-Data aided Estimation: Block diagram. . . . 103
6.4 Pilot-Data-aided estimation: Flow chart. . . . 105
6.5 Pilot-Data channel estimation: MISO case. . . . 108
6.6 Virtual pilots - Selection Processing. . . . 109
6.7 Pilot-Data-aided estimation: Block-diagram. . . . 110
6.8 MSE performance: Scenario #1 and ITU Pedestrian Model A. . . . 114
6.9 MSE performance: Scenario #1 and ITU Pedestrian Model B. . . . 115
6.10 MSE performance: Scenario #2 and ITU Pedestrian Model A. . . . 115
6.11 MSE performance: Scenario #2 and ITU Pedestrian Model B. . . . 116

6.12 MSE performance: Scenario #3 and ITU Pedestrian Model A. 116
6.13 MSE performance: Scenario #3 and ITU Pedestrian Model B. 117

List of Tables

3.1 Summary of LS implementation complexity (per symbol estimation) 44
3.2 Summary of MMSE implementation complexity (per symbol estimation) 44
3.3 a and b vary according to a modulation scheme 46

4.1 Simulation parameters 60

5.1 Two transmit antenna SFBC mapping 72
5.2 Simulation parameters 92

6.1 Simulation parameters 111
6.2 Assessed links statistics 112

List of Symbols

- **Choice of Notation**

Regular small letters denote variables in the frequency domain whereas boldface small and capital letters denote vectors and matrices, respectively in the frequency domain as well. Variables, vectors or matrices in the time domain are denoted by ($\sim$). All estimates are denoted by ($\wedge$).

Symbol	**Connotation**
A	Gain related to the AF protocol
α	Gain related to the EF protocol
B_c	Coherent frequency band
β	Complex amplitude of a path
c	Light speed in vacuum
c_s	Clutter size
$\mathcal{CN}$	i.i.d complex Gaussian Noise
d	Regenerated data symbol
d	Superscript related to the data-aided estimation
d_t	Distance between the transmitter and the receiver
D	Regenerated data symbol matrix
diag($\cdot$)	Diagonal matrix

$\det(\cdot)$	Determinant of a matrix
Δh	Surface undulation
Δf	Frequency shift
Δt	Time shift
E_b	Energy per bit
f_D	Doppler frequency
$f_{D\max}$	Maximum Doppler frequency
f_k	Frequency subcarrier
f_s	frequency spacing
$\mathfrak{F}\{\cdot\}$	Fourier transform
$\mathfrak{F}^{-1}\{\cdot\}$	Inverse Fourier transform
ϕ	Angle between the direction of the motion and the path.
G	Number of antennas at the RN
$\mathcal{G}$	MRC equalisation coefficients
h	Channel frequency response
$\tilde{h}$	Channel impulse response
$\imath$	Imaginary unit
i	Iteration index
$\mathbf{I}$	Identity matrix
j	Data subcarrier
$\mathfrak{j}$	Subset of data subcarrier
J	Size of the data subcarrier set
$\mathfrak{J}$	Data subcarriers set

$\mathcal{J}\{\cdot\}$	Bessel function
k	Frequency domain subcarrier index
K	Number of subcarriers
l	Channel path
L	Number of channel paths
λ	Wavelength
$\mathcal{M}$	$\mathcal{M}$-ary constelation
m	Number of encoded bits per symbol
n	Time domain sample index
$\mathfrak{n}$	Variable index
$\mathbb{N}$	Set of the Natural numbers
N	Number of time samples
N_{cp}	CP size
N_f	Pilot distance in frequency dimension
N_r	Noise power
N_t	CIR replica separation
N_v	Pilot distance in time dimension
N_0	One sided noise power spectrum density
p	Pilot symbol
p	Superscript related to pilot-based estimation
P	Size of the pilot subcarrier set
$\mathfrak{P}$	Pilot subcarriers set
P_s	Signal power

Q	Number of antennas at the BS
$\mathcal{Q}$	Q-function
$R(\Delta t)$	Temporal autocorrelation
$R(\Delta f)$	Spectral autocorrelation
s	data-symbol
S	soft-decision variable
S_D	Doppler power spectral density
σ^2_{ch}	Channel power
$\sigma^2_{h,l}$	Average power of l-th path
σ^2_{bu}	Noise variance related to the link BS-UT
σ^2_{br}	Noise variance related to the link BS-RN
σ^2_{ru}	Noise variance related to the link RN-UT
σ^2_n	Noise variance related to a generic link
σ^2_{t}	Noise variance of the overall noise
t	Time instant
t_{cp}	CP duration
t_s	Data-symbol duration
t_S	OFDM symbol duration
T_c	Coherent time
T_s	Sampling interval
T_S	OFDM symbol duration with CP
τ	Delay of a path
$\tau_{\max}$	Maximun excess delay

v	Mobile terminal speed
W	Filter FIR
x	An OFDM symbol in frequency domain
y	Received signal
z	Additive Noise
$\circ$	Point-wise operation
$\circledast$	Circular convolution
$\| \cdot \|$	2-Norm
$\| \cdot \|$	Absolute value
$(\cdot)^*$	Hermitian
$(\cdot)^T$	Transpose
$\widehat{(\cdot)}$	Estimate of $(\cdot)$
$\widetilde{(\cdot)}$	$(\cdot)$ in the time domain
$\mathbb{E}\left\{ \cdot \right\}$	Expectation operator

Chapter 1

Introduction

1.1 The Mobile Communications Journey

The breakthrough in wireless communications was the successful use of the electromagnetic waves for transmitting information, which allowed the long-distance transmission [1], [2]. The wireless communications has had a remarkable journey from the Marconi's first experiments with radio communication in 1890's to the cellular systems of nowadays.

Analogue cellular are referred to as the first generation of mobile communication systems, 1G, based on Frequency Division Multiple Access (FDMA) that was launched for voice service. In Japan the first operational cellular system was deployed by Nippon Telephone and Telegraph (NTT) in 1979, followed in Scandinavia by the Nordic Mobile Telephony (NMT) system in 1981. At the same year the Advanced Mobile Phone Service (AMPS) was introduced in North America by AT & T. In 1982 Total Access Communication System (TACS) was launched in the United Kingdom and afterwards, in 1985 the Radicom 2000 was introduced in France and the C-450 cellular system was introduced in Germany and Portugal. At mid 80's with the advances in integrated circuits and digital communication the cellular systems, with rudimentary Quality of Service (QoS), based on analogue signalling techniques were becoming obsolete and the cellular service in Europe had several interoperable cellular systems [3].

The digital technology brought the opportunity to develop a second generation of mobile systems. The digital generation increased the capacity of the systems, spectral efficiency, provided better QoS and smaller mobile devices. In addition, the digital encryption provided secrecy and safety to the voice calls and data that were initially 9.6 kbp/s of peak data rates [4]. In order to develop a European-wide digital cellular standard the Telecommunication Com-

mission of European Conference of Postal and Telecommunications Administrations (CEPT) established a group of study called *Groupe Speciale Mobile* (GSM) that were in 1989 continued within the European Telecommunication Standards Institute European Telecommunication Standards Institute (ETSI). The second generation of mobile communication, 2G, deployed in the 90's with the GSM standard built on Time Division Multiple Access (TDMA). Simultaneous development of a digital cellular standard was done by Telecommunications Industry Association (TIA) in the USA yielding in the IS-54, also a TDMA-based standard, referred to as North American TDMA Digital Cellular or United States Digital Cellular. Later on, with revised standards, such a system has been renamed IS-136, often called D-AMPS, and with the development of a CDMA standard the IS-95 was completed by TIA in 1993. In Japan, a 2G TDMA standard was also developed, referred to as Pacific Digital Cellular (PDC). Shortly, the IS-95 CDMA system, marketed as CDMAOne, has been introduced in Japan as well. The 2G systems provided voice e-mail and the primary data service, Short Message Service (SMS), that is considered in all likelihood the most successful mobile service to date, after voice. In 2006 several countries have reached more than 80% cellular phone penetration and the global GSM subscribers counted more than 2 billion – 15 years after the launching of the its first network [5].

Higher data rates were later introduced in the 2G systems with the General Packet Radio Service (GPRS) that could provide rates from 56 kb/s up to 115 kb/s. Such rates could provide other services other than SMS such as Multimedia Messaging Service (MMS), Wireless Application Protocol (WAP), Internet access. Subsequently, similar services with data rates up to 384 kb/s could be provided by Enhanced Data Rates for GSM Evolution (EDGE) [6] that later on yielded into Evolved EDGE.

The third generation system, 3G, was a worldwide efforts to develop and deploy more advanced cellular networks with a range of higher data rates multimedia communication such as person-to-person communication (push-to-talk over cellular, real time video sharing, voice over IP (VoIP) and online games) with high-quality images/ videos, Global Positioning System (GPS) and access to information/ services whether on public or private networks with improved QoS. The Universal Mobile Telecommunication Services (UMTS) was developed as the 3G replacement for GSM therefore, UMTS is considered a synonymous with W-CDMA standard that is also referred to as IMT-2000 standard. W-CDMA higher-bandwidth radio

interface of Universal Terrestrial Radio Access (UTRA) was developed by the partnership project 3rd Generation Partnership Project (3GPP) whereas the CDMA2000 1 x Evolution-Data Optimized (EV-DO) Advanced standard, the 3G technology developed from the 2G CDMA-based standard IS-95, was developed by the 3GPP2. These standards projects were created in 1998 and 1999, respectively, as a collective effort of standardisation bodies in Europe, Japan, South Korea, USA, and China with relevant International Telecommunication Union (ITU) recommendations [5], [7]. Figure 1.1 shows the evolution of the 3G wireless technologies and their expected peak network performance capabilities, to date [8].

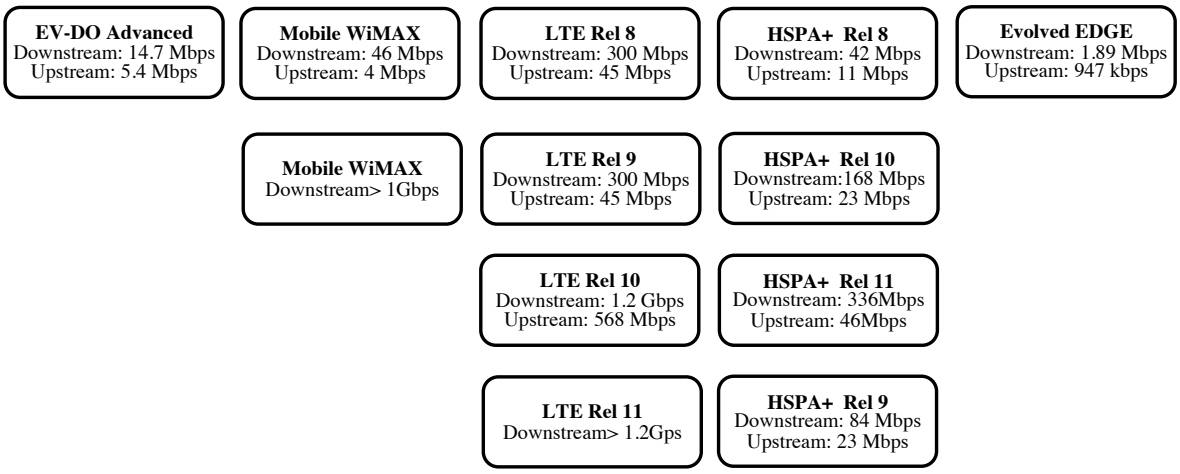

Figure 1.1: Expected peak network performance capabilities.

Subsequent developments yielded into enhanced 3G networks. 3GPP specifications yielded into a radio access standard referred to as Long Term Evolution (LTE) and major extensions of the W-CDMA radio interface evolved High-Speed Packet Access (HSPA) evolution, also referred to as HSPA+. Other deployment with the Institute of Electrical and Electronics Engineers (IEEE) 802 family, that are the standards related to the broadband Wireless Metropolitan Area Networks (Wireless- MAN), within the Worldwide Interoperability for Microwave Access (WiMAX) forum have led to the fixed WiMAX (802.16d-2004) and the mobile WiMAX (802.16e-2005) standards. The fourth generation system, 4G, was envisaged offering a seamless connectivity, i.e., the capability to roam across cellular networks, wireless LANs and WANs, satellites, and IP interoperability according to the user need. Currently, 4G network supports Multiple-Inputs and Multiple-Outputs (MIMO) and, to date, there three different

types of 4G networks: LTE using Orthogonal Frequency-Division Multiple Access (OFDMA); HSPA+, sometimes using W-CDMA; WiMAX using OFDMA [9]. Current 4G applications include mobile telemedicine and monitoring, high-bandwidth mobile applications, mobile entertainment and multi-party games. According to ITU the 4G term is undefined however, it applies to technologies beyond IMT-2000 or evolved 3G technologies providing a substantial level of improvement in performance and capabilities with respect to the initial third generation systems [10]. ITU refers to technologies beyond IMT-2000 as IMT-Advanced which the response from 3GPP evolved the LTE-Advanced (LTE-A), Release 10.

The smartphones has become a focal point for many people's digital lives, displacing the PC as the primary means of accessing the Internet [11]. Worldwide, the total number of smartphones is expected to exceed 3 billion by 2017 and as the cost of cellular devices decrease and their functionality increases, it is expected that the vast majority of people will hold in their hand a device with higher processing power than the most powerful computers from the 1980's [12].

Whilst voice remains as the basic service offered by the worldwide mobile operators the data traffic, which has been driven by the diffusion of smart devices and apps, has been growing at an impressive rate between 2007 and 2012, according to the Figure 1.2 that depicts the total monthly traffic split for voice and data[1]. The data traffic doubled between Q3 2011−Q3 2012 and the quarterly growth between Q2 2012−Q3 2012 was 16 percent [13].

Mobile data traffic is expected to grow approximately 14 times between 2012 and 2018 as it continues the trend of doubling each year, according to the Figure 1.3. The smartphone traffic is expected to grow faster due to the high growth in subscriptions. In the latter years of the forecast period, the data traffic will be split fairly equally between mobile phones on one hand and mobile PCs, tablets and mobile routers on the other [13].

[1]Traffic does not include DVB-H, Wi-Fi, or Mobile WiMAX

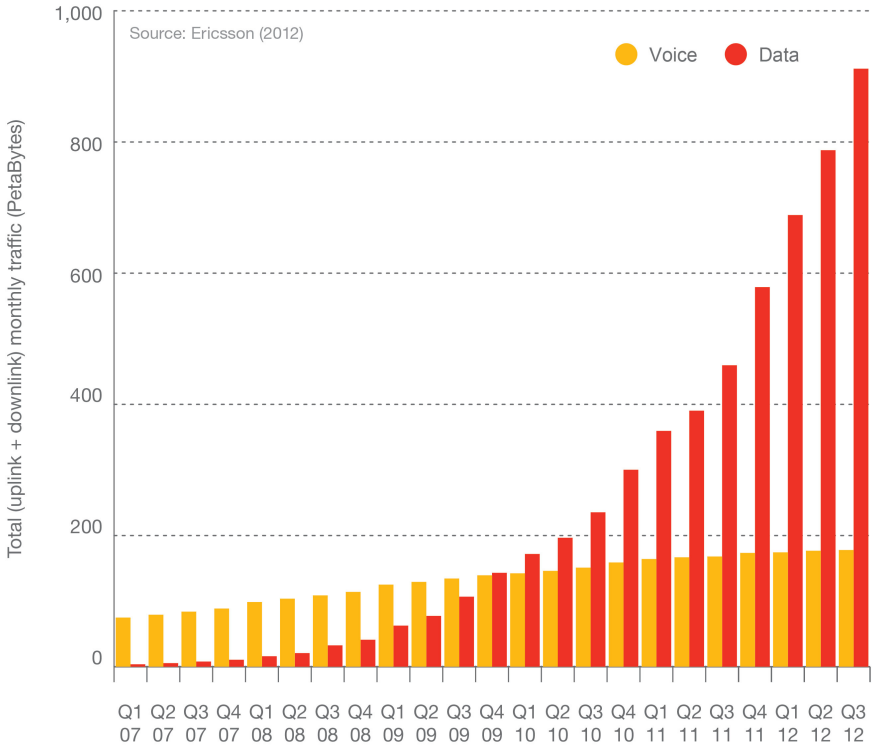

Figure 1.2: Global total traffic in mobile networks, 2007 – 2012, from *Traffic and Market Data Report, Ericsson, 2012.*

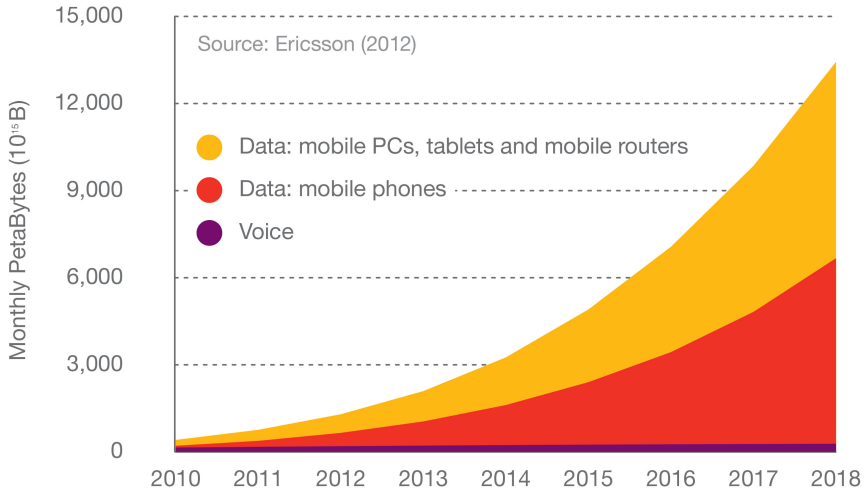

Figure 1.3: Global mobile traffic: voice and data 2010 – 2018, from *Traffic and Market Data Report, Ericsson, 2012.*

Nowadays 4G connections represent only 0.2% of mobile connections, they already account for 6% of mobile data traffic, to date. In 2016, 4G is expected to represent 6% of connections, but 36% of total traffic. To date, a 4G connection generates 28 times more traffic than a non-4G connection as many of the 4G connections today are for residential broadband routers and laptops, which have a higher average usage. In addition, the higher speeds encourage the adoption and usage of high-bandwidth applications, therefore a smartphone on a 4G network is likely to generate 50% percent more traffic than the same model smartphone on a 3G network [14].

According to the predictions, in the end of 2012 the total number of mobile subscriptions was around 6.6 billion, being 1.5 billion of broadband connections. By the end of 2018 total mobile subscriptions are predicted to reach 9.3 billion, being 1.5 billion of broadband accesses. These figures do not include Machine-to-Machine (M2M) subscriptions, which will also add to the number of subscriptions [13].

In order to satisfy the peak data rate of 100 Mb/s for high mobility and 1 Gb/s for low mobility required by the IMT-Advanced as well as the roaming seamlessly between networks [15], [16], promising approaches have been foreseen for the LTE-A, such as:

- Relaying: Additional nodes are included in the communication link in order to exchange information and improve link reliability.

- Carrier Aggregation: Multiple component carriers of smaller bandwidth are aggregated. It is an attractive alternative to increase data rate. Aggregating non-contiguous carriers, fragmented spectrum can be more efficiently utilised in various deployment scenarios [17].

- Multi-user MIMO (MU-MIMO): Spatial diversity is exploited by serving different users on different spatial streams on the same time/frequency resource, that is, assigning the same resource block to different users.

- Coordinated MultiPoint (CoMP) Transmission: It refers to the possibility to coordinate the transmission towards the same user adopting multiple base stations, in case of downlink transmission. CoMP techniques imply into use resource allocation techniques, coordination and synchronisation in order to cope with multi-point transmissions [18].

- Scheduling in Heterogeneous Networks: It addresses radio resource management problems, such as dynamic frequency allocation and inter-cell interference management by

means of dynamic spectrum access [19].

Whilst LTE was initially designed to be as decentralised as possible, in LTE-A enhanced Intercell Interference Coordination (ICIC) [20] is now being introduced such that interference-related information is exchanged among base stations and resource usage decisions are performed in a hierarchical manner.

Further standardisation of LTE-A will continue to follow the evolutionary phases in the form of releases. The future steps towards such an evolution is expected to lead to the LTE-B, LTE-C and so on in order to indicate the steps after LTE-A [21].

1.2 Motivations and Goals

As referred in the previous section, in order to continuously provide the demand for wireless services and ubiquitous access, more innovative techniques should be considered. In LTE-A and WiMAX standards cooperative techniques as well as virtual MIMO and Space Frequency Block Code (SFBC)/Space Time Block Code (STBC) are regarded in order to cope with the IMT-Advanced requirements.

When it comes to virtual MIMO or Relay Assisted (RA) techniques, a new paradigm arises, i.e., instead of having a point-to-point link between the transmitter and the receiver the connection may involve several nodes and this raises new challenges in channel estimation. The availability of accurate channel estimates is crucial to the performance of any link and, although there is abundant literature in the context of point-to-point links, when multiple links are involved (e.g. through the relays), these techniques require modifications and few studies have been done to date. Therefore, efficient channel estimation techniques for RA cooperative schemes are needed.

The estimation of a channel involving relays has been addressed for several scenarios and protocols, e.g., for the Decode-and-Forward (DF) protocol the relaying channel is regarded as two point-to-point channels whereas for the Amplify-and-Forward (AF) a compound channel estimate is addressed. Regarding RA scenarios where the Relay Node (RN) is equipped with a single antenna and employs the AF relaying protocol, some channel estimation techniques have been proposed, as mentioned in the following chapters. Nevertheless, restricting the RN to a single antenna is a limitative approach since the diversity associated with multiple antennas is

not explored. When it comes to a scenario where the RN is equipped with an antenna array, the available literature is scarce, specially concerning the used transmission/reception scheme.

This thesis addresses Orthogonal Frequency-Division Multiplexing (OFDM)-based systems employing RA cooperative approaches. It aims at: identifying the impact that the RN has on the estimation performance as well as its constrains; contributing with efficient channel estimation schemes for RA scenarios such that at the RN low complex processing are performed and the diversity provided by antenna array is achieved; proposing and assessing techniques with aid of the regenerated data-symbols, as virtual pilots, in order to compensate the impairments brought by the RN insertion.

1.3 Main Contributions and Dissemination

The main contributions of this thesis is summarised as follows:

- Proposal of a pilot-based channel estimation scheme for RA cooperative systems employing the Equalise-and-Forward relaying protocol;
- Proposal of a pilot and data aided channel estimation method for an EF MIMO cooperative using Alamouti coding;
- Proposal of a modified MMSE channel estimator for RA cooperative systems employing the Amplify-and-Forward relaying protocol;
- Assessment of the aforementioned proposals in realistic scenarios with ITU multipath channel models including evaluation of the impact of pilot density in the performance the RA cooperative systems;

The contributions presented in this thesis were disseminated in the following scientific publications.

- (J1) D. Neves, C. Ribeiro, A. Silva, and A. Gameiro. An Iterative Pilot-Data-Aided Estimator for SFBC Relay-Assisted OFDM-Based Systems. *EURASIP Journal on Advances in Signal Processing*, 2012:74, 2012.

- (B1) D. Neves, C. Ribeiro, A. Silva, and A. Gameiro. Channels and Parameters Acquisition in Cooperative OFDM Systems. In *Vehicular Technologies: Increasing Connectivity*. Intech, 2011.

- (C1) D. Neves, C. Ribeiro, A. Silva, and A. Gameiro. An Iterative Pilot-Data Aided Estimator for OFDM-Based Relay-Assisted Systems. In *Proceedings of IEEE Third Latin-American Conference on Communications*, Belem, Brazil, October 2011.

- (C2) D. Neves, C. Ribeiro, A. Silva, and A. Gameiro. A Pilot-Data Based Channel Estimation Method for OFDM Relay-Assisted Systems. In *Proceeding of IEEE Vehicular Technology Conference - Fall*, San Francisco, United States, September 2011.

- (C3) D. Neves, C. Ribeiro, A. Silva, and A. Gameiro. A Time Domain Channel Estimation Scheme for Equalize-and-Forward Relay-Assisted Systems. In *Proceeding of IEEE 72nd Vehicular Technology Conference - Fall*, Ottawa, Canada, September 2010.

- (C4) D. Neves, C. Ribeiro, A. Silva, and A. Gameiro. Channel Estimation Schemes for OFDM Relay-Assisted Systems. In *Proceeding of IEEE 69th Vehicular Technology Conference - Spring*, Barcelona, Spain, April 2009.

1.4 Thesis Organisation

The remaining of this thesis is organised in seven chapters that present the contributions of the work and directions for future research.

Chapter 2 presents the concepts related to the wireless medium such as the mechanisms of propagation, channel modelling as well as the channel characterisation. The basic principles of OFDM-based transmission are presented as well as the concept of diversity in wireless communications, RA cooperative systems and some relaying protocols are described.

Chapter 3 addresses the channel estimation related issues such as pilot density and pilot pattern as well as their impact on the estimation performance. The conventional pilot-based channel estimators are addressed, following by the OFDM pilot-based transmission and assumptions that are considered in this thesis. In addition, the metrics carried out throughout of the evaluation of overall system performance are also presented.

Chapter 4 presents the mathematical model for the RA cooperative system employing the AF protocol and the corresponding relay channel statistics. Also, the proposals for modifying the classical point-to-point estimators, according to the AF relaying channel statistics, are presented and it is discussed the impact of the pilot density on the relaying channel estimation performance.

Chapter 5 addresses the mathematical model for RA cooperative scenarios employing the Equalise-and-Forward (EF) protocol, where in one of them the RA MIMO cooperative transmission is complemented by the use of Alamouti coding. A pilot-based channel estimation scheme is proposed in order to provide the required relaying channel estimates and other parameters that may be useful in the equalisation processing at the User Terminal (UT).

Chapter 6 presents an iterative pilot and data-aided channel estimation method for an EF MIMO cooperative scenario. The performance of the channel estimation scheme, presented in Chapter 5, is improved by using the energy of the regenerated data symbol. In addition, it is assessed the impact of the pilot density in the relaying channel estimates performance.

Chapter 7 summarises the findings and provides directions for future works exploiting the concepts addressed by the this thesis.

This thesis was written as a comprehensive complement to the published papers that contain most of the information. All the numerical simulations were carried out through Monte-Carlo simulations in a simulation platform implemented in Matlab® programming language.

Chapter 2

Basic Principles of Wireless and Cooperative Communications

This chapter discusses aspects of cooperative communication and relaying capabilities. The channel modelling, OFDM-based systems and the assumptions considered throughout this work are discussed as well.

2.1 Wireless Medium

In wireless systems the signal, i.e., the electromagnetic wave, propagates through free space and through or through off the objects cluttered in the surrounding the environment, therefore, the term wireless channel refers to the medium between the transmitting and receiving antenna. Since the propagation of signal leads to distortions, delays and losses, the space-time-frequency characteristics of the wireless channel play an important role in the system performance.

2.1.1 Propagation: Mechanisms and Effects

Depending on the relationship between the radio-frequency signal wavelength λ, the distance between transmitter and receiver d_t, the clutter size c_s and its surface ripples Δh, the mechanisms of propagation are categorised according to the following.

- Free space propagation: There is no clutter between the transmitter and receiver, i.e., the signal propagates through the Line-of-Sight (LOS). This propagation obeys the Friis' transmission formula [22].

- Reflection and refraction: A part of the signal reflects off the clutter's surface, if $\lambda \gg \Delta h$, and the remaining part refracts into the clutter, if $c_s \gg \lambda$. Both are represented in Figure 2.1 a).

- Diffraction: Occurs when, between the transmitter and receiver, there is no LOS and the clutter has edges that are smaller or of the same size of λ. The diffraction causes the formation of secondary waves that can still reach a zone shadowed by an object, according to Figure 2.1 b).

- Scattering: It is due to the constructive and destructive addition of the reflected waves off surface elements of heights differing of Δh. If $c_s \geqslant \lambda$ and $\lambda \approx \Delta h$ the signal is known to be scattered off the clutter's surface, represented in Figure 2.1 c).

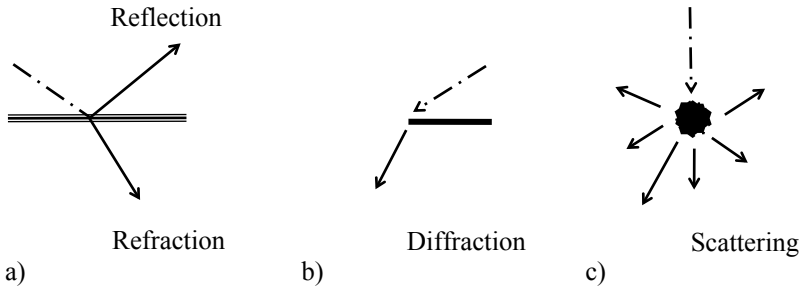

Figure 2.1: Reflection, refraction, diffraction and scattering propagations.

A signal may undergo all these propagations mechanisms before coupling into the receive antenna. Consequently, these phenomena may lead to the following distortions, depicted in Figure 2.2.

- Multipath Propagation: The signal and its copies, i.e., the replicas, transverse multiple propagation paths such that the received signal corresponds to a sum of signals with different delays, amplitude, phase angle of arrival and therefore this effect causes fading to the signal. If the multiple paths change rapidly this effect is referred as fast-fading.

- Path-loss: It corresponds to the attenuation of the signal power with the distance. Path-loss limits interference but also rapidly diminishes the useful signal power [23].

- Shadowing: It is caused by obstructions between the transmitter and receiver and it is also referred as shadow loss. Likewise the path-loss effect, it is noticeable over long distances and it leads to fluctuations in the average received signal power.

The fluctuation in the signal power caused either by path-loss or shadowing can be compensated by techniques provided by network planners [24]. Therefore, in this thesis it is considered that the multipath is the only effect distorting the transmitted signal.

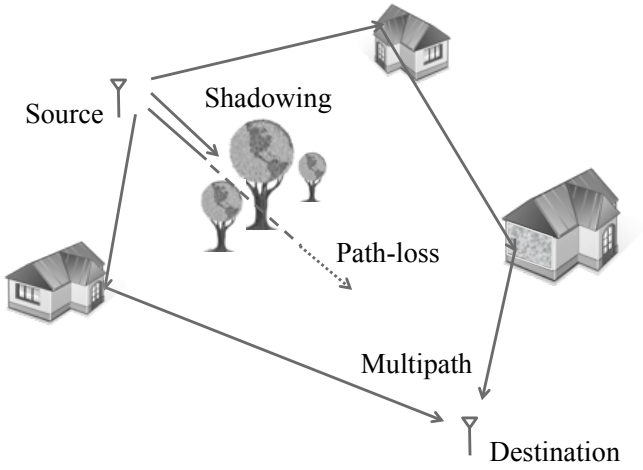

Figure 2.2: Multipath, path-loss and shadowing effects.

2.1.2 Channel Modelling

In the designing process of wireless systems the channel model is a key aspect as it influence the performance behaviour, power budget dimensioning and transceiver design.

Regarding the channel models, there are statistical, deterministic and hybrid channel modellings [3]. The statistical model considers random variables in order to describe the channel behaviour. The deterministic one is based on the electromagnetic wave propagation whereas the hybrid model is obtained based on indoor or outdoor measures and mathematical approximations. The statistical model is commonly used in literature due to its low complex implementation and hence it is considered in this thesis.

According to the statistical model, the multipath fading channel can be characterised as complex-valued, time variant, low-pass equivalent Channel Impulse Response (CIR) given by [?]

$$\tilde{h}(t,\tau) = \sum_{l=0}^{L-1} \beta_l(t)\delta(t-\tau_l), \tag{2.1}$$

where τ_l is the delay of the l-th path and β_l is the corresponding complex amplitude.

The Channel Frequency Response (CFR) corresponds to Fourier Transform (FT) of Eq. (2.1) w.r.t. τ and corresponds to

$$h(t,k) = \sum_{l=0}^{L-1} \beta_l(t) e^{-\imath 2\pi k \tau_l}. \tag{2.2}$$

2.1.3 Channel Characterisation

The channel can be statistically characterised according its temporal and spectral properties. The behaviour of the channel impacts the transmitted signal and therefore, the autocorrelations functions dependent on CIR and CFR play an important role in the system performance.

2.1.3.1 Spectral Domain

The spectral autocorrelation function determines how correlated the channel is after an observation frequency shift of Δf. It is expressed by

$$R(\Delta f) = \mathbb{E}\left\{h(f)h^*(f+\Delta f)\right\} = \sum_{l=0}^{L-1} \frac{\sigma_{h,l}^2}{\sigma_{\text{ch}}^2} e^{-\imath 2\pi \Delta f \tau_l}, \tag{2.3}$$

where $\sigma_{h,l}^2$ is the average power of l-th path, i.e., $\sigma_{h,l}^2 = \mathbb{E}\left\{|\beta_l|^2\right\}$ and σ_{ch}^2 is the total power average which is given by $\sigma_{\text{ch}}^2 = \sum_{l=0}^{L-1} \sigma_{h,l}^2$.

The Inverse Fourier Transform (IFT) of the spectral autocorrelation function gives the average power of the multiple delayed replicas, i.e., the Power Delay Profile (PDP), which determines how dispersive a channel is [23]. The dispersion of the channel is characterised by the Root Mean Square (RMS) delay spread τ_{RMS} which corresponds to the second central moment of the PDP, according to the following expression.

$$\tau_{\text{RMS}} = \sqrt{\overline{(\tau^2)} - (\bar{\tau})^2}, \tag{2.4}$$

with $\bar{\tau}$ being the the first moment of the PDP, i.e., the average delay $\bar{\tau} = \sum_l \sigma_{h,l}^2 \tau_l / \sum_l \sigma_{h,l}^2$ and $\bar{\tau^2} = \sum_l \sigma_{h,l}^2 \tau_l^2 / \sum_l \sigma_{h,l}^2$. In this thesis, the total power average is assumed to be normalised to one, i.e., $\sigma_{\text{ch}}^2 = 1$.

The spectral autocorrelation function characterises whether a channel is frequency selective or flat fading. Such a characterisation depends of the coherent frequency band B_c which corresponds to the shift Δf over which $R(\Delta f)$ remain unchanged or insignificantly changed, i.e., it is a range of frequency where the multipath channel affects the transmitted signal with similar gain and linear phase. The coherence frequency band depends on the environment through its impact onto the PDP. The literature presents several numerical approximations to B_c [3],[25],[26]. Generally, it is considered inversely proportional to the maximum excess delay $\tau_{\max}$, i.e., the time interval between the last resolvable tap and the earliest significant one, that is $B_c \approx 1/\tau_{\max}$.

Considering the transmitted signal bandwidth B, if $B < B_c$ all the spectral components of the signal are affected by the same attenuation and by a linear change of phase. In such a case, the channel is classified as flat fading or narrow band channel. If $B > B_c$, then the spectral components of the signal are affected by different attenuations, making it harder to equalise the received signal for accurate detection [26]. In this case, the channel is classified frequency selective fading or broadband channel.

2.1.3.2 Temporal Domain

The temporal autocorrelation determines how correlated the channel is after an observation time shift of Δt. The temporal autocorrelation depends on the environment and the movement of transmitter and/or receiver. Such a mobility makes the channel time-variant and hence, makes the signal may be perceived at a different frequency than the actual emitted. This effect is referred as Doppler shift and the perceived frequency is called Doppler frequency f_D. The normalised temporal autocorrelation function is expressed as [3]

$$R(\Delta t) = \jmath_0(2\pi f_{D\max}\Delta t), \tag{2.5}$$

where $\jmath_0$ is the zero order Bessel function of the first kind and $f_{D\max}$ corresponds to the maximum Doppler frequency that is obtained for $\phi = 0$ or $\phi = \pi$, according to the following expression.

$$f_D = \frac{\mathrm{v}}{\lambda_k}\cos(\phi), \tag{2.6}$$

where v is the speed of motion, either of transmitter or receiver, λ_k is the corresponding wavelength of the carrier and ϕ is the angle between the direction of the motion and the path.

Signals undergoing different paths experience different Doppler shifts and therefore, the received signal power spectral density is spread over the bandwidth limited by the $f_{D\max}$. The FT of the temporal autocorrelation corresponds to the Jakes spectrum [24], also referred as Doppler Power Spectrum Density (PSD) S_D which is

$$S_D(f_D) = \begin{cases} \dfrac{1}{\pi f_D \sqrt{1-(\frac{f_D}{f_{D\max}})}}, \ |f_d| \leqslant f_{D\max} \\ 0, \ \text{remaining} \end{cases} . \tag{2.7}$$

The temporal autocorrelation function categorises whether a channel is slow or fast fading. Such categorisation depends on the the coherent time T_c which is the shift Δt over which $R(\Delta t)$ remains invariant, i.e., the channel impulse response remains insignificantly unchanged. Similarly to the frequency coherent band, the literature presents several numerical approximations to T_c [3]-[26]. Generally, it is considered inversely proportional to maximum Doppler frequency, that is $T_c \approx 1/f_{D\max}$.

Considering the transmitted signal duration t_S, if $t_S > Tc$ the channel impulse response changes over a period of time longer than the signal duration. In such case, the channel is categorised as slow fading. If the converse applies, the channel is said to have fast fading [26].

The channel modelling previously described is classified as Wide Sense Stationary Uncorrelated Scattering (WSSUS) since neither the coherence time or frequency depend on time and since the paths presents uncorrelated scattering. If the multipath fading channel is only made up of non-LOS components, which is a common assumption in urban scenarios, the envelope of the channel is Rayleigh distributed and the channel is said Rayleigh fading channel [27]. In cases where there is a dominant scatter in the medium, e.g. a LOS component, the envelope of the channel is described by a Rice distribution and the channel is said to be Ricean fading channel [27].

2.2 OFDM-based Systems

In single carrier modulation techniques, a carrier occupies the entire bandwidth whereas in multi-carrier techniques each carrier occupies a small part of it. OFDM can be address as a special case of a multi-carrier technique that modulates independent data on several orthogonal and overlapped subcarriers therefore, the available bandwidth is efficiently used.

Let us consider a digital multi-carrier transmitter with K subcarriers where T_s is the sampling interval, i.e., $t = nT_s$ for $n = 0, 1, \cdots, N-1$. s_k corresponds to a complex data-symbol generated by a modulation scheme. Each s_k is modulated according to a frequency f_k, therefore, the multi-carrier transmitter output is given by

$$\tilde{s}(nT_s) = \sum_{k=0}^{K-1} s_k e^{\imath 2\pi f_k nT_s}. \tag{2.8}$$

A multi-carrier transmitter consists of a bank of modulators and for complexity and costs reasons such a structure is not appropriate for actual implementation.

Considering that $k = 0, 1, \cdots, K$ are the indices of the baseband frequencies that are uniformly spaced in frequency domain by a frequency spacing of f_s, such that $f_k = kf_s$. Then, assuming that $f_s = 1/(KT_s)$ is the minimum separation among the subcarriers in order to make them orthogonal, thus Eq. (2.8) can be written as

$$\tilde{s}_n = \tilde{s}(nT_s) = \sum_{k=0}^{K-1} s_k e^{\imath 2\pi nk/K}. \tag{2.9}$$

Equation (2.9) corresponds to an OFDM signal. Except for the missing multiplying factor $1/\sqrt{K}$, it corresponds to the equation of a K-point Inverse Discrete Fourier Transform (IDFT). If K is power of two, it can be implemented by a Inverse Fast Fourier Transform (IFFT) which means that OFDM allows low-complexity and computationally efficient implementations [26], [4] and a bank of parallel modulators is no longer required.

In Figure 2.3 is shown a representative block diagram of an OFDM baseband system where K represents the number of subcarriers, for $k = 0, 1, \cdots, K$, and the corresponding bandwidth is $B = Kf_s$. This system presents the components that are relevant to the purpose of this thesis. Others features, despite being essential in an OFDM system, are not represented here.

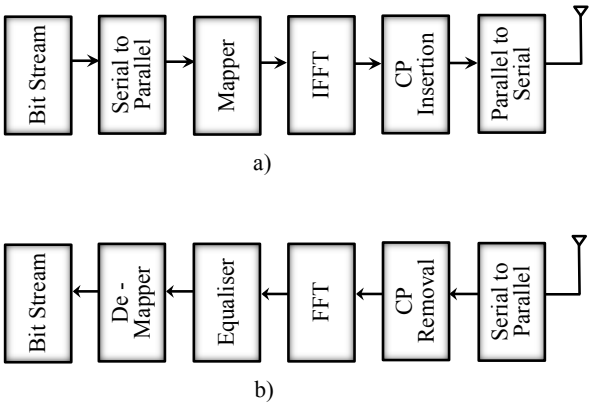

Figure 2.3: OFDM System. a) Transmitter. b) Receiver.

In the transmitter, the Serial to Parallel block arranges the serial bit stream into parallel lower rate bits. In the Mapper block, sets of parallel bits are mapped into complex constellation points, i.e., data-symbols, according to a constellation. In the IFFT block, at time K subcarriers moulds the amplitude and phase of K data-symbols. The output of this block corresponds to an OFDM symbol vector $\tilde{\mathbf{x}}$ that is made up of N elements, according to

$$\tilde{s}_n = \frac{1}{\sqrt{K}} \sum_{k=0}^{K-1} s_k e^{\imath 2\pi nk/K}, \quad \text{for} \quad n = 0, 1, \cdots, N. \tag{2.10}$$

Since each data-symbol has period of t_s hence, an OFDM symbol period is $t_S = Nt_s$. Considering that the duration of an OFDM symbol corresponds to the inverse of the frequency spacing and the orthogonal subcarriers follows $f_s = 1/(KT_s)$, the sampling interval can be express as

$$T_s = \frac{t_s}{K}. \tag{2.11}$$

OFDM systems may suffer sever interferences that may compromise the system performance. The high speed motion may destroy the orthogonality leading to power leakage among the subcarriers, referred as Inter-Carrier Interference (ICI). Also, the delay of the received signals makes an OFDM symbol disturbs the subsequent one generating Inter-Symbol Interference (ISI). In order to mitigate ISI, a Cyclic Prefix (CP), i.e., a copy of the last samples of the corresponding upcoming symbol, should be inserted between the symbols. Inserting a CP with duration equal or higher than the maximum delay guarantees ISI free and allows the channel matrix to be circular so that it prevents ICI. It should be pointed out that the asyn-

chronism between the received signal and the local oscillator at the receiver can cause ICI as well. A long enough CP and perfect synchronisation are common requirements of a system free of ISI and ICI.

The CP is inserted by the CP Insertion block resulting in $N + N_{\text{cp}}$ samples with period of $T_S = t_S + t_{\text{cp}}$ where t_{cp} is the period of the corresponding N_{cp}, the size of the CP.

In the receiver side, Figure 2.3 b), after remove the CP the OFDM symbol is brought into the Frequency Domain (FD) by the Fast Fourier Transform (FFT) block. The Equaliser block is designed to mitigate distortions introduced by the channel, assuming that this block can access the channel estimates. Without the equalisation, if no noise was considered, the bit stream could not be recovered. The optimal equaliser is the Maximum Ration Combining (MRC) [26] and its coefficients correspond to the complex conjugate of the CFR. Following the equalisation at the De-mapper block the demodulation takes place and the the bit stream is recovered.

In contrast to Figure 2.3 OFDM systems can also be implemented with the block Serial to Parallel before the IFFT at the transmitter and with the Parallel to Serial following the FFT block at the receiver [3],[28]. Without loss of generality, the OFDM modulator generates the same result.

2.3 Diversity in Wireless Communications

Diversity corresponds to transmitting additional copies of a signal over multiple uncorrelated paths, each one exhibiting a fading process as much independent from the others as possible. Such a transmission improves the overall links' reliability and leads to diversity gains.

Techniques that aim at providing multiple and independent signal paths are known as diversity techniques [28]. Such techniques may mitigate the fading effects of the multipath channel, basically by ensuring multiple channels that vary in time, frequency, space or polarization. The deployment of multiple antennas inducing space diversity generates copies of the transmitted signal at the transmitter and/or receiver. The benefits of diversity are significant, but they can be summarized by the performance improvement that is manifested by the communication symbol error probability P_{ser} decreasing at a much larger rate at a high channel Signal-to-Noise Ratio (SNR) than systems with less or no diversity, according to the

expression

$$D_0 = \lim_{\mathrm{SNR}\to\infty} \frac{\log P_{\mathrm{ser}}}{\log \mathrm{SNR}}. \tag{2.12}$$

The diversity gain stem from the fact that with the amount of additional copies increasing, the probability of all of them being illegible decreases. According to Eq. (2.12), for a high value of SNR a large diversity gain means that the probability of symbol error is reduced at a faster rate [28] hence, the chance that there is at least one sufficiently strong path is improved. In the following, is described the main diversity techniques.

- Time Diversity: Multiple copies of the signal are transmitted at different times instants. The interval between the transmissions should be greater than the coherence time of the channel therefore, the copies experience channel realizations that are highly uncorrelated, i.e., independent fading.

- Frequency Diversity: Copies of the signal are transmitted using different carriers. If the frequency spacing between the carrier frequencies is greater than the channel frequency coherence band, the received signals would suffer from uncorrelated fading.

- Space Diversity: Also referred as antenna diversity it corresponding to either transmit or receive, or both, copies of the signal over uncorrelated propagation paths by using multiple and physically separated antennas.

- Space-time or Space-frequency diversity: The space diversity could be increased by its combination with a frequency diversity or a time-diversity method, generating the spatial diversity and thus increasing the frequency and time selectivity of the resulting channels.

- Polarization Diversity: Copies of the signal are transmitted and received via antennas with orthogonal polarisation.

Furthermore, multiple diversity techniques can be combined to provide even greater performance improvement. These translates into decreasing transmission powers, higher capacity or better cell coverage [28].

Alternatively, diversity may be achieved by using a third terminal, a helper node, it is so called cooperative diversity. This form of diversity uses the broadcast nature of the wireless channels and the available or idle nodes willing to cooperate within a wireless network.

The cooperative network can be regarded as a system implementing a distributed multiple antenna in order to create diverse signal paths, as depicted in Figure 2.4, where node U cooperates with neighbours to send information to B.

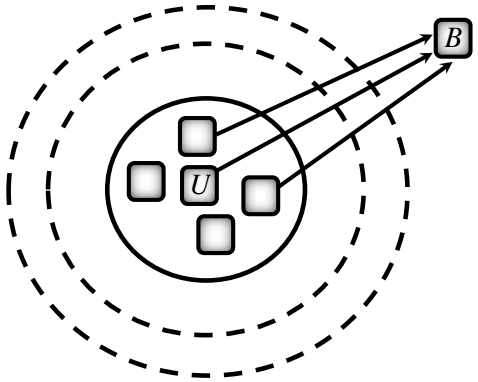

Figure 2.4: Cooperative transmission.

Similarly to the space diversity case, in such a diversity as the number of cooperating nodes increases the diversity increases as well.

2.4 Cooperative Communications

MIMO communications can improve the system throughput and reliability based on space diversity. The concept of transmitting information over different antennas is behind of the MIMO techniques and such approaches provide very higher data rates in comparison with Single-Input and single-output (SISO) or Multiple-Inputs and Single-Output (MISO) techniques. In order to make use of the MIMO advantages the devices should be equipped with multiple antennas and they should experience independent channel characteristics, i.e., the equivalent channel matrix should be full-rank. In practice, MIMO devices may experience propagation environment that cannot support MIMO requirements, i.e., the paths between transmitter and receiver may be highly correlated [28]. The use of an extra source, distant several wavelengths from the primary one, makes the relay channel, e.g. Base Station (BS)-RN-UT or UT-RN-BS, varies independently from the direct channel, e.g. BS-UT or UT-BS. This may generate a full-rank channel matrix between the sources and receiver.

The cooperation concept is not new, in the 70's Van der Meulen [29] and Cover [30]

had introduced the three-terminal relay channel and the information theoretic properties of the relay channel, respectively. Later on in [31] an user cooperation protocol was suggested in order to boost the uplink capacity and in [32]-[33] a two user cooperation system was proposed such that pairs of terminals in the wireless network are coupled to help each other forming a distributed two-antenna. Cooperative communications is a new paradigm shift for the future wireless systems that will guarantee high data rates to all users in the network, and we anticipate that it will be the key technology aspect in the forthcoming wireless networks [28]. The key aspect in cooperation is sharing the resources among multiple nodes in a network and plenty of lessons have been learned ever since and current standards developing bodies are picking up on the relaying and the cooperative concept. The IEEE 802.16j standard [34] has developed a relay enabled mode to WiMAX in the hope of giving it a competitive edge in 3GPP LTE developments and the LTE-A includes cooperative relay features in order to extend coverage by means of relay nodes [15],[35].

Cooperative receivers consider the information received by the direct and the multi-hop links. On account of that, cooperative communications offers several advantages such as:

- Extend the coverage area
- Reduce battery consumption and extend network lifetime
- Improve system performance and capacity
- Increase the throughput and stability region for multiple access schemes
- Provide cooperation trade-off beyond source–channel coding for multimedia communications
- Infrastructure-Less Deployment: The use of relays allows the roll-out of a system that has minimal or no infrastructure available prior to deployment. Relaying can be used to facilitate communications even though the cellular system is non-functioning, e.g. in disaster struck areas. For hybrid deployments, that is a cellular system coupled with relays, the deployment and maintenance costs can be lowered [23].

The "Anyone, Anywhere and Any time" paradigm fits perfectly the cooperative communications. Any terminal, static or mobile, can act as a RN or make use of relay link and therefore can provide or obtain higher gains as cooperative entity than as autonomous terminal.

2.4.1 Cooperative Systems

In wireless communications, initially, relay-assisted communication was designed to generate virtual antennas for single-antenna devices in a multi-user environment. The concept of cooperation has been extended to antenna arrays devices in order to merge benefits from space and cooperative diversity. In cooperative scenarios the receiver, e.g. UT, may combine the signal transmitted by two sources: the source, e.g., BS and a helper node, a RN. This approach has major impact especially in devices where the integration of more antennas is not suitable either for size or power constraints.

In non-cooperative systems the simplest channel corresponds to a point-to-point one, according to Figure 2.5. Such channels present significant attenuation of the signal with distance, which makes them impractical in long-range communications. The simplest form of user cooperation is multi-hopping that corresponds to a chain of point-to-point links from the source to the destination, according to Figure 2.6 where is depicted a two-hop link.

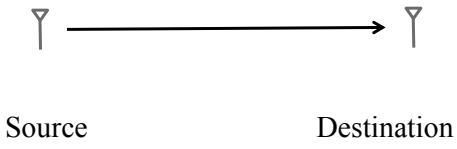

Figure 2.5: Point-to-point link.

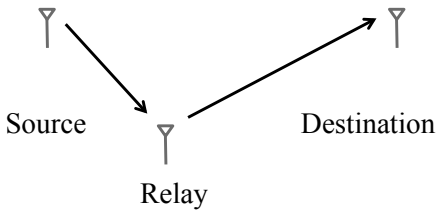

Figure 2.6: Two-hop link.

Such links represent scenarios where the direct link is shadowed by the clutter or offers poor conditions compared to the relay channel. The WiMAX standards has included the relay enable mode since 2009 [34],[36] in order to leverage coverage problems however, they act as repeater not as cooperative entities. Since, at least, one helper node is included the cooperative communications no longer have a point-to-point links but instead they have a

multi-links from the transmitter to the receiver, according to Figure 2.7 that depicts a three-terminal relay link.

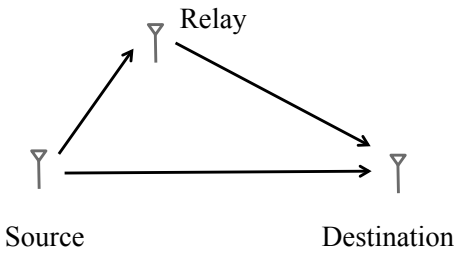

Figure 2.7: Three-terminal relay link.

Furthermore, the two-hop channel in Figure 2.6 can be extended by including more than one helper node, as depicted in Figure 2.8. Optimally designed cooperative schemes that involve μ terminals can achieve μ-th order diversity.

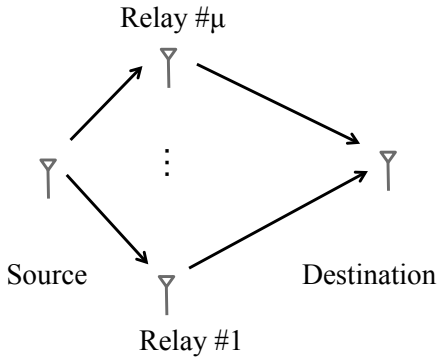

Figure 2.8: Multiple relay scenario.

2.4.2 Relaying Protocols

The cooperation is enabled by a relaying protocol that establish the processing to be performed at the RN. A protocol is termed as half-duplex when the reception and transmission are processed in different phases, i.e., different times in the same band, otherwise they are referred as full-duplex and the transmitted/received signals must be orthogonal. In real systems is difficult to ensure enabling simultaneous transmission and reception in the same band since the transmitted signals could cause severe interference to the incoming signals. The-

oretically, the relay could cancel out the interference since the transmitted signal is known however, errors in interference cancellation could compromise the received signal. Due to the difficulty of accurate interference cancellation it is more common using half-duplex protocols. Nevertheless, advances in analogue processing could potentially enable full-duplex relaying [37].

The half-duplex protocols, as depicted in Figure 2.9, present two phases:

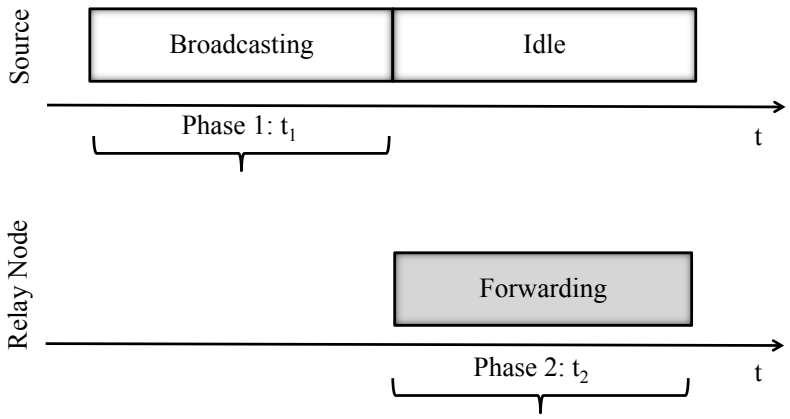

Figure 2.9: Half-duplex relaying protocols.

- Phase 1: The BS broadcasts the signal. The UT keeps the received signal in a buffer whereas the RN processes it.
- Phase 2: The RN forwards the signal and the BS may remain idle. At the UT the signals received in both phases are combined in order to be hard decoded.

The relaying protocol also can be classified as transparent or regenerative. The later one requires digital baseband operations therefore, considering the involved links with comparable conditions, they are likely to outperform the transparent ones [37]. Transparent relaying essentially implies that the relay does not access the information contents but receives the signal in one frequency band, performs analogue changes to it and momentarily retransmitted on another frequency band [28]. Some relaying protocols are described in the following.

- AF: The RN scales the signal received from the BS. The Normalisation block normalises the amplified signal before transmitting it to the UT. It is described in Figure 2.10, where

A corresponds to the amplification factor [38]. The amplification gain may follow three choices: constant, average or variable. In the first case, the relay node transmits at a constant output power that has been set during the node manufacturing. In the second choice, the relay fixes the amplification factor over a given time widow to a value that depends on long term statistics in the channel. In the third case, the amplification gain is adapted to instantaneous changes in the channel or network. The major disadvantage of this protocol is the amplification of the noisy components.

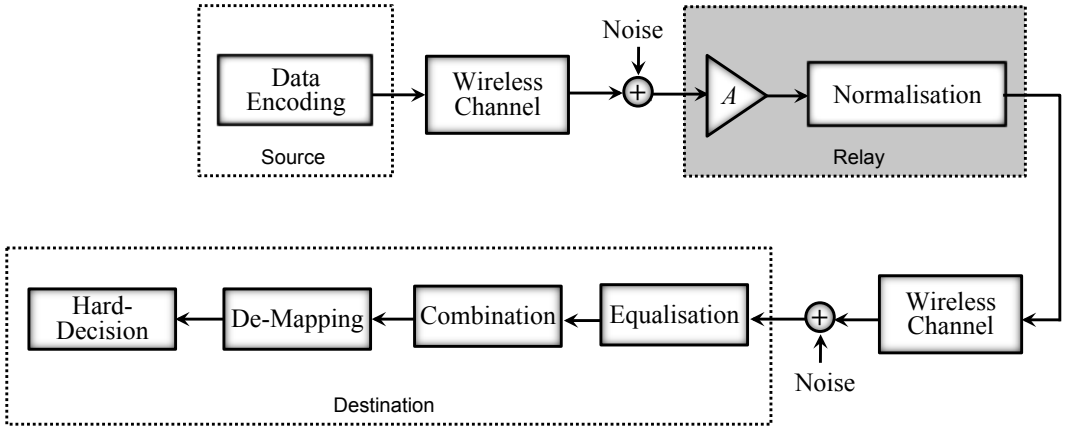

Figure 2.10: Block diagram of the cooperative link with the RN employing the AF protocol.

- DF: The received signal is hard-decoded, re-encoded and then transmitted to the UT, according to Figure 2.11 [39]-[40]. Since this protocol decodes the received signal it has the advantage over the AF in reducing the effects of the noise. If the channel source-relay offers excellent conditions, this protocol achieves optimal performance. However, if the first hop of the channel presents poor conditions it entails the possibility of forwarding erroneously detected signals to the destination, causing error propagation. An effective approach of this protocol is referred as Selective DF. According to it, the relay only processes the signal if its SNR excess a certain threshold. If the SNR falls below the threshold, the relay idles. Such approach overcome the problem in DF relaying in which the relay forwards all decoded signals to the destination although some decoded signals are incorrect.

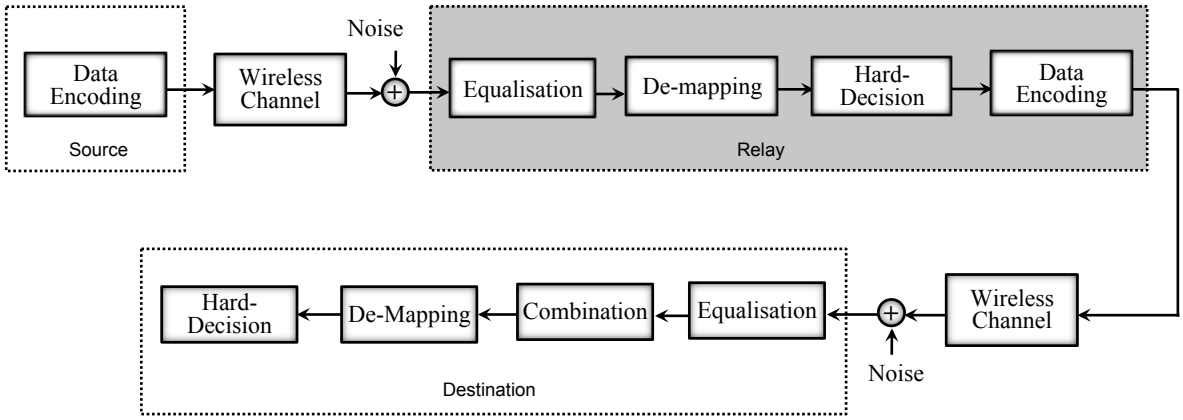

Figure 2.11: Block diagram of the cooperative link with the RN employing the DF protocol.

- Compress-and-Forward (CF): The RN does not transmit a copy of the received signal, instead it transmits a quantised and compressed version of it [41]-[42], according to Figure 2.12. Therefore, at the destination the signal transmitted by the BS is combined with its quantised version. Depending on the quantisation partition the second phase of the protocol may be made arbitrarily short.

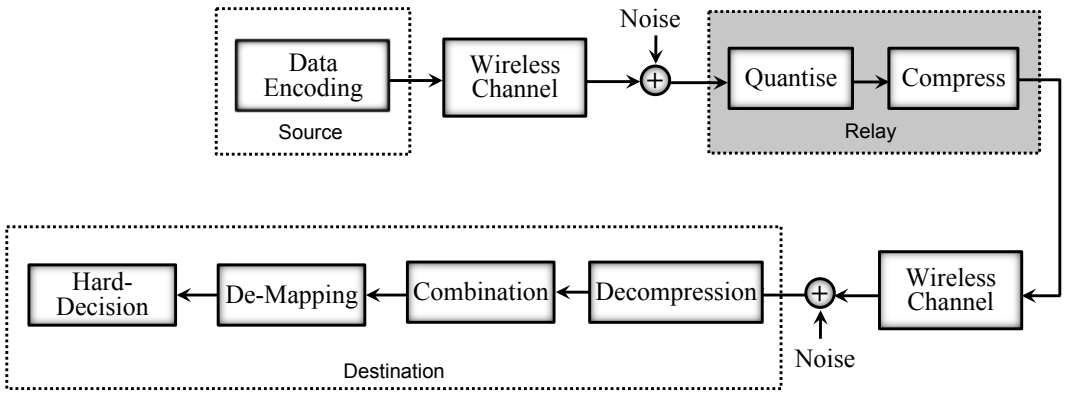

Figure 2.12: Block diagram of the cooperative link with the RN employing the CF protocol.

- EF: As depicted in Figure 2.13, at the RN only an equalisation is performed and then the resulting signal is transmitted to the UT [43]. In case of the first hop of the channel presents poor conditions this protocol avoids premature decisions at the RN, leading to advantage over the DF.

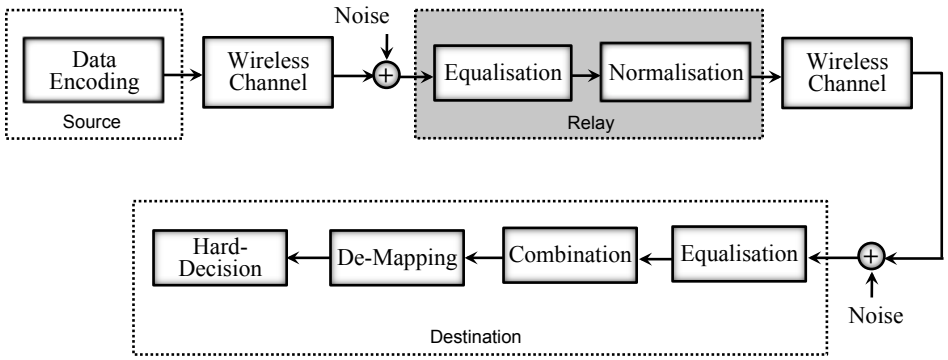

Figure 2.13: Block diagram of the cooperative link with the RN employing the EF protocol.

From the aforementioned protocols only the AF is classified as transparent, the others are regenerative.

2.4.3 Relay-Assisted Approach Scenarios

Cooperative schemes can be envisaged according to the employed scenario such that they can be drawn regarding the number of relays or the availability of the direct link. Such scenarios can realise transparent or regenerative relaying as well as any combination thereof. The involved entities can work together in a ad-hoc fashion style without centralisation or they can work under centralized control [44]. Furthermore, regarding the mobility in such scenarios the RN may assume mobile or fixed states. The terminals may be or not aware that they are exploiting a relay-assisted link or they are acting as RN. Likewise non-cooperative communication the link conditions play an important role in the relay selection for which many techniques have been proposed [45]-[47].

Apparently there are many possibilities for exploiting the principle of cooperative diversity in wireless communications nevertheless, the vast majority of the concepts and techniques are based on the basic three-terminal scenario, i.e, source (BS) - relay - destination (UT), according to Figure 2.14. For a scenario based on such channel, with slightly changes one may obtain different possibilities of cooperation [48].

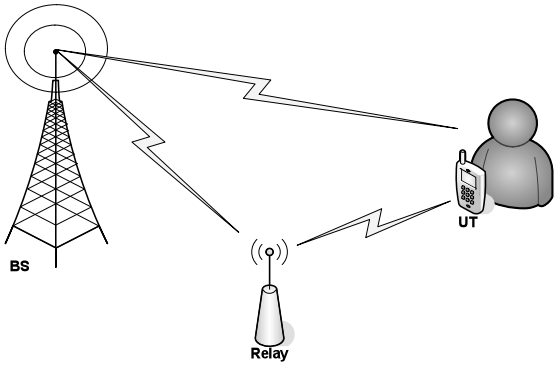

Figure 2.14: Traditional relaying.

The basic cooperative scenario can be exploited in order to obtain a set of sub-scenarios. In Figure 2.15 is presented a scenario that makes use of two relay links. Considering that the relay nodes are slightly apart such scenario provides relay links with minimal correlation which leads to higher diversity. For any cooperative scenario, the mobility of the UT and the RN has a great impact on issues related to synchronisation or coherent time which determine the ability to exploit channel state information.

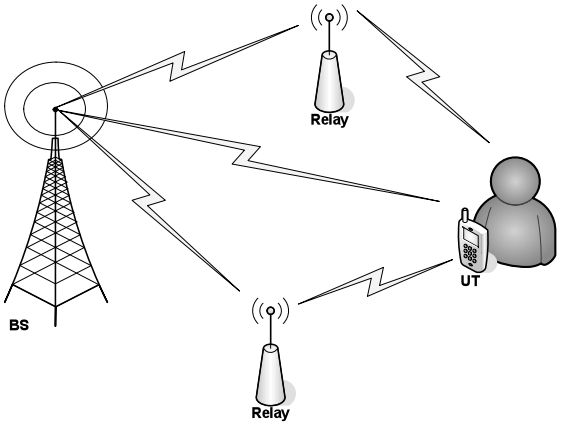

Figure 2.15: Diversity enhancement scenario.

Furthermore, whether the environment corresponds to indoor or outdoor, rural or urban also impacts on the cell size, the expected number of users in the cell and in the nature of the channel, i.e., multipath, shadowing or interferences. In Figure 2.16 is depicted a scenario where a UT or a group of UT is far beyond the realistic transmission range of the BS. In such case, there is no direct link and the coverage enlargement is reached by using the relay nodes.

Moreover, considering a cluttered environment a cooperative scenario can provide fairness enhancement by using the relays as a clutter bypass as depicted in Figure 2.17.

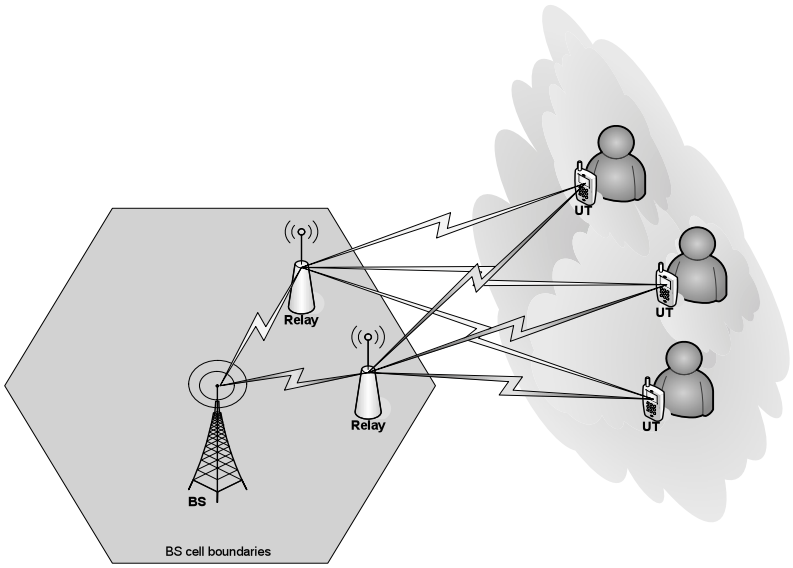

Figure 2.16: Coverage enlargement scenario.

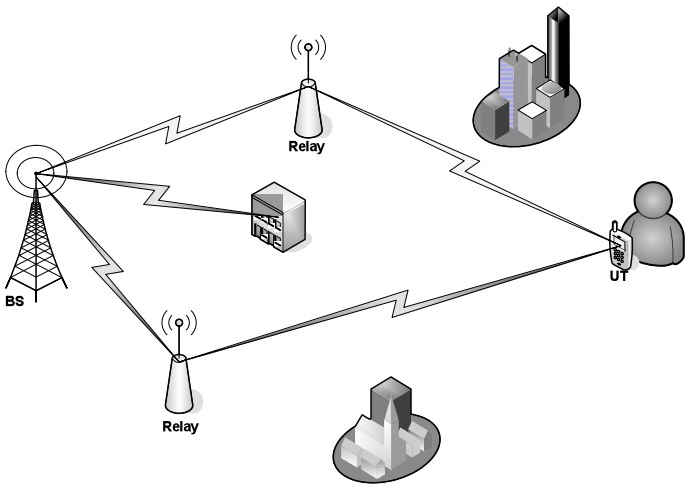

Figure 2.17: Fairness enhancement scenario.

Using the relay concept more additional scenarios can envisaged such as the scenario in Figure 2.18. In this case the relays are linked and can exchange information, forming a sub-net or a cluster.

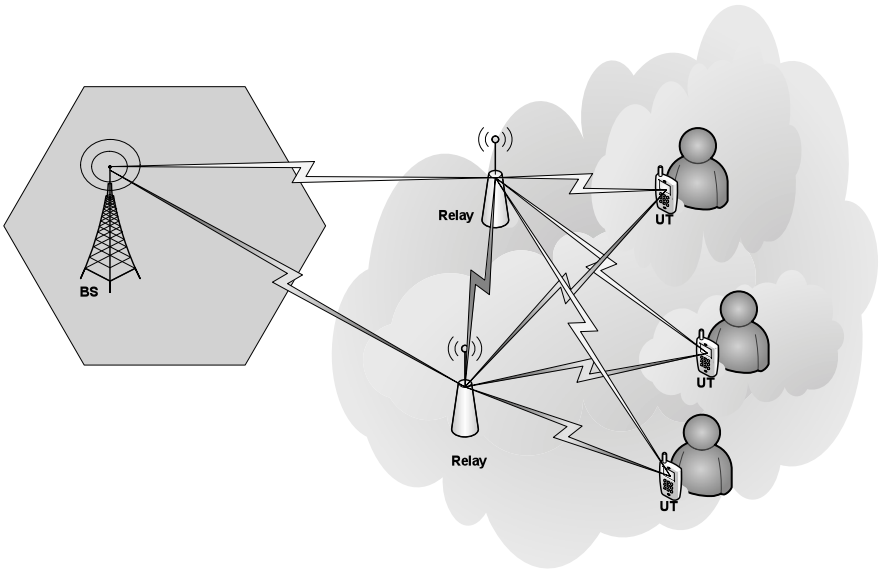

Figure 2.18: Cluster scenario.

In addition, more scenarios can be conceived considering the two-way relay channels, e.g. two user terminals are out of the coverage but can communicate through a RN. Such cooperative strategies are based upon the communication link is bidirectional and the transmissions/receptions can be performed simultaneously. Hence, the two-way relaying communications are promising spectral efficient transmissions for wireless networks with relay terminals employing half-duplex-protocols [49]-[50].

Chapter 3

Channel Estimation in OFDM Systems

3.1 Introduction

For coherent detection, accurate channel is essential and plays an important role since estimation inaccuracies degrade the system performance. Hence, the factors that may lead to errors or poor estimation performance should be analysed. This chapter addresses issues related to channel estimation and strategies that may impact its processing.

3.2 Pilot-Assisted OFDM-Based Systems

As aforementioned in Section 2.2, the OFDM systems are designed such that the transmitted signal follows the ensuing properties:

- The outcome of the IFFT block is a signal which corresponds to a sum of sinusoids with amplitude variations.
- Since the transmitter uses the CP longer than the CIR there is no ISI.
- The OFDM symbol duration is longer than the CIR and consequently, the channel impact corresponds to a multiplication by a complex scalar.

Accordingly, the receiver needs to compensate, per subcarrier, the amplitude and phase distortions imposed by the multipath fading channel. Such a processing is performed by an equaliser that is also fed by the channel estimator block, the provider of the channel estimates.

In contrast to Figure 2.3, the block diagrams in Figure 3.1 a) and b) show the channel estimation features required at the transmitter and the receiver sides in a pilot-aided OFDM-based system. Regarding the channel estimation, the Channel Estimator block in continuous line represents an estimation performed in the frequency domain whereas the block in dashed line represents one performed in the time domain. Channel estimation processing performed in the frequency or the time domains are discussed in Section 3.4. At the transmitter side, Figure 3.1 a), the Framing block multiplexes pilots and data-symbols in disjoint subcarriers, according to a pilot pattern. Such a block organises the OFDM symbols in a frame and according to that an OFDM system explores time and frequency diversity.

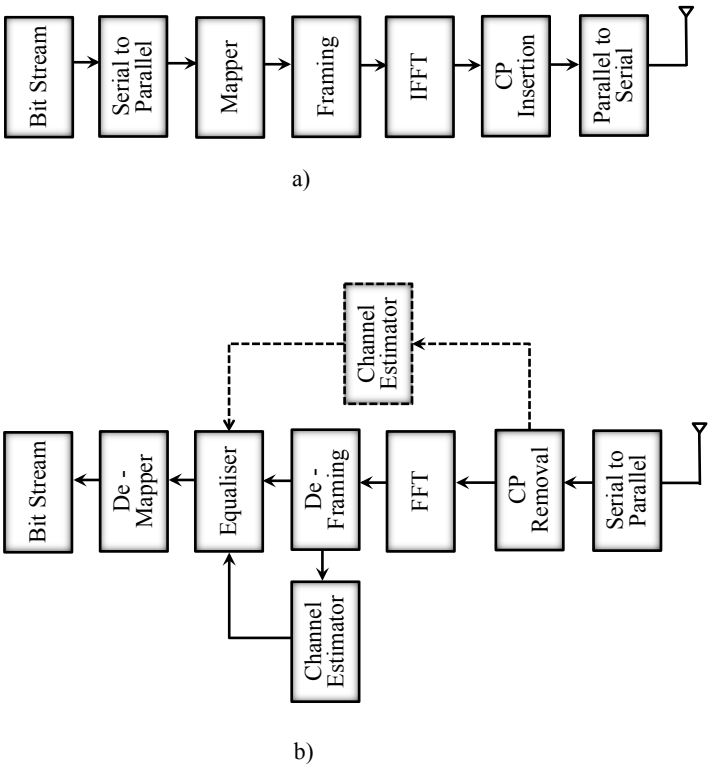

Figure 3.1: OFDM System. a) Pilot-aided OFDM-based transmitter. b) Pilot-aided OFDM-based receiver

The output of the Framing block is $\mathbf{x}$ that corresponds to the resulting signal vector in frequency domain given by

$$\mathbf{x} = \mathbf{s} + \mathbf{p}, \tag{3.1}$$

where $\mathbf{p}$ and $\mathbf{s}$ correspond to the pilot and data-symbol vectors.

Therefore, $\tilde{\mathbf{x}}$ corresponds to the output of the IFFT block, i.e., an OFDM symbol. After appending the N_{cp} samples related to the CP, the resulting signal in time domain corresponds to

$$\tilde{\mathbf{x}}_{\text{cp}} = \mathbf{C}\mathbf{F}^H\mathbf{x} = \mathbf{C}\Big(\tilde{\mathbf{s}} + \tilde{\mathbf{p}}\Big), \tag{3.2}$$

being $\mathbf{C} = \begin{bmatrix}\mathbf{I}_{K\times N_{\text{cp}}} & \mathbf{I}_K\end{bmatrix}^T$ the matrix that adds the CP, where $\mathbf{I}_K$ denotes the identity matrix $(K \times K)$ and $\mathbf{I}_{K\times N_{\text{cp}}}$ denotes the last N_{cp} columns of $\mathbf{I}_K$. The vectors $\tilde{\mathbf{p}}$ and $\tilde{\mathbf{s}}$ represent the pilot and data-symbols in time domain, respectively. $\mathbf{F}$ is the matrix $(K \times K)$ that represents the Discrete Fourier Transform (DFT) operation such that $\mathbf{F}\mathbf{F}^H = \mathbf{I}$.

At the receiver side, Figure 3.1 b), assuming perfect synchronisation and the sampling rate of $1/T_s$, the output of the CP Removal block followed by the FFT block corresponds to the received signal in frequency domain that is given by

$$\mathbf{r} = \mathbf{F}\bar{\mathbf{C}}\tilde{\mathbf{y}} = \mathbf{F}\bar{\mathbf{C}}\tilde{\mathbf{H}}_{\text{lin}}\tilde{\mathbf{x}}_{\text{cp}} + \mathbf{F}\bar{\mathbf{C}}\tilde{\mathbf{z}}, \tag{3.3}$$

where $\bar{\mathbf{C}} = \begin{bmatrix}\mathbf{0}_{K\times N_{\text{cp}}} & \mathbf{I}_K\end{bmatrix}$ is the matrix that removes the CP with $\mathbf{0}_{K\times N_{\text{cp}}}$ representing the null matrix $(K \times N_{\text{cp}})$, $\tilde{\mathbf{H}}_{\text{lin}}$ is the lower triangular Toeplitz channel convolution matrix $(K + N_{\text{cp}} \times K + N_{\text{cp}})$. Since the CP insertion and perfect synchronisation guarantees ISI and ICI free conditions, $\mathbf{F}\bar{\mathbf{C}}\tilde{\mathbf{z}}$ represents the noise at the receiver.

Substituting Eq.(3.2) into Eq.(3.3)

$$\mathbf{r} = \mathbf{F}\tilde{\mathbf{H}}_{\text{cir}}\mathbf{F}^H\mathbf{x} + \mathbf{z}, \tag{3.4}$$

where $\tilde{\mathbf{H}}_{\text{cir}} = \bar{\mathbf{C}}\tilde{\mathbf{H}}_{\text{lin}}\mathbf{C}$ is the circulant matrix $K \times K$ and $\mathbf{z} = \mathbf{F}\bar{\mathbf{C}}\tilde{\mathbf{z}}$.

According to the DFT property, $\mathbf{F}\tilde{\mathbf{H}}_{\text{cir}}\mathbf{F}$ yields in a diagonal matrix $(K \times K)$ where each diagonal element corresponds to the channel frequency response at the corresponding subcarrier, hence $\mathbf{H} = \text{diag}(\mathbf{h})$. Therefore, Eq. (3.4) can be rewritten according to

$$\mathbf{r} = \mathbf{H}\mathbf{x} + \mathbf{z}. \tag{3.5}$$

where $\mathbf{x} = [x_0 \;\; x_1 \;\; \cdots \;\; x_{K-1}]^T$.

De-Framing block detaches the received signal into pilot and data subcarriers. Based on pilot subcarriers the Channel Estimator block provides the estimates that generate the CFR for

the OFDM frame. Also, the Channel Estimator block may perform an interpolation whether it is required. The CFR estimate feeds the Equaliser block that performs the equalisation of the signal.

In order to guarantee the conditions ISI and ICI free a long enough CP and perfect synchronisation are also common assumptions of pilot-assisted OFDM systems. Also, considering that the channel impulse response is sampled at instants $t = n\Delta t$ and is constant over the duration of one OFDM, an element of it is represented by $\tilde{h}_n$, according to

$$\tilde{h}_n = \tilde{h}(n\Delta t) = \sum_{l=0}^{L-1} \beta_l(t)\delta(t - \tau_l), \tag{3.6}$$

where $n = 0, 1, \cdots, N$. Hereinafter L is the number of resolvable paths, the delay τ_l are multiple of the OFDM system sampling interval.

The corresponding element of the channel frequency response is represented by h_k as

$$h_k = h(k\Delta f) = \sum_{l=0}^{L-1} \beta_l(t)e^{-\imath 2\pi k\tau_l/K}, \tag{3.7}$$

where $k = 0, 1, \cdots, K$.

3.3 Channel Estimation

The channel estimation processing can be classified according to the information that is used to perform channel estimation at the receiver. They are:

- Pilot-assisted estimators: These class of estimators use deterministic information that are known at the receiver side. These symbols are used for synchronisation and/or channel estimation purposes and they are allocated to pilot subcarriers, that do not carry data information [51]-[52].

- Blind estimators: Have no knowledge of the transmitted information and use statistical properties of the signal. It corresponds to a high latency class of estimators since a large number of statistics data should be collected and processed in order to provide accurate channel estimates [53].

- Pilot and data assisted: Make use of pilots symbols and the information provided by

the data as well [54].

The estimators aforementioned can be recursively or iteratively implemented. Such approaches refine an initial estimation that was obtained by using pilots, data or statistics measure.

In this work blind channel estimations are not considered and hereinafter it is assumed that the estimators are aided by pilot symbols.

3.3.1 Pilot Density and Pilot Patterns

In a system with K subcarriers the number of pilot subcarriers is given by $P = K - J$, where J is the number of subcarriers allocated to carry data. P is related to the spectral efficiency and to the pilot density in an OFDM frame thus, the design of a pilot pattern impacts the estimation performance. It has been shown that the pilot patterns that explore time and frequency diversity, i.e., 2-D pattern, outperform those that only allocate pilots in one dimension. 2-D patterns provides the estimator with enough information to track the channel variations in both domains.

A time-frequency OFDM frame is often illustrated as depicted in Figure 3.2 with white and gray representing the data and pilot symbols and with N_v and N_f being the pilot separation in time and frequency dimensions, respectively.

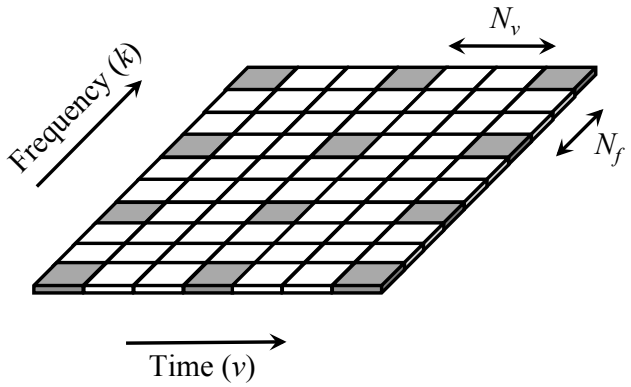

Figure 3.2: Time-Frequency OFDM frame with regular scattered pilot arrangement.

In such a frame columns represent the OFDM symbols and rows corresponds to the OFDM subcarriers. In order to provide the channel estimates for the entire frame, interpolations in

time and frequency are required. This pilot pattern, also referred as regular scattered pilot arrangement, reduce the pilot density and consequently improve the spectral efficiency. Others pilot patterns with adaptive, hexagonal and parallelogram-shaped arrangements can be found in the literature [26], [55].

A pilot pattern can be described by a sampling matrix $\mathbf{P}$ that is formed by two spanning vectors $\mathbf{p}_k$ and $\mathbf{p}_v$ [26]. Such vectors generate the doubly sub-structures of all pilots in the time-frequency grid. The pilot grid depicted in Figure 3.2 may be represented by a non-singular matrix $\mathbf{P}$ formed by 2 basis vector $\mathbf{p}_k = [N_f \quad 0]^T$ and $\mathbf{p}_v = [0 \quad N_v]^T$ so that $\mathbf{P} = [\mathbf{p}_k \quad \mathbf{p}_v]$ and therefore, D_p the pilot density of a pattern is given by

$$D_p = \mid \det(\mathbf{P}) \mid^{-1}. \tag{3.8}$$

The pilot density must satisfy the 2-D sampling theorem in order to properly estimate the channel [56], that is according to

$$f_{D\max} N_v T_S \leqslant 1 \tag{3.9}$$

$$\tau_{\max} N_f f_s \leqslant 1 \tag{3.10}$$

Equations (3.9) and (3.10) shows that the relative variation of the channel in time and frequency domain plays an important role regarding N_v and N_f. These measures are highly related to the channel characteristics specially to T_c the coherent time and to B_c the coherent frequency band that are related to $f_{D\max}$ the maximum Doppler frequency and $\tau_{\max}$ the maximum excess delay, respectively. Also, Eq. (3.9) and (3.10) show that the pilot symbols should have a sufficiently high density in both the time and frequency dimension in order to be able to provide estimates for the OFDM frame also in case of radio channels subject to high frequency and /or time selectivity [4]. A more conservative approach may consider an oversampling rate of two for the pilot symbols be used to suppress channel noise and improve the estimation performance [25], [57]. The distortion, due to an insufficiently high sampling, is irrevocable and is known as aliasing.

An OFDM symbol may transmit only pilots, according to Figure 3.3 a), also referred as block-type arrangement. In such a case, the estimator is able to provide the channel estimates for the entire symbol and in frequency dimension no interpolation is required. For this pilot

grid $N_v T_S$ must be significantly shorter than T_c therefore, this pilot grid is appropriate for slow fading channels, such as indoor environment.

Similar approach is also applicable in time dimension, i.e., a number of subcarriers are allocated to transmit pilots throughout the frame, as depicted in Figure 3.3 b), also referred as comb-type arrangement. In this case $N_f f_s$ must be less than B_c hence, this arrangement may be used for fast fading channels and requires interpolation in frequency domain. Such a pilot grid is advisable for fine-tuning of carrier frequency offset or to compensate error phase [55].

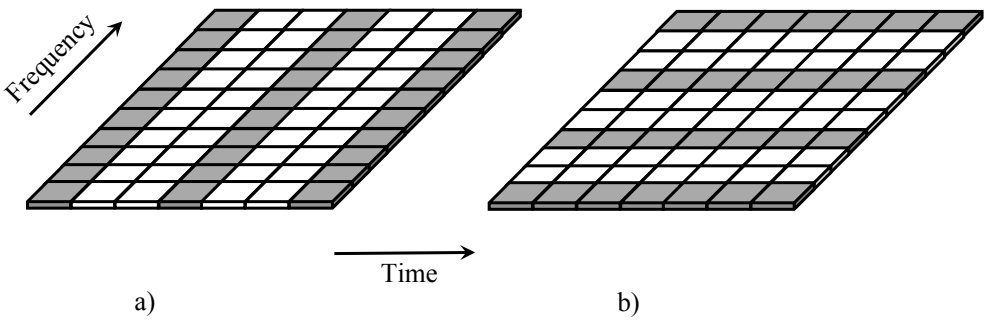

Figure 3.3: a) Block-type arrangement b) Comb-type arrangement.

Equispaced and equipowered pilot symbols have been shown superior channel estimation performances [58]-[59] and without loss of generality, pilots often assume an unitary and constant value during an OFDM symbol transmission. Therefore, at k subcarrier the element p_k of a vector $\mathbf{p}$ may be expressed by a pulse train equispaced by N_f with unitary amplitude. The corresponding expression in Time Domain (TD) is also given by a pulse train with elements at the instants $(n - mK/N_f)$ for $m \in [0; N_f - 1]$, according to the expression

$$p_n = \begin{cases} \dfrac{1}{N_f}, & \text{if } \; n = m\frac{K}{N_f}, \quad m = 0, 1, \cdots, N_f - 1 \\ 0, & \text{remaining.} \end{cases} . \tag{3.11}$$

Considering a pilot arrangement according to Figure 3.2, in frequency dimension it follows

that $\frac{K}{N_f} = N_t \in \mathbb{N}$. Correspondingly, Eq. (3.11) yields in

$$p_n = \frac{1}{N_f} \sum_{m=0}^{N_f-1} \delta_{n-N_t} \quad \overset{\mathfrak{F}^{-1}}{\underset{\mathfrak{F}}{\longleftrightarrow}} \quad p_k = \sum_{m=0}^{N_t} \delta_{k-mN_f}. \tag{3.12}$$

Combining Eq. (3.5), in time domain, and Eq. (3.12) the received signal presents three components, namely, data-symbol, pilot symbol and noise, as follows

$$\tilde{r}_n = \sum_{k=0}^{K-1} \tilde{h}_k \tilde{x}_{n-k} + \frac{1}{N_f} \sum_{m=0}^{N_f-1} \tilde{h}_{n-mK/N_f} + \tilde{z}_n. \tag{3.13}$$

3.4 Classical Channel Estimators

3.4.1 Least Squares Estimator

The Least Square (LS) estimation corresponds to an optimisation problem with no constrains [60]. For a given subset p, the solution corresponds to minimise the error square norm $\mathbf{e}$ [61].

$$\underset{h}{\text{Minimize}} \quad \|\mathbf{y} - \mathbf{ph}\|^2, \tag{3.14}$$

where $\|\cdot\|$ is the norm operator, the vectors $\mathbf{y}$, $\mathbf{p}$ and $\mathbf{h}$ are the observed signal, the pilot symbol and the channel, respectively.

Regarding the pilot grid in Figure 3.2, where the set of pilot subcarriers is $\mathfrak{P}$ and according to the system described in Section 3.2, the LS channel estimation, corresponds to [26]

$$\hat{h}_{\text{ls},k} = \frac{y_k}{p_k}, \quad \forall\ k \in \mathfrak{P}, \tag{3.15}$$

where y_k is the received signal in frequency domain and p_k is the corresponding pilot symbol at k subcarrier.

The LS channel estimates for the remain subcarriers are obtained via an interpolation with factor N_f.

For one OFDM symbol, two consecutive pilot subcarriers are spaced by N_f. According to the Nyquist theorem, i.e., the time domain sampling effect [26], summing N_f delayed (by N_t) replicas of the input signal is equivalent to filter the pilot positions in frequency domain, and

therefore the LS estimate in time domain is made up of N_f replicas of the CIR separated by N_t, according to the expression

$$\hat{\tilde{h}}_{\mathrm{ls},n} = \frac{1}{N_f} \sum_{m=0}^{N_f-1} \tilde{h}_{n-mN_t} + \sum_{m=0}^{N_f-1} \tilde{z}_{n-mN_t}, \tag{3.16}$$

where $n = mN_t,\ m = 0,\ 1, \cdots, N_t - 1$ and $\tilde{z}$ is the Additive White Gaussian Noise (AWGN) noise.

According to [62] similar and quite less complex estimation is achieved by averaging the received signal in Eq. (3.13). Such average operation performed directly in time domain yields in Eq. (3.17) that is referred as TD-LS or the LS implementation in time domain.

$$\hat{\tilde{h}}_{\mathrm{ls},n} = \begin{cases} \sum_{m=0}^{N_f-1} \tilde{r}_{n+mN_t}, & n = 0, 1, \cdots, N_t - 1 \\ 0, & \text{remaining.} \end{cases} . \tag{3.17}$$

For one OFDM symbol the channel estimation vector $K \times 1$ related to Eq. (3.17) can be express by Eq. (3.18) and the CFR is obtained via an IFFT.

$$\hat{\tilde{\mathbf{h}}}_{\mathrm{ls},K} = \begin{bmatrix} \hat{\tilde{\mathbf{h}}}_{\mathrm{ls},N_t} & \mathbf{0}_{K-N_t} \end{bmatrix}^T . \tag{3.18}$$

The LS estimate takes place for all OFDM symbols that carry pilots and in order to obtain the channel estimates for the remaining symbols, an interpolation with factor N_v should be performed in time dimension.

3.4.2 Minimum Mean Square Error

The Minimum Mean Square Error (MMSE) filtering corresponds to a minimisation problem regarding the expected error norm $\mathbf{e}$, according to

$$\underset{h}{\text{Minimise}} \quad \mathbb{E}\Big\{ \|\hat{\mathbf{h}} - \mathbf{h}\|^2 \Big\}, \tag{3.19}$$

where the vectors $\mathbf{h}$ and $\hat{\mathbf{h}}$ are the channel and its corresponding estimate.

The MMSE channel estimation, according to the system described in Section 3.2 is given

by [63]

$$\hat{\mathbf{h}}_{\text{mmse}} = \mathbf{R}_{h\hat{h}_{\text{ls}}} \mathbf{R}^{-1}_{\hat{h}_{\text{ls}}\hat{h}_{\text{ls}}} \hat{\mathbf{h}}_{\text{ls}}, \tag{3.20}$$

where the correlation matrices $K \times K$ are

$$\mathbf{R}_{h\hat{h}_{\text{ls}}} = \mathbb{E}\left\{ \mathbf{h}\hat{\mathbf{h}}^{H}_{\text{ls}} \right\} \tag{3.21}$$

$$\mathbf{R}_{\hat{h}_{\text{ls}}\hat{h}_{\text{ls}}} = \mathbb{E}\left\{ \hat{\mathbf{h}}_{\text{ls}}\hat{\mathbf{h}}^{H}_{\text{ls}} \right\} \tag{3.22}$$

The estimator in Eq. (3.20) improves the LS estimation by making use of the correlation properties of the channel and also provides the channel estimates for the remaining subcarriers. Regarding the minimisation problem in Eq. (3.19) the MMSE estimator corresponds to the optimal solution. However, such an estimation requires an full matrix inversion that can large depending on the number of subcarriers in the system, followed by an interpolation in time dimension. Several versions of the MMSE estimator has been proposed in order to reduce the computational load [64]-[68]. Basically, the number of multiplications can be reduced by reducing the number of coefficients in the LS estimates. Such approaches, referred as DFT-based estimations, are performed via linear operations or other techniques in time domain and then the result is transformed back into the frequency domain.

For an arbitrary pilot grid a MMSE implementation can be performed considering a 2-D MMSE estimator that is able to provide the channel estimates for the pilot subcarriers, interpolate the channel estimates for the remain subcarriers and OFDM symbols [69]. The 2-D MMSE estimator also has high complexity load and, since the correlation functions of the channel frequency responses along the time and frequency axis are independent, its performance is quite similar to the performance of two one-dimensional MMSE estimators [26]. Therefore, channel estimation based on pilot grid are often treated as two one-dimension estimations.

For one OFDM symbol and considering the system described in Section 3.2, the MMSE filter also can follow the implementation in time domain according to

$$\widetilde{\mathbf{W}}_{\text{mmse}} = \mathbf{R}_{\tilde{h}\hat{h}} \mathbf{R}^{-1}_{\hat{h}\hat{h}}, \tag{3.23}$$

where the correlation matrices $N_t \times N_t$ are given by [62]

$$\mathbf{R}_{\tilde{h}\hat{\tilde{h}}} = \mathbb{E}\left\{\tilde{\mathbf{h}}\hat{\tilde{\mathbf{h}}}^H\right\} = \mathbf{R}_{\tilde{h}\tilde{h}} + \frac{\sigma_n^2}{N_t}\mathbf{I}_{N_t} \tag{3.24}$$

$$\mathbf{R}_{\hat{\tilde{h}}\hat{\tilde{h}}} = \mathbb{E}\left\{\hat{\tilde{\mathbf{h}}}\hat{\tilde{\mathbf{h}}}^H\right\} = \mathbf{R}_{\tilde{h}\tilde{h}} = \text{diag}\left(\sigma_{h,0}^2 \;\; \sigma_{h,1}^2 \;\; \cdots \;\; \sigma_{h,L-1}^2 \;\; \cdots \;\; 0\right). \tag{3.25}$$

Assuming that the channel taps are separated by the sampling interval, the MMSE filter corresponds to a sparse diagonal matrix with non-null elements whose number is equal to the number of taps L occurring only in the diagonal.

If Eq. (3.18) and Eq. (3.23) are simultaneously implemented the CIR estimate presents L non-null elements and zeros in the remaining, hence significant complexity is reduced with the same performance of the frequency domain implementation [70]. Such an estimation is referred as TD-MMSE or MMSE implementation in time domain. The final CFR is obtained by performing a FFT.

Similarly to the LS case, such an estimation is performed for all OFDM symbols that carry pilots hence, in order to obtain the channel estimates for the remaining symbols an interpolation with factor N_v should be performed in time dimension.

3.4.3 Complexity Analysis

The complexity and computational load of implementing pilot-assisted channel estimation algorithms with regularly scattered pilots is presented using as metrics the number of required operations (multiplications and sums) and the memory usage. Such analysis focus on LS and MMSE, either implemented in frequency or time domain.

The operation of the analysed channel estimation algorithms can be divided into two main tasks: estimation of the channel in the pilot positions and interpolation in-between pilots for remaining subcarriers.

3.4.3.1 LS Channel Estimation with FIR Interpolation Filter

The complexity and computational load of implementing the LS estimation on the pilot density and the size of the OFDM frame.

The design of the FIR interpolation filter is only performed in the initial phase as it depends only on N_f. Therefore, the computational load associated with this operation can

be neglected. Table 3.1 summarises the complexity of performing the LS channel estimation algorithm.

Table 3.1: Summary of LS implementation complexity (per symbol estimation)

Estimator	**Multiplications**	**Sums**	**Memory Elements**
LS	$N_t + lK$	lK	$N_t + K$

For each received OFDM symbol that carries pilots, i.e., pilot-carrying symbol, the implementation of the LS estimation requires N_t multiplications. In order to hold the initial estimates N_t memory elements are needed. In addition, in order to perform the interpolation using an l-th order FIR interpolation filter, lK multiplications and sums are performed. K memory elements hold the channel estimate that are used throughout the frame.

3.4.3.2 MMSE Channel Estimation

The MMSE interpolation filter performs the two tasks of estimating the channel in the pilot positions and interpolating in-between them with a single operation. The complexity and computational load of implementing also depends the pilot density, the size of the OFDM frame and if the filter in applied in frequency or time domain. The implementation of the MMSE estimation scheme in time domain achieves a significant reduction of complexity when compared to the frequency domain counterpart, as detailed in Table 3.2 that summarises the complexity of performing the MMSE channel estimation algorithm.

Table 3.2: Summary of MMSE implementation complexity (per symbol estimation)

Estimator	**Multiplications**	**Sums**	**Memory Elements**
FD MMSE	K^2/N_f	K^2/N_f	$N_t + K$
TD MMSE	$L + K\log_2(K)/2$	$LN_f + K\log_2(K)$	K

The design of MMSE filter includes a $(N_t \times N_t)$ matrix inversion that requires $O(N_t)^3$

operations. For each received pilot-carrying symbol, the N_t values received in the pilot subcarriers are stored in memory elements and feed to the input of the filter that outputs the channel estimate for the symbol. To perform this operation K^2/N_f multiplications and sums are required. The final estimate is stored in K memory elements.

Due to the independence of the channel taps, the complexity associated with the filter design, i.e, the diagonal matrix with L non-zero elements, is negligible in comparison with the implementation cost. Considering that the time MMSE filter is used in conjunction with the LS estimator, also implemented in time domain, this estimation yields in an overall operation that requires L multiplications and LN_f sums for each received pilot-carrying symbol. The outputted CIR estimate must be transformed to the frequency domain with an FFT that requires $K\log_2(K)/2$ multiplications and $K\log_2(K)$ sums. The final estimate in stored in K memory elements.

3.4.4 Metrics of Assessment

In order to assess a system performance appropriate figures should be adopted. This section presents the figures used to assess a system performance throughout this thesis.

3.4.4.1 Bit Error Rate

In information theory, one of the main measures of performance is system capacity. However, in real systems it is more appropriate the use of other figures such as Bit Error Ratio (BER). The BER for a variate of modulation schemes can be calculated as

$$P_b \approx \mathbb{E}\left\{ a\mathcal{Q}\left(\sqrt{2b\frac{P_s}{N_r}}\right)\right\}, \tag{3.26}$$

where $\mathcal{Q}(\cdot)$ represents the $\mathcal{Q}$-function

$$\mathcal{Q}(x) = \frac{1}{2\pi}\int_x^\infty e^{-\frac{y^2}{2}}\,dy, \tag{3.27}$$

and the ratio P_s/N_r corresponds to the instantaneously received SNR, a and b are parameters that depend on a modulation scheme, according to Table 3.3.

Table 3.3: a and b vary according to a modulation scheme

Modulation scheme	a	b
BPSK	1	1
QPSK	1	0.5
$\mathcal{M}$-ary PAM	$2(\mathcal{M}-1)/\mathcal{M}$	$3/(\mathcal{M}^2-1)$
Minimum $\mathcal{M}$-ary PSK	2	$\sin^2(\pi/\mathcal{M})$

By replacing Eq.(3.27) into Eq.(3.26) one may obtain

$$P_b \approx \frac{a\sqrt{b}}{2\sqrt{\pi}} \int_0^{\infty} \frac{e^{-b\gamma} F_\gamma(\gamma)}{\sqrt{\gamma}}\, dy, \tag{3.28}$$

where $\gamma = P_s/N_r$ and $F_\gamma(\gamma)$ is the Cumulative Distribution Function (CDF) of γ.

Equation (3.28) shows that the BER can be obtained by using the CDF. In addition, the asymptotic BER in the high SNR regime can be obtained directly by using the CDF or the Probability Density Function (PDF) of γ [23].

The BER can be calculated by comparing the transmitted and the received bit stream as well. Such a comparison can be performed via simulations, also referred as Monte-Carlo simulations [71]. Furthermore, BER expressions also can be derived as a function of ρ, the correlation between the channel and its estimate. Considering that the communication link is established and the use of Quadrature Phase-Shift Keying (QPSK) modulation with coherent MRC detection, such an expression is expressed by [27]

$$P_b \approx \frac{1}{2}\left[1 - \frac{\rho}{\sqrt{2-\rho^2}} \sum_{l=0}^{L-1} \binom{2l}{l} \left(\frac{1+\rho^2}{4-2\rho^2}\right)^l\right], \tag{3.29}$$

where l corresponds to a multipath component.

Equation (3.29) shows that with the amount of paths increasing the P_b increases as well and as the channel differs from its estimate, i.e., ρ tends towards zero, the BER decreases. In addition, the above expression shows that the channel estimate may degrade a system

performance.

The BER as a function of the SNR should be measure on the basis of a fixed symbol rate R_s, i.e., the inverse of the symbol duration (baud), or equivalently a fixed bit rate R_b (bits/s) as the constellation order increases the SNR requirement also increases for the same BER performance. The relationship between R_b and R_s is given by $R_b = R_s \log_2(\mathcal{M})$, where $\mathcal{M}$ is the constellation order such that $\mathcal{M} = 2^m$, being m the number of encoded bits per symbol.

Therefore, it is appropriate the use of the BER as a function of the power efficiency, E_b/N_0, where E_b the energy per bit and $\frac{1}{2}N_0$ is the PSD of the AWGN noise at the receiver.

Considering the OFDM system described in Sections 2.2 and 3.2, E_b is given by

$$E_b = \frac{\bar{S}_S T_S}{m}, \tag{3.30}$$

where $\bar{S}_S$ is the average OFDM symbol power.

Since in this work it is considered an pilot-assisted OFDM system, in an OFDM frame there are also pilot subcarriers that do not carry data symbol. Consequently, the average number of bits per OFDM symbol depends on the pilot density, D_p, according to

$$m = K \log_2(\mathcal{M})(1 - D_p). \tag{3.31}$$

Replacing Eq.(3.31) into Eq.(3.30), E_b can be rewritten as

$$E_b = \frac{\bar{S}_S T_S}{K \log_2(\mathcal{M})(1 - D_p)}. \tag{3.32}$$

Accordingly, the one sided PSD N_0 is expressed by

$$N_0 = \frac{\sigma_n^2}{K\Delta f} = \frac{\sigma_n^2 t_s}{K}. \tag{3.33}$$

Consequently, the system's power efficiency follows

$$E_b/N_0 = \frac{\bar{S}_S T_S}{\sigma_n^2 \log_2(\mathcal{M})(1 - D_p)}. \tag{3.34}$$

3.4.5 Mean Square Error - MSE

The channel estimation performance is assessed in terms of Mean Square Error (MSE). For an arbitrary parameter θ and its corresponding estimate $\hat{\theta}$ the MSE expression is given according to the following

$$\text{MSE} = \frac{\mathbb{E}\left\{ \mid \theta - \hat{\theta} \mid^2 \right\}}{\mathbb{E}\left\{ \mid \theta \mid^2 \right\}}. \tag{3.35}$$

Considering the OFDM system with K subcarriers described in Sections 2.2 and 3.2, the corresponding channel estimate MSE is

$$\text{MSE} = \frac{1}{K} \sum_{k=0}^{K-1} \frac{\mid h_k - \hat{h}_k \mid^2}{\mid h_k \mid^2}. \tag{3.36}$$

Without loss of generality it is assumed $\mathbb{E}\left\{|h_k|^2\right\} = 1$. In addition, it is assumed that $P_s = 1$ and therefore, the SNR $= 1/\sigma_n^2$. If the channel estimate is corrupted by AWGN noise and if the interpolation errors are negligible, the numerator of the expression above yields in the noise variance and then the channel estimate MSE is expected to follows the inverse of the SNR. Consequently, Eq. (3.36) in dB can be written as

$$\text{MSE}_{\text{dB}} = -\text{SNR}_{\text{dB}}. \tag{3.37}$$

Chapter 4

Channel Estimation for AF Relay-Assisted OFDM-Based Systems

4.1 Introduction

The concept of cooperative communication was rediscovered recently in relation to great potential applications in cellular and wireless sensor networks [72]. In cooperative systems, independent paths are generated between the source and the destination via the introduction of RNs. Therefore, the relaying channel corresponds to an auxiliary channel to the direct one.

Channel estimation is one of the key challenges in cooperation since the relaying channel is made up of multi-hop links the channel estimator is expected to cope with the noise component related to each link. In order to skip such a challenge some cooperative schemes consider differential modulation-based approaches [73]-[75] as the Channel State Information (CSI) is not needed at either relays or destination and non-coherent detection does not require the channel estimation as well. Nevertheless, it has been reported that the performance of non-coherent cooperative systems present losses when comparing with systems employing coherent cooperative modulation techniques [75]-[76]. Early researchs on cooperative communications worked on regenerative and non-regenerative relay-assisted schemes that assumed perfect CSI at some or all the involved nodes [77]-[79]. However, such a assumption is not realistic since some of the network elements may require accurate CSI in order to perform coherent detection and demodulation at the destination or at both relay and destination. Since then, several work have addressed channel estimation in the cooperative context [80]-[93].

Like point-to-point systems, pilot-aided channel estimation in relay-assisted systems, also depends on channel statistics and the pilot density. In addition, it also depends on the em-

ployed relaying protocol and the scenario. Channel estimation in the context of regenerative relaying consists of individual estimation of source-to-relay and relay-to-destination links. Therefore, the traditional pilot patterns and estimation algorithms designed for point-to-point links can be applied. Hence, besides improving the system performance by employing cooperation, others problems related to performance degradation can be addressed in conjunction, such as synchronisation and Channel Frequency Offset (CFO).

The main advantage of the AF, in comparison with regenerative protocols, is its low complexity. In order to keep the relay as simple as possible, it is advantageous to estimate all channel parameters at the destination. Specially in the context of such relaying where a cascaded channel consisting of source-to-relay and relay-to-destination links needs to be estimated.

This chapter provides analytical studies on the relaying channels statistics in RA OFDM-based cooperative scenario employing the half-duplex AF protocol. It is shown that compound channel entail statistics that comply to a proper equalisation and filter designs. Since the relay channel is not a single-hop link, the estimation algorithms LS and MMSE, designed for such channels, may require changes. Throughout this chapter it is proposed some adjustments that should be done in the estimators in order to provide accurate channel estimates.

4.2 System Model

We consider an OFDM transmission, described according to Section 2.2. The OFDM symbol transmitted by each antenna element corresponds to $\mathbf{x} = \mathbf{s} + \mathbf{p}$, where $\mathbf{x}$, $\mathbf{p}$ and $\mathbf{s}$ are vectors $K \times 1$, being $\mathbf{p}$ the pilots that are multiplexed within the data $\mathbf{s}$ symbols according to a regular scattered pilot arrangement, as depicted in Figure 3.2. The OFDM symbol vector is transmitted over a flat fading channel which the discrete CIR and the corresponding CFR expressions are restated below.

$$\tilde{h}_n = \sum_{l=0}^{L-1} \beta_l(t)\delta(t - \tau_l), \tag{4.1}$$

$$h_k = \sum_{l=0}^{L-1} \beta_l(t)e^{-\imath 2\pi k\tau_l/K}, \tag{4.2}$$

where L is the number of resolvable paths, τ_l are multiple of the OFDM system sampling interval. $\beta_l(t)$ is modelled as a zero mean complex Gaussian variable with variance σ_h^2 determined by the power delay profile such that $\sigma_{\text{ch}}^2 = 1$. Although the channel is time-variant we assume it quasi-static, i.e. constant during one OFDM symbol interval. The channel gains, h_k for $k = 0, \cdots, K-1$, are therefore also zero mean complex Gaussian variables with unit variance. It is assumed that $\mathbb{E}\left\{|x_k|^2\right\} = 1$, $\mathbb{E}\left\{|h_k|^2\right\} = 1$ and the average transmitted power is unitary. It is widely known that in typical OFDM systems the subcarrier separation is significantly lower than the frequency coherence band of the channel. Accordingly, the fading in two adjacent subcarriers can be considered flat and without loss of generality it can be assumed for generic channel $h_k \approx h_{k+1}$.

The Doppler's effect is considered in all channels as the RN and UT are mobile terminals. Throughout this analysis the subscripts *br*, *bu* and *ru* are related to the links BS-RN, BS-UT and RN-UT, respectively.

4.2.1 Relay-Assisted Scenario

In this chapter considers a downlink AF relaying scheme where the cooperation is assisted by one RN and the involved entities namely the BS, RN and UT are single antenna devices, according to Figure 4.1.

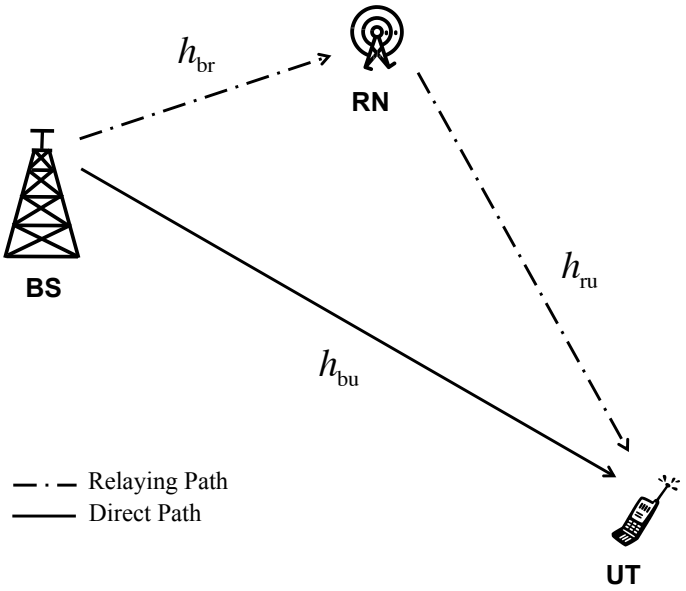

Figure 4.1: AF relay-assisted scenario.

According to the scenario, there are three channels involved h_{bu}, h_{br} and h_{ru} that represent the links BS-UT, BS–RN and RN–UT, respectively. The corresponding block diagram is depicted in Figure 4.2. The block Joint Processing combines the signals received in both phases of the protocol.

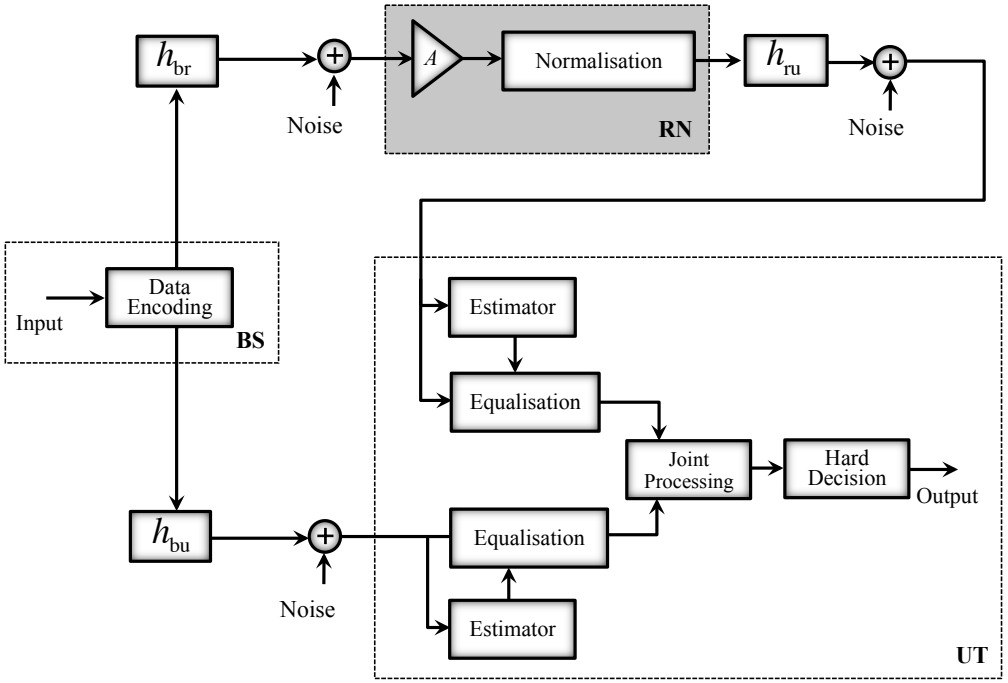

Figure 4.2: AF relay-assisted scenario: Block diagram.

In the first phase of the protocol, the signal received at the UT is given by

$$y_{k,\mathrm{bu}} = x_k h_{k,\mathrm{bu}} + z_{k,\mathrm{bu}}, \tag{4.3}$$

where $h_{k,\mathrm{bu}}$ is the channel between the BS and the UT, z_k corresponds to the independent and identically distributed (i.i.d) complex zero-mean Gaussian noise with a variance σ_n^2, that is assumed to be uncorrelated with h_k. Since BS-UT corresponds to a single hop link the corresponding channel estimation is performed by point-to-point estimators at the destination.

At the RN, the transmitted signal is obtained by amplifying the received signal $y_{k,\mathrm{br}}$. In the second phase, the UT receives the signal $y_{k,\mathrm{ru}}$ from the RN as follows

$$y_{k,\mathrm{ru}} = r_{k,\mathrm{ru}} h_{k,\mathrm{ru}} + z_{k,\mathrm{ru}}, \tag{4.4}$$

being $r_{k,\mathrm{ru}}$ the signal transmitted by the RN and $h_{k,\mathrm{ru}}$ the channel between the RN and the UT. Therefore, Eq. (4.4) can be rewritten as

$$y_{k,\mathrm{ru}} = h_{k,\mathrm{c}} x_k + A h_{k,\mathrm{br}} z_{k,\mathrm{br}} + z_{k,\mathrm{ru}}, \tag{4.5}$$

being $h_{k,\mathrm{c}}$ the compound channel given by $h_{k,\mathrm{c}} = A h_{k,\mathrm{ru}} h_{k,\mathrm{br}}$, where $h_{k,\mathrm{br}}$ is the channel between the BS and the RN. A corresponds to the amplifying factor that is selected such that the destination is able to perform the equalisation. The amplifying factor is inversely proportional to the received power thus, for a variable gain A is expressed by

$$A = \sqrt{\frac{1}{\frac{1}{K}|\sum_k \sigma_k^2|^2 + \sigma_n^2}}, \tag{4.6}$$

where $\sigma_k^2 = |h_{k,\mathrm{br}} h_{k,\mathrm{ru}}|^2$ is the instantaneous power at k subcarrier.

For variable amplifying gain the complexity at the RN is increased as it is necessary to compute the instantaneous channel power. The average amplifying factors refer to the case where amplification is a function of the average channel conditions, which change very slowly and can generally be considered constant over typical communication durations [28]. Considering that the average transmitted power is unitary, A is expressed by

$$A = \sqrt{\frac{1}{\frac{1}{K}\mathbb{E}\{|\sum_k \sigma_k^2|^2\} + \sigma_n^2}}. \tag{4.7}$$

4.2.2 Relay Channel Statistics

The AF relay channel can be modelled by cascading the fading of individual channels of each hop. According Eq. (4.5) the signal arriving at the UT, via the RN, is in fact the output of the cascaded links BS–RN and RN–UT which the corresponding channel is referred as compound channel, i.e. $A h_{k,\mathrm{ru}} h_{k,\mathrm{br}}$. The involved channels $h_{k,\mathrm{br}}$ and $h_{k,\mathrm{ru}}$ are independent flat Rayleigh fading channels and the product of them, the product of two complex Gaussian processes that is not Gaussian, corresponds to a double Rayleigh distribution as depicted in Figure 4.3.

Such channel presents a short coherent frequency band and hence limits the pilot separation in the frequency dimension. According to Section 3.3.1 the pilot symbols should have a sufficiently high density such that the pilot separation must satisfy the sampling theorem

in order to properly estimate the channel. Otherwise, the channel estimates present an irrevocable distortion. The double-cascaded Rayleigh channels yield even more severe system performance degradations than simple Rayleigh fading channels [23].

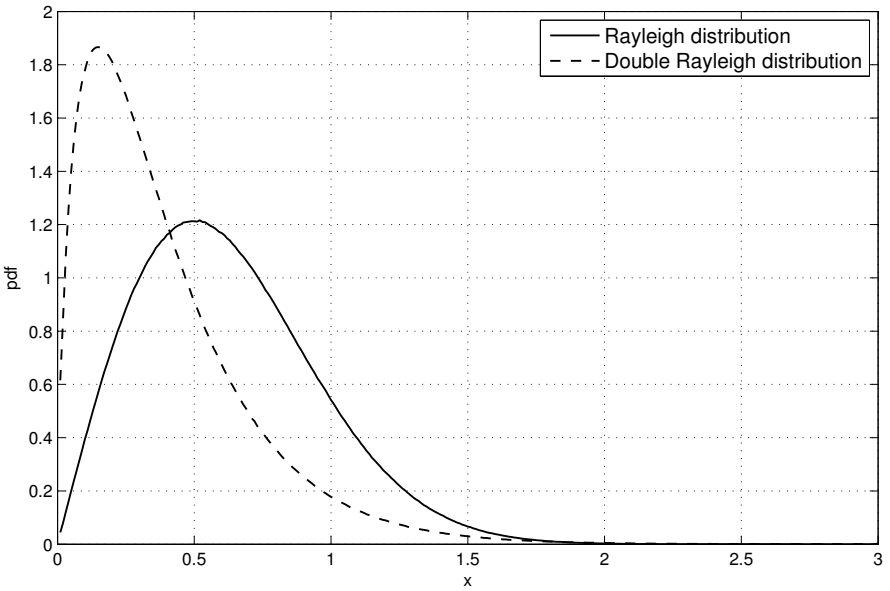

Figure 4.3: PDF: Rayleigh and double Rayleigh distributions.

Assuming that the amplifying gain is absorbed in the product $h_{k,\mathrm{ru}}h_{k,\mathrm{br}}$, in the time domain the compound channel channel corresponds to $\tilde{h}_{\mathrm{br}} \circledast \tilde{h}_{\mathrm{ru}}$. Such a channel is given by two independents paths therefore, the autocorrelation matrices (in time or frequency) depend on the individual channel autocorrelation matrices [94]. As mentioned in Section 2.1.3.1 the temporal autocorrelation of a generic channel h is given by

$$R(\Delta t) = \mathbb{E}\{h(t)h^*(t+\Delta t)\}. \tag{4.8}$$

Correspondingly, the temporal autocorrelation function of the compound channel corresponds to

$$R_{h_c}(\Delta t) = \mathbb{E}\Big\{h_{\mathrm{br}}(t)h^*_{\mathrm{br}}(t+\Delta t)h_{\mathrm{ru}}(t)h^*_{\mathrm{ru}}(t+\Delta t)\Big\}. \tag{4.9}$$

Considering that $h_{k,\mathrm{br}}$ and $h_{k,\mathrm{ru}}$ are statistically independent Eq. (4.9) can be rewritten as

$$R_{h_c}(\Delta t) = \mathbb{E}\Big\{h_{\mathrm{br}}(t)h^*_{\mathrm{br}}(t+\Delta t)\Big\}\mathbb{E}\Big\{h_{\mathrm{ru}}(t)h^*_{\mathrm{ru}}(t+\Delta t)\Big\} \tag{4.10}$$

$$R_{h_c}(\Delta t) = R_{\mathrm{br}}(\Delta t) R_{\mathrm{ru}}(\Delta t). \tag{4.11}$$

$$R_{h_c}(\Delta t) = \jmath_0(2\pi f_{D\mathrm{max,br}} \Delta t) \jmath_0(2\pi f_{D\mathrm{max,ru}} \Delta t), \tag{4.12}$$

where $f_{D\mathrm{max,br}}$ and $f_{D\mathrm{max,ru}}$ correspond to the maximum Doppler frequency related to the paths BS-RN and RN-UT, respectively.

For a generic channel h the spectral autocorrelation is given by

$$R(\Delta f) = \mathbb{E}\{h(f) h^*(f + \Delta f)\}. \tag{4.13}$$

Similarly, the spectral autocorrelation function of the compound channel corresponds to

$$R_{h_c}(\Delta f) = \mathbb{E}\Big\{ h_{\mathrm{br}}(f) h^*_{\mathrm{br}}(f + \Delta f) h_{\mathrm{ru}}(f) h^*_{\mathrm{ru}}(f + \Delta f) \Big\}. \tag{4.14}$$

Considering that $h_{k,\mathrm{br}}$ and $h_{k,\mathrm{ru}}$ are statistically independent Eq. (4.14) can be rewritten as

$$R_{h_c}(\Delta f) = \mathbb{E}\Big\{ h_{\mathrm{br}}(f) h^*_{\mathrm{br}}(f + \Delta f) \Big\} \mathbb{E}\Big\{ h_{\mathrm{ru}}(f) h^*_{\mathrm{ru}}(f + \Delta f) \Big\} \tag{4.15}$$

$$R_{h_c}(\Delta f) = R_{\mathrm{br}}(\Delta f) R_{\mathrm{ru}}(\Delta f). \tag{4.16}$$

For a generic channel, the IFFT of the spectral correlation function corresponds to its PDP. Therefore, the PDP of the compound channel corresponds to [94]

$$\mathrm{PDP}_c = \mathrm{PDP}_{\mathrm{br}} \circledast \mathrm{PDP}_{\mathrm{ru}}. \tag{4.17}$$

Equation (4.17) shows that the number of the taps of the compound channel, i.e., L_{c} depends on the individual channels taps L_1 and L_2 which typically leads to a channel with a delay spread being approximately the sum of the delay spreads in each segment BS-RN and RN-UT, i.e, $L_c \approx L_1 + L_2$. Therefore, the compound channel taps should be taken into account when designing the CP in an OFDM system. Figure 4.4 - Figure 4.7 show the PDP of the point-to-point and the compound channels considering the ITU Pedestrian Model A

and B, respectively [35].

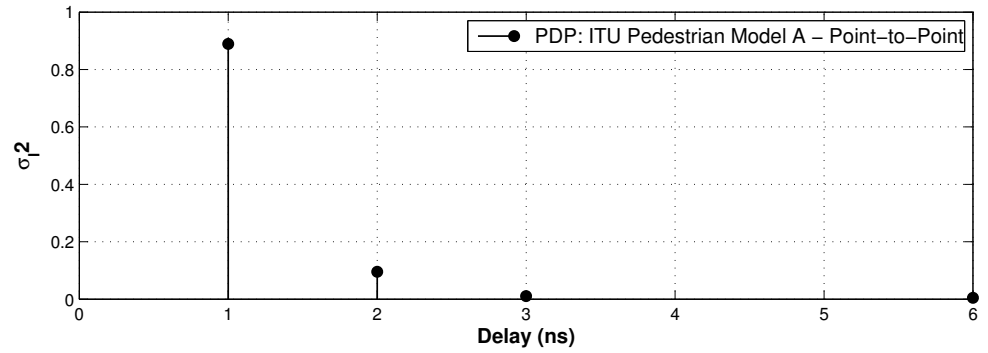

Figure 4.4: PDP: ITU Pedestrian Model A - point-to-point link.

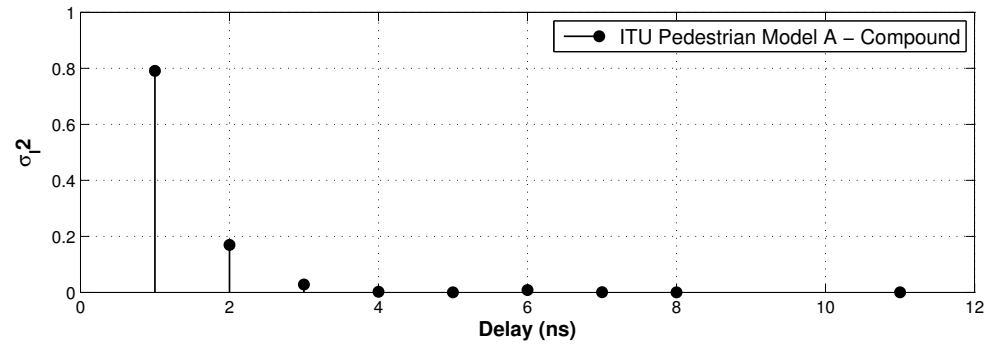

Figure 4.5: PDP: ITU Pedestrian Model A - compound link.

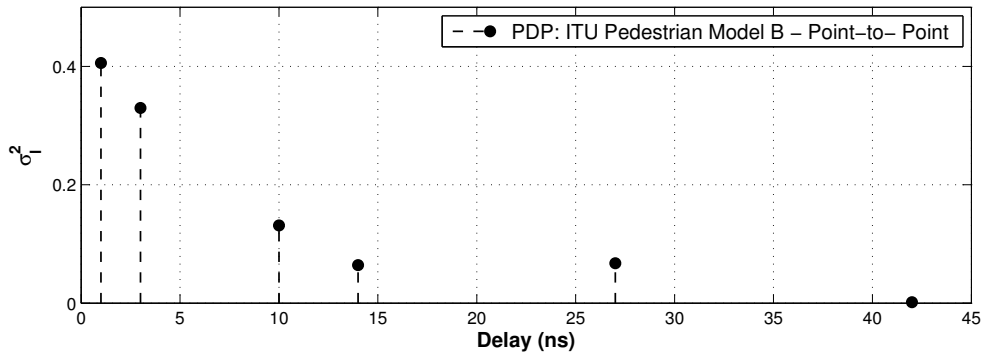

Figure 4.6: PDP: ITU Pedestrian Model B - point-to-point link.

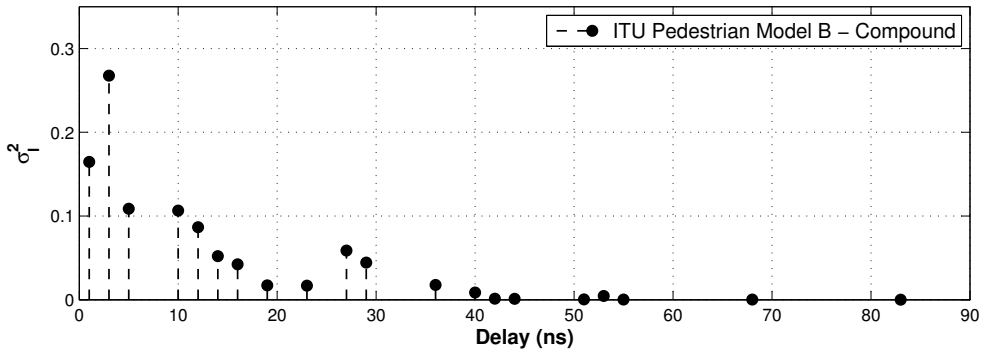

Figure 4.7: PDP: ITU Pedestrian Model B - compound link.

Regarding the noise, as aforementioned, the AF protocol exhibits noise amplification and propagation. According to Eq. (4.5), the overall received noise corresponds to

$$z_{\mathrm{t}} = A h_{k,\mathrm{br}} z_{k,\mathrm{br}} + z_{k,\mathrm{ru}}. \tag{4.18}$$

According to Eq. (4.18), the overall noise is made up by the product of two complex Gaussian random variables, $h_{k,\mathrm{br}}$ and $z_{k,\mathrm{br}}$. Consequently, z_{t} the does not present a Gaussian distribution and the noise variance has components that depend on $h_{k,\mathrm{br}}$, i.e., it cannot be considered power flat over the bandwidth.

Conditioned to the instantaneous channel realisation, and assuming that both noise components have the same variance σ_n^2, the noise variance of the overall noise $\sigma_{k,\mathrm{t}}^2$ follows Eq. (4.19) which shows that the noise affecting each subcarrier is also no longer white as well.

$$\sigma_{k,\mathrm{t}}^2 = A^2 |h_{k,\mathrm{ru}}^2| \sigma_n^2 + \sigma_n^2. \tag{4.19}$$

Assuming that $\mathbb{E}\left\{|h_k|^2\right\} = 1$, the average value of σ_{t}^2 corresponds to

$$\sigma_{\mathrm{t}}^2 = \mathbb{E}\left\{|z_{\mathrm{t}}|^2\right\} = A^2 \sigma_n^2 + \sigma_n^2. \tag{4.20}$$

In order to perform optimal equalisation the variance of the overall noise is assumed to be known at the UT which follows Eq. (4.20). Moreover, according to Eq. (4.5) the received SNR is a function of channel realisations, amplifying factor and noise. However, for an average amplifying factor, considering that $\mathbb{E}\left\{|x_k|^2\right\} = 1$, $\mathbb{E}\left\{|h_k|^2\right\} = 1$ and one RN, the average

received SNR at the UT is given by

$$\mathrm{SNR_r} \approx \frac{\mathbb{E}\Big\{|h_c x|^2\Big\}}{\mathbb{E}\Big\{|z_t|^2\Big\}} \approx \frac{\mathbb{E}\Big\{|A|^2|h_{br}|^2|h_{br}|^2|x|^2\Big\}}{\mathbb{E}\Big\{|A|^2|h_{br}|^2|z|^2+|z|^2\Big\}} \tag{4.21}$$

For an average amplifying gain, assuming that the channels have identical statistics and $\mathbb{E}\Big\{|h_k|^2\Big\} = 1$, the following relation can be found

$$A^2 = \frac{1}{1+\sigma_n^2}. \tag{4.22}$$

Therefore, Eq. (4.21) can be rewritten as

$$\mathrm{SNR_r} \approx \frac{1}{2\sigma_n^2 + (\sigma_n^2)^2}. \tag{4.23}$$

According to Eq. (4.21) for the AF relay assisted scheme it is expected that the average received SNR is reduced asymptotically by 3 dB. Therefore, if the system performance is assessed considering only the noise added at the destination, the performance curves must be shifted by 3 dB.

4.3 Relay Channel Estimation

The LS and the MMSE are two classical estimator that were designed to estimate point-to-point links. Here, they are considered to provide the channel estimates in a two-hop AF relay-assisted scenario.

The LS channel estimation does not take into the channel statistics. Therefore, the statistics presented in the previous section for a relay channel cannot be used in the LS estimation. Hence, at destination the LS estimates are obtained according to

$$\hat{h}_{ls} = \frac{y_{p,ru}}{p} = \frac{r_{p,ru}h_{p,ru}}{p} + \frac{z_{p,ru}}{p}. \tag{4.24}$$

$$\hat{h}_{ls} = \frac{Ah_{p,ru}h_{p,br} + Ah_{p,br}z_{p,br}}{p} + \frac{z_{p,ru}}{p}. \tag{4.25}$$

Equation (4.25) shows that the LS estimation is corrupt by two noise components therefore,

the estimates are expected to present severe degradation.

The LS estimation can be improved by the MMSE filter. The MMSE estimator in the time domain is described in Section 3.4.2 for a point-to-point link, as follows

$$\widetilde{\mathbf{W}}_{\text{mmse}} = \mathbf{R}_{\tilde{h}\hat{\tilde{h}}}\mathbf{R}^{-1}_{\hat{\tilde{h}}\hat{\tilde{h}}}, \tag{4.26}$$

where the correlation matrices are given by

$$\mathbf{R}_{\tilde{h}\hat{\tilde{h}}} = \mathbb{E}\Big\{\tilde{\mathbf{h}}\hat{\tilde{\mathbf{h}}}^H\Big\} = \mathbf{R}_{\tilde{h}\tilde{h}} + \frac{\sigma_n^2}{N_t}\mathbf{I}_{N_t} \tag{4.27}$$

$$\mathbf{R}_{\hat{\tilde{h}}\hat{\tilde{h}}} = \mathbb{E}\Big\{\hat{\tilde{\mathbf{h}}}\hat{\tilde{\mathbf{h}}}^H\Big\} = \mathbf{R}_{\tilde{h}\tilde{h}} = \text{diag}\left(\sigma_h^2[0] \;\; \sigma_h^2[1] \;\; \cdots \;\; \sigma_h^2[L-1] \;\; \cdots \;\; 0\right). \tag{4.28}$$

This estimator considers the statistics of the channel such as the noise variance, as presented in Eq. (4.27). According to Eq. (4.5) for the AF relay link there is an extra source of noise that should be considered in order to design the filter properly. Therefore, for the AF relay link it is proposed that the variance of the overall noise, σ_{t}^2, be considered into the filter designing.

Furthermore, for such channel the corresponding autocorrelation function in time domain, i.e., the PDP should be considered as well, according to Eq. (4.17). Hence, it proposed that the expression for the AF relay channel the MMSE filter in the time domain be expressed by

$$\widetilde{\mathbf{W}}_{\text{mmse}} = \mathbf{R}_{\tilde{h}_c\hat{\tilde{h}}_c}\mathbf{R}^{-1}_{\hat{\tilde{h}}_c\hat{\tilde{h}}_c}, \tag{4.29}$$

where the correlation matrices are given by

$$\mathbf{R}_{\tilde{h}_c\hat{\tilde{h}}_c} = \mathbb{E}\Big\{\tilde{\mathbf{h}}_c\hat{\tilde{\mathbf{h}}}_c^H\Big\} = \mathbf{R}_{\tilde{h}_c\tilde{h}_c} + \frac{\sigma_{\text{t}}^2}{N_t}\mathbf{I}_{N_t} \tag{4.30}$$

$$\mathbf{R}_{\hat{\tilde{h}}_c\hat{\tilde{h}}_c} = \mathbb{E}\Big\{\hat{\tilde{\mathbf{h}}}_c\hat{\tilde{\mathbf{h}}}_c^H\Big\} = \mathbf{R}_{\tilde{h}_c\tilde{h}_c}. \tag{4.31}$$

As aforementioned the for a generic channel, the IFFT of the spectral correlation function corresponds to its PDP. Therefore, for compound channel the delay spread that is much more

large than the single-hop channel is also considered in the MMSE estimator, according to

$$\mathbf{R}_{\tilde{h_c}\tilde{h_c}} = \text{diag}\left(\sigma_h^1[0] \;\; \sigma_h^2[1] \;\; \cdots \;\; \sigma_h^2[L_c-1] \;\; \cdots \;\; 0\right). \tag{4.32}$$

4.4 Performance Assessment

The results obtained considers only the compound channel $h_{k,c} = Ah_{k,\text{ru}}h_{k,\text{br}}$. Such a scheme represents a scenario where the direct link has poor conditions. For reference the results considering the channel estimation results for point-to-point is included. The simulation parameters are summarised in Table 4.1.

Table 4.1: Simulation parameters

Modulation	QPSK
Carrier Frequency	2 GHz
Sampling Interval	89.3 ns
# Subcarriers	1024
OFDM frame	9 symbols
Channel Taps	4 and 6 taps
Channel Statistics	Identical
Velocity	3 km/h
Link Analysed	Compound Link
For Reference	Point-to-Point

The channel estimation performance is presented in terms of MSE and E_b/N_0. If the channel performance is assessed using E_b/N_0' where N_0' represents only the noise added at the user terminal, the MSE performance curve of the scenarios employing AF relay protocol must be shifted by 3 dB).

The pilot symbols assume deterministic value $p = 1$ and for simplicity only average amplifying gain is considered. Therefore normalised MSE of relay channel estimate corresponds

to

$$\text{MSE} = \mathbb{E}\left\{ \frac{|\hat{h}_{\text{ls}} - h_c|^2}{A^2} \right\}. \tag{4.33}$$

It is considered that the pilot separation in time dimension is $N_v = 1$ that provides a channel estimate per OFDM symbol. It is considered the following pilot separations in frequency dimension are $N_f = 4,\ 8$ and 16. The ITU Pedestrian A and B are considered as channel models with the tap delays modified according to the sampling interval. Both the UT and the RN are considered as mobile terminals hence, the Doppler effect is considered in both links BS - RN and RN - UT.

The results considering the MMSE estimation for the AF relay link with the ITU Pedestrian model A are depicted in Figure 4.8. Regarding the pilot separation N_f, for a point-to-point link, as the pilot density increases by a factor of 2 the MSE performance is expected to improve in approximately 3 dB. In the results presented in Figure 4.8 and Figure 4.9 as the density increases the MSE performance increases as well. However, the maximum delay spread of the compound channel as well as the short frequency coherency band causes degradation in the estimation performance. Contrarily to the results presented in Figure 4.9, the results related to the compound channel show that the improvements related to the pilot density does not follow the expected gain of 3 dB. For $E_b/N_0 = 6$ dB and $N_f = 16$ an increase in the pilot density, $N_f = 8$, provides 2.5 dB gain. Similar gain is obtained for $E_b/N_0 = 9$ and $N_f = 8$, considering an increase in the pilot density by a factor of 2, $N_f = 8$. For the compound channel case there is a loss of approximately 0.5 dB in the MSE performance.

The results for the LS estimation for the AF relay link with the ITU Pedestrian model A are presented in Figure 4.10. Contrastingly to the MMSE results for a point-to-point link, increasing the pilot density does not provide a gain, as depicted in Figure 4.11. Since the LS estimator does not consider the channel statistics in order to improve the channel estimates, it provides a noisy estimation. In addition, the LS estimator presents errors related to interpolation. As the pilot density increases the errors related to the interpolation decreases however, more noise components are added to the estimation yielding in degradation. The LS estimation for the AF relay channel presents a performance degradation for low SNR in comparison with the point-to-point link estimation however, asymptomatically the performance are similar.

Considering the ITU Pedestrian model B, the MMSE estimation results for the AF relay

channel are depicted in Figure 4.12. Regarding the increase of power efficiency stemmed from the insertion of pilots, the MSE performance achieves only 2 dB gain whereas the point-to-point link estimation achieves 2.5 dB, as depicted in Figure 4.13. As this channel model is a high selective channel both results present degradation in comparison with the results obtained for the MMSE estimation in Figure 4.8 and Figure 4.9, respectively. For all N_f values and in the E_b/N_0 range, the increased maximum delay of the compound channel causes, approximately, a loss of 4 dB in comparison with the point-to-point link whereas the comparable loss in the slowly selective ITU Pedestrian model A is, approximately, 2 dB.

The LS channel estimation performance for the AF relay channel with the ITU Pedestrian model B is presented in Figure 4.14 whereas Figure 4.15 depicts the results for the point-to-point link. The channel estimation performance presented in Figure 4.15 shows minor degradations in comparison with the results in Figure 4.11, with the ITU Pedestrian model A. The high selectivity of the ITU Pedestrian model B does not impact significantly on the MSE performance as this estimator does not consider the channel statistics in the estimation process. The poor performances presented in Figure 4.14 and Figure 4.15 are related to errors introduced either by interpolation or noisy components insertion. The results for the AF link also show minor degradations for the pilot separations $N_f = 4$ and $N_f = 8$. On the other hand, the result considering $N_f = 16$ presents significant saturation. Such effect stem from the large pilot separation which causes undersampling of the channel, yielding in distortions by causing an irreducible error floor. The high selectivity of such channel model and the AF relay link statistics limits the maximum pilot separation. Therefore, for the AF relay scenario the pilot symbols should have a sufficiently high density such that the estimator is able to provide the channel estimates in case of channels subject to high frequency selectivity.

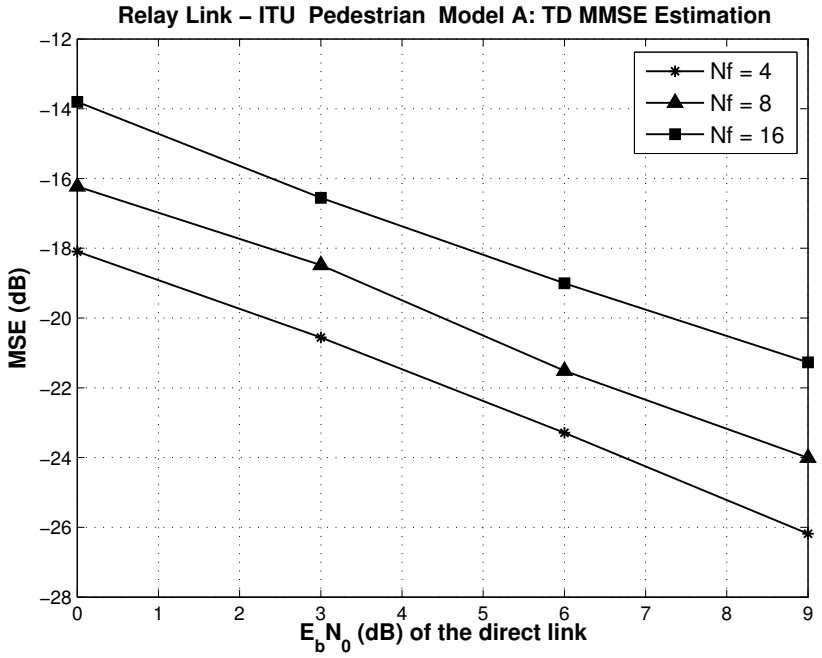

Figure 4.8: MMSE channel estimation performance for AF relay channel with ITU Pedestrian model A.

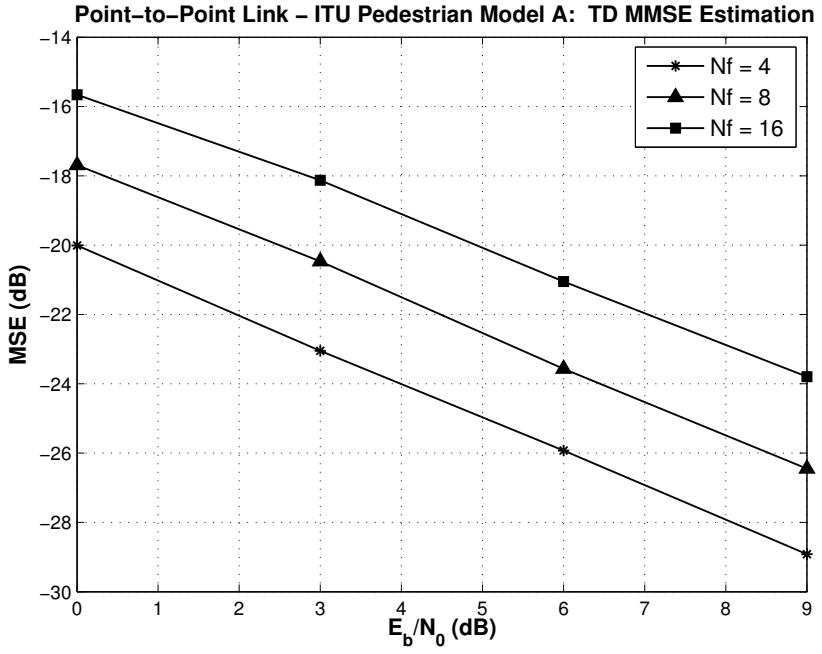

Figure 4.9: MMSE channel estimation performance for point-to-point link with ITU Pedestrian model A.

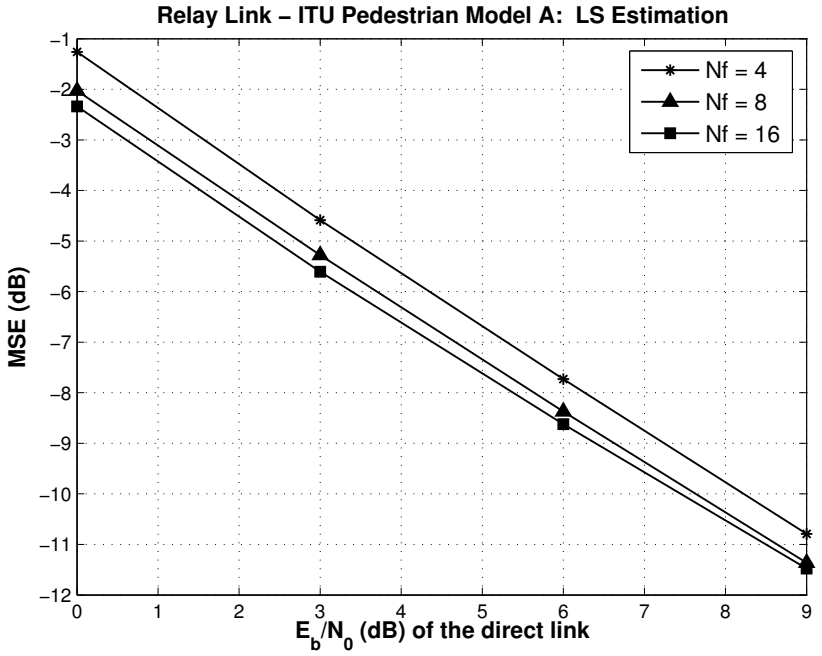

Figure 4.10: LS channel estimation performance for AF relay channel with ITU Pedestrian model A.

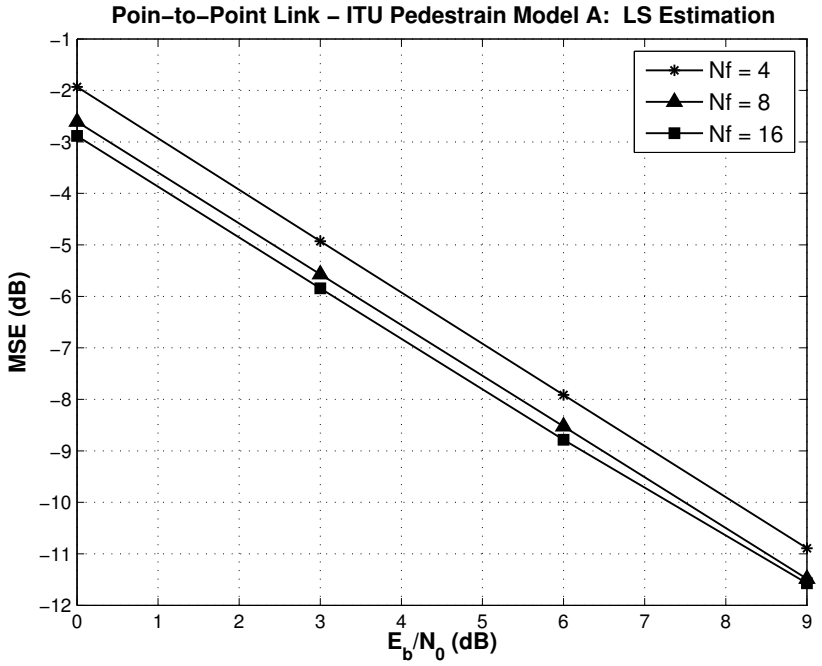

Figure 4.11: LS channel estimation performance for point-to-point link with ITU Pedestrian model A.

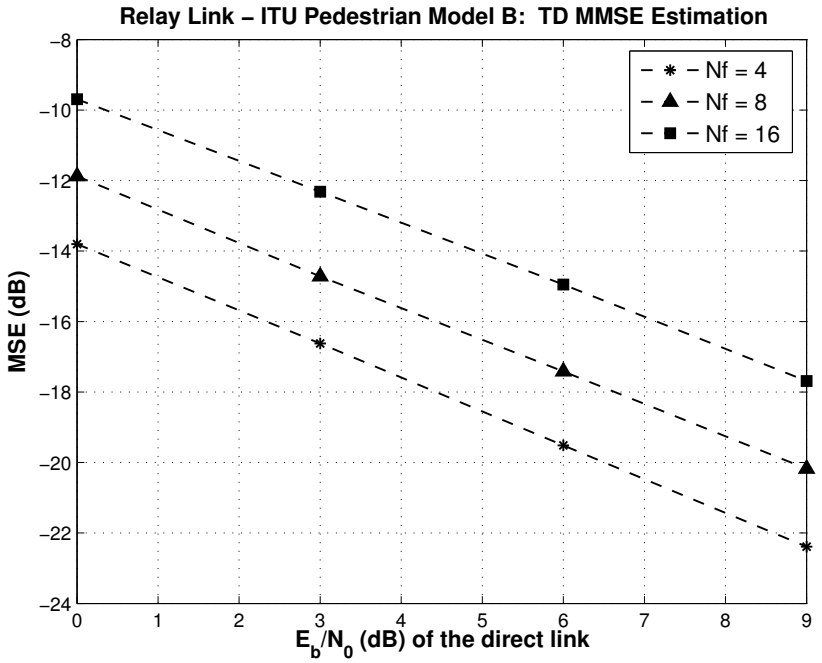

Figure 4.12: MMSE channel estimation performance for AF relay channel with ITU Pedestrian model B.

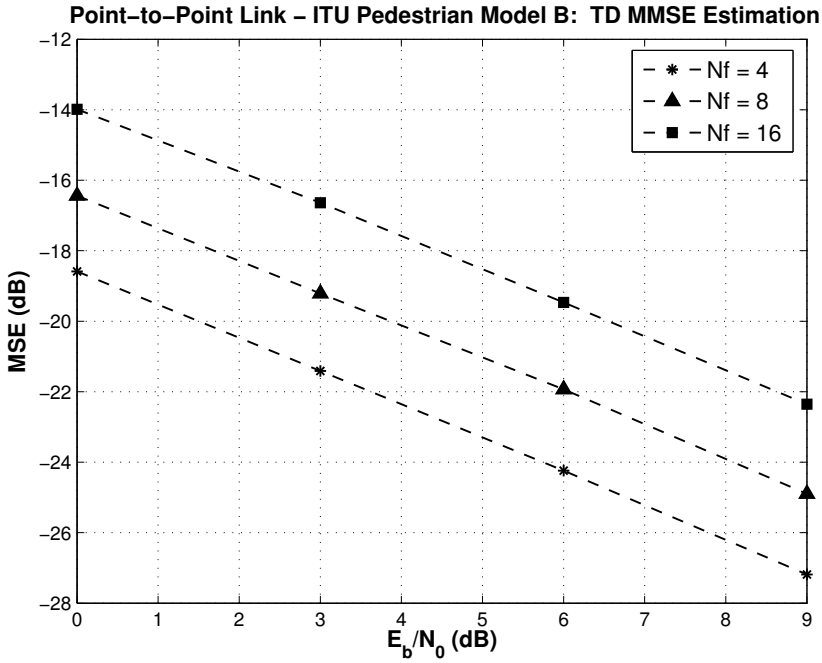

Figure 4.13: MMSE channel estimation performance for point-to-point link with ITU Pedestrian model B.

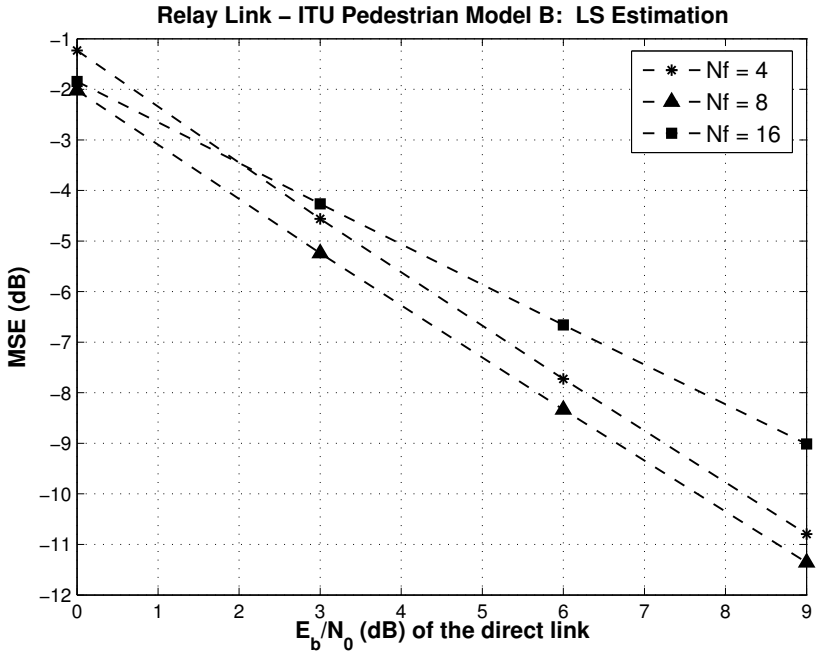

Figure 4.14: LS channel estimation performance for AF relay channel with ITU Pedestrian model B.

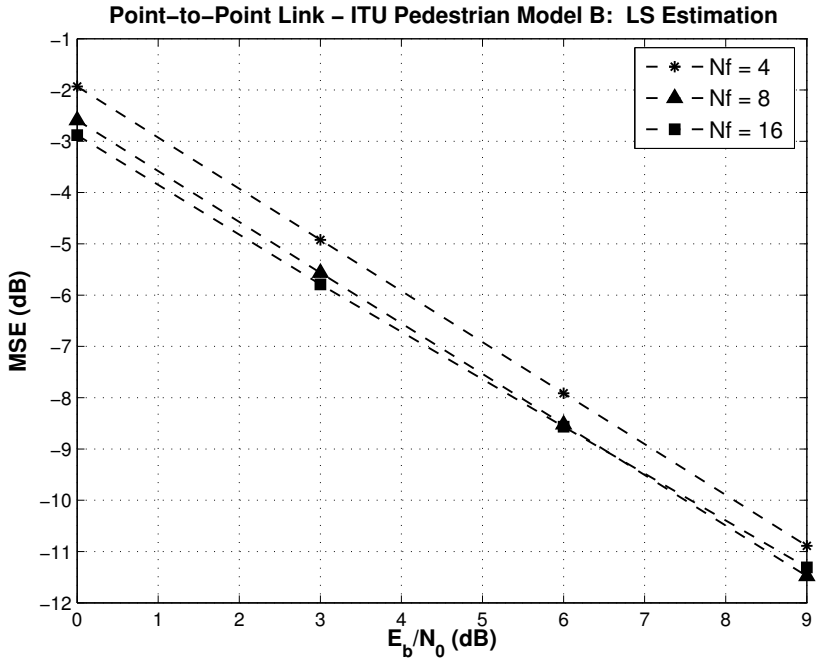

Figure 4.15: LS channel estimation performance for point-to-point link with ITU Pedestrian model B.

4.5 Conclusion

We have presented the channel estimation performance of an AF relay-assisted scheme whereby two classical pilot-based estimators designed for point-to-point links were employed.

The results for the MMSE estimation show that the maximum delay of the compound channel limits the expected gain provided by the increase of the pilot density, causing losses of approximately 0.5 dB and 1 dB in the MSE performance for slowly and highly selective channels, respectively. In addition, in comparison with the point-to-point link, the overall MMSE estimation performance for the AF relay link is degraded in 2 dB and 4 dB for slowly and highly selective channels, respectively. The results considering the LS estimation show that its poor performance is related to interpolation errors and the insertion of noisy components than to the statistics of a slowly selective channel. Moreover, the LS results show that a highly selectivity channel merged with the increased maximum delay of the AF relay link limits the maximum pilot separation. Therefore, for the AF relay scenario the pilot grid should have a sufficiently high density in case of channels subject to high frequency selectivity.

Chapter 5

Channel Estimation for EF Relay-Assisted OFDM-Based Systems

5.1 Introduction

In the previous chapter we have considered the AF protocol. This technique is appealing for relaying schemes because of its low complexity implementation, as it does not need any a priori information in order to amplify and forward the received signal.

As discussed in Section 2.4, the use of MIMO has been recognised as a key technique to explore the scattering inherent to the wireless channel in order to provide high capacity through channel multiplexing or spatial diversity. The extension of MIMO to systems employing relays can bring additional capacity and diversity to cooperative systems [95], [96], [97] and in fact the integration of multiple antennas does not represent significant constraints both at the BS and at the RN, when dedicated. However, if we consider the AF protocol its simplicity does not allow us to achieve the benefits from MIMO in the BS-RN links. In AF MIMO cooperative systems, considering for example two antennas at the source, the channel from the BS to one antenna element at the RN corresponds to the sum of two Gaussian variables. Hence, directly amplifying the received signal simply destroys the space-time or space-frequency coding that may have been performed at the BS. In such a scenario (two antennas at the BS with space frequency/time coding and AF at the RN) the space diversity asymptotically achieves the same diversity as a system where the RN is a single antenna terminal [43] and therefore, the spatial diversity benefits are not fully explored. In order to achieve the diversity, it is necessary that at the RN we are able to separate the different paths from the BS to the RN. This requires, for the SFBC case, that we are able to separate the different subcarriers properly and then,

after the appropriate combination, the amplification is performed. This technique has been reported as EF in Section 2.4. This represents obviously additional complexity at the RN but allows us to make use of MIMO without going for a full regeneration at the RN.

Although there is an absorbing literature on channel estimation for point-to-point MIMO [98], [99], [100] when it comes to systems employing relays, most of literature dealing with the AF considers single antenna at the RNs (see Chapter 4). In DF MIMO cooperative systems, conventional point-to-point link channel estimation schemes can be used since the regeneration isolates the links. However, when employing the AF relaying protocol, transmission schemes departing significantly from the conventional space time/frequency techniques have to be devised in order to get benefits from diversity. Few works have however tackled the problem of channel estimation in AF cooperative systems. For example in [95] a joint estimation of the channel vectors is proposed for a distributed STBC. As such, each channel vector is decomposed into the product of its length and direction that are then combined to obtain a ML-based estimation. [96] concentrates on the problem of estimation for the channel when both the BS and the RN have multiple antennas and the RN employs the AF protocol. They found necessary and sufficient conditions on the pilot amplifying matrix sequence at the RN to ensure feasible relay channel estimation at the destination. However nothing is mentioned concerning the data transmission. A similar MIMO model is considered in [97] where a Least-Squares (LS) based channel estimation algorithm is developed, that provides the destination with full knowledge of all channel responses involved in the transmission, but again nothing is referred about the data transmission arrangement.

Publications considering the EF protocol, to the best of our knowledge, have mainly dealt with performance analysis assuming ideal channel estimation [101], [102]. Since in the EF MIMO cooperative systems there are no regeneration but an equalisation at the RN, the BS-RN-UT links are not just the cascade of the BS-RN and RN-UT links but a more complex channel. Consequently, the channel estimator at the UT needs to estimate an equivalent channel in order to perform the optimal equalisation.

The derivation of a proper channel estimation scheme for the EF MIMO cooperative system is the objective of this chapter. In the studied scenario, both the BS and the RN are equipped with an antenna array whereas the UT is a single antenna device. The BS-RN channels are estimated at the relaying terminal and the information related to the equivalent channel is

inserted at the pilot tons. At the UT, the MMSE estimator estimates the equivalent channel taking into account the SFBC equalisation performed at the RN. The estimator scheme is considered operating in the time domain because of the reduced complexity in comparison with its implementation in frequency domain.

The remaining of this chapter is organised as follows. Section 5.2 and Section 5.3 introduce the scenario and the system description. In Section 5.4 the relay-assisted scheme is designed. Section 5.5 presents the channels and parameters to be estimate at the RN or at the UT. The system performance is evaluated in terms of BER and MSE in Section 5.6. Lastly, some concluding remarks are presented in Section 5.7.

5.2 EF Relay-Assisted Scenario

This chapter considers a downlink EF relaying scheme where the cooperation is assisted by a single RN. The BS and RN are equipped with Q and G antennas, respectively, whereas the UT is a single antenna device, according to Figure 5.1.

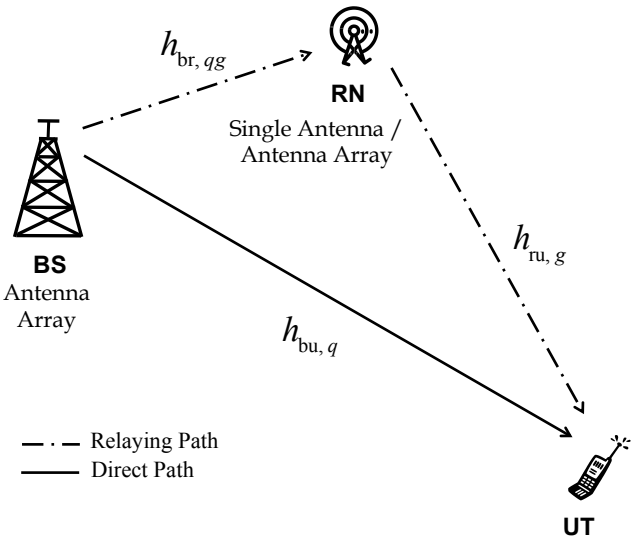

Figure 5.1: EF relay-assisted scenario.

Throughout this analysis the subscripts *br*, *bu* and *ru* are related to the links BS-RN, BS-UT and RN-UT, respectively. The scenarios are referred as $Q \times G \times 1$ schemes. Correspondingly, the following channels are involved:

- $Q \times G$ channels, for $Q = 2$ and $G = 1,\ 2$. The channels BS–RN are represented by $h_{\mathrm{br},qg}$, for $q = 1,\ 2$ and $g = 1,\ 2$;
- $Q \times 1$ channels. The MISO channels BS-UT are represented by $h_{\mathrm{bu},q}$, for $q = 1,\ 2$;
- $G \times 1$ channels. The SISO or MISO channels RN–UT are represented by h_{ru} and $h_{\mathrm{ru},g}$, for $g = 1$ and $g = 1,\ 2$, respectively;

5.3 System Model

We consider an OFDM transmission as described according to Section 2.2 and the channel model as described in Section 4.2. Let $\mathbf{s} = [s_1\ s_2\ \cdots\ s_J]^T$ be the data symbol sequence to be transmitted, for $k \in J$ where J is the set of data symbols. s_k follows the Alamouti (SFBC) mapping rule defined in Table 5.1, such that they are assumed to have unitary average energy, i.e., $\mathbb{E}\left\{|s_k|^2\right\} = 1$. Therefore, the factor $1/\sqrt{2}$ used in the mapping is to ensure that the total energy transmitted is normalised to 1. Consequently, the power transmitted by the terminals equipped with an antenna array is equally allocated between the two antennas.

Table 5.1: Two transmit antenna SFBC mapping

Subcarrier	**Antenna #1**	**Antenna #2**
k	$s_k/\sqrt{2}$	$-s_{k+1}^*/\sqrt{2}$
$k+1$	$s_{k+1}/\sqrt{2}$	$s_k^*/\sqrt{2}$

The data symbols and pilots are conveyed in different sets of subcarriers. The pilot separation at the BS and RN follows the pattern depicted in Figure 5.2 where the pilot spacing in frequency and time dimension is N_f and N_v, respectively.

The terminals equipped with two antennas allocate for each antenna element a different subset of pilot subcarriers therefore, for a specific antenna, the pilot separation is $2N_f$. The corresponding symbols arrangement, including pilots and the SFBC mapped data symbol per antenna element, is depicted in Figure 5.3 where $\varnothing$ means that neither pilot or data symbol is transmitted.

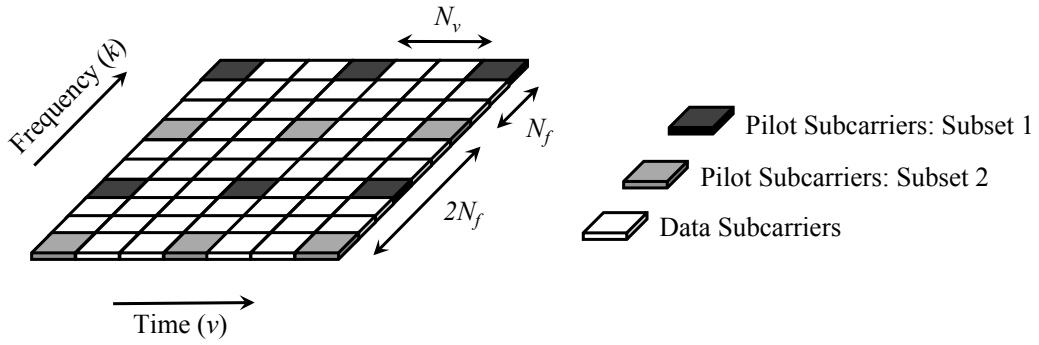

Figure 5.2: Pilot Pattern.

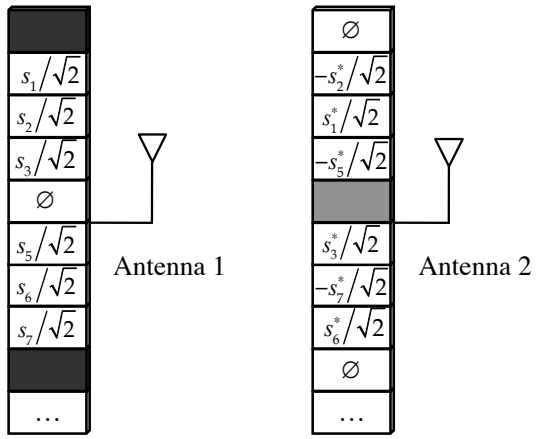

Figure 5.3: Symbols arrangement per antenna element.

5.4 EF Relay-Assisted System

The corresponding block diagram of the scenario depicted in Figure 5.1, for $Q = 2$ and $G = 2$, is presented in Figure 5.4 considering the broadcasting and reception processing. The Soft-Decision block performs the SFBC de-mapping and equalisation operations and its output corresponds to soft-decision variables. The Joint Processing block combines the soft-decision variables obtained in Phases I and II, as described in following sections.

The combining processing performed in both receiving phases are summarised in Figure 5.5. In Phase I, in the scenario $2 \times 2 \times 1$, at the RN the SFBC de-mapping and equalisation operations are performed for each antenna element. In such case, the resulting soft-decision variable is obtained after combining the soft-decision variables related to each antenna. In the scenario $2 \times 1 \times 1$ at the RN this combining processing is not required as the RN is equipped

with a single antenna. In Phase II, either in the $2 \times 2 \times 1$ or $2 \times 1 \times 1$ scenario, at the UT the combining operation is processed in order to combine the signals received from the BS and the RN.

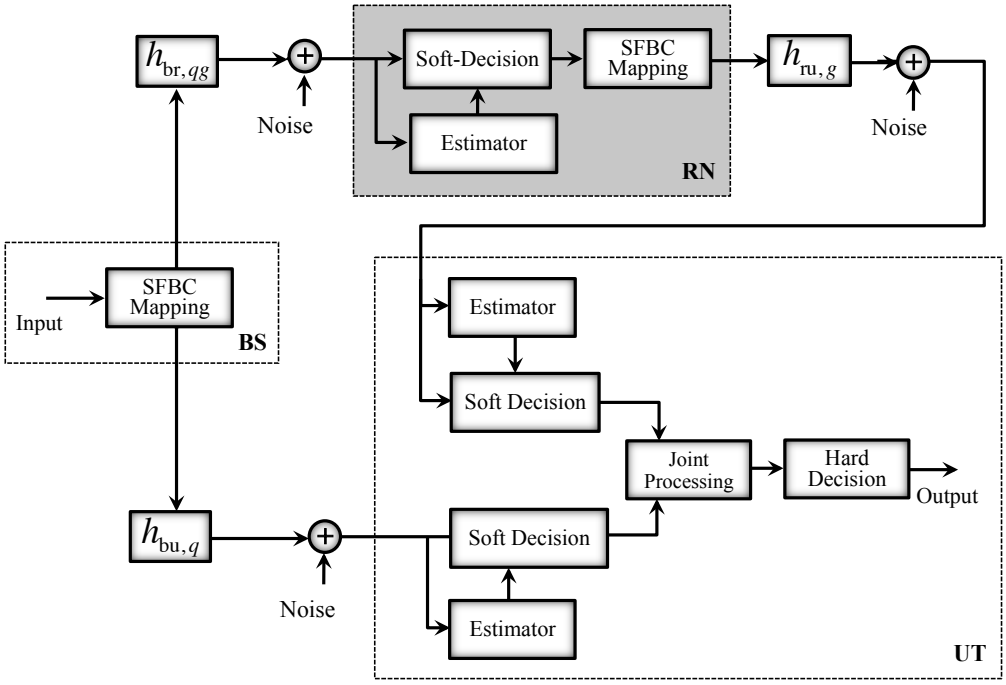

Figure 5.4: EF relay-assisted scenario: Block diagram.

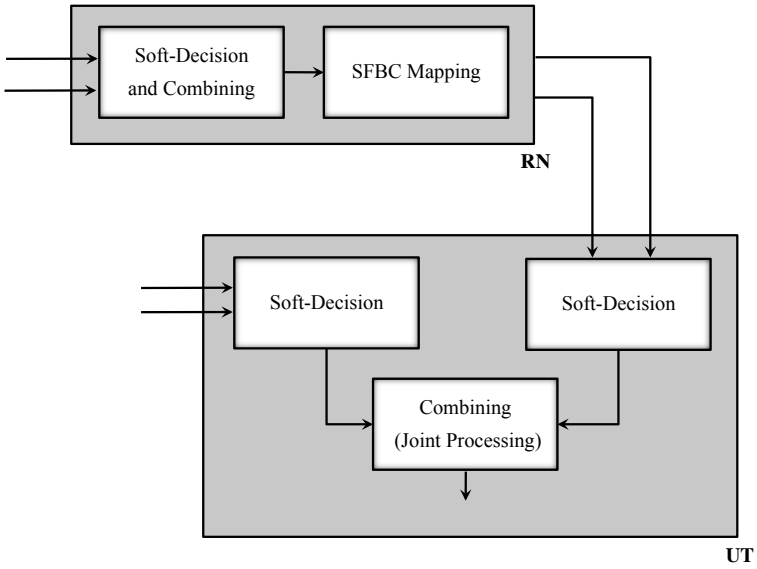

Figure 5.5: Combining processing related to both transmission phases.

5.4.1 Phase I

- **At the UT**

During the first phase of the transmission the information is broadcasted by the BS. The signals received at the UT on data subcarriers k and $k+1$ are given by

$$y_{k,\mathrm{bu}} = \frac{1}{\sqrt{2}}\Big(s_k h_{k,\mathrm{bu},1} - s^*_{k+1} h_{k+1,\mathrm{bu},2}\Big) + z^1_{k,\mathrm{bu}} \ , \tag{5.1}$$

$$y_{k+1,\mathrm{bu}} = \frac{1}{\sqrt{2}}\Big(s^*_k h_{k,\mathrm{bu},2} + s_{k+1} h_{k+1,\mathrm{bu},1}\Big) + z^1_{k+1,\mathrm{bu}} \ , \tag{5.2}$$

where $z^1_{k,\mathrm{bu}}$ is the AWGN noise with zero mean and variance σ^2_n, i.e., $\mathcal{CN}(0,\sigma^2_n)$.

Since the data symbol are SFBC mapped at the transmitters the SFBC de-mapping at the receivers also includes the MRC equalisation, which coefficients depend on the channels estimates. The corresponding soft decision-variables are given by

$$S_{k,\mathrm{bu}} = y_{k,\mathrm{bu}}\mathcal{G}^*_{k,\mathrm{bu},1} + y^*_{k+1,\mathrm{bu}}\mathcal{G}_{k+1,\mathrm{bu},2} \ , \tag{5.3}$$

$$S_{k+1,\mathrm{bu}} = -y^*_{k,\mathrm{bu}}\mathcal{G}_{k,\mathrm{bu},2} + y_{k+1,\mathrm{bu}}\mathcal{G}_{k+1,\mathrm{bu},1} \ , \tag{5.4}$$

where the MRC equalisation coefficients on k and $k+1$ data subcarriers correspond to $\mathcal{G}_{k,\mathrm{bu},q} = \hat{h}_{k,\mathrm{bu},q}\Big/\sqrt{2}$ and $\mathcal{G}_{k+1,\mathrm{bu},q} = \hat{h}_{k+1,\mathrm{bu},q}\Big/\sqrt{2}$, respectively, for $q = 1,\ 2$. After some mathematical manipulation, assuming $h_k \approx h_{k+1}$, these soft-decision variables may be expressed as:

$$S_{k,\mathrm{bu}} = \Gamma_{k,\mathrm{bu}} s_k + \frac{\hat{h}^*_{\mathrm{bu},1}}{\sqrt{2}} z^1_{k,\mathrm{bu}} + \frac{\hat{h}_{\mathrm{bu},2}}{\sqrt{2}} z^{*1}_{k+1,\mathrm{bu}} \ , \tag{5.5}$$

$$S_{k+1,\mathrm{bu}} = \Gamma_{k+1,\mathrm{bu}} s_{k+1} + \frac{\hat{h}^*_{\mathrm{bu},1}}{\sqrt{2}} z^1_{k+1,\mathrm{bu}} - \frac{\hat{h}_{\mathrm{bu},2}}{\sqrt{2}} z^{*1}_{k,\mathrm{bu}} \ , \tag{5.6}$$

where for k and $k+1$ data subcarriers $\Gamma_{k,\mathrm{bu}} = \dfrac{1}{2}\displaystyle\sum_{q=1}^{Q}\left|\hat{h}_{k,\mathrm{bu},q}\right|^2$ and $\Gamma_{k+1,\mathrm{bu}} = \dfrac{1}{2}\displaystyle\sum_{q=1}^{Q}\left|\hat{h}_{k+1,\mathrm{bu},q}\right|^2$.

- **At the RN**

Similarly, the signals received at the RN per g antenna on data subcarriers k and $k+1$ are

expressed according to

$$y_{k,\mathrm{br},g} = \frac{1}{\sqrt{2}}\Big(s_k h_{k,\mathrm{br},1g} - s^*_{k+1} h_{k+1,\mathrm{br},2g}\Big) + z^1_{k,\mathrm{br}} \ , \tag{5.7}$$

$$y_{k+1,\mathrm{br},g} = \frac{1}{\sqrt{2}}\Big(s^*_k h_{k,\mathrm{br},2g} + s_{k+1} h_{k+1,\mathrm{br},1g}\Big) + z^1_{k+1,\mathrm{br}} \ , \tag{5.8}$$

where $z_{k,\mathrm{br}}$ is the noise $\mathcal{CN}(0, \sigma_n^2)$.

For $G = 1$ the soft decision variables on k and $k+1$ data subcarriers are given by

$$S_{k,\mathrm{br}} = y_{k,\mathrm{br},1}\mathcal{G}^*_{k,\mathrm{br},11} + y^*_{k+1,\mathrm{br},1}\mathcal{G}_{k+1,\mathrm{br},21} \ , \tag{5.9}$$

$$S_{k+1,\mathrm{br}} = -y^*_{k,\mathrm{br},1}\mathcal{G}_{k,\mathrm{br},21} + y_{k+1,\mathrm{br},1}\mathcal{G}_{k+1,\mathrm{br}11} \ , \tag{5.10}$$

where the MRC equalisation coefficients for k and $k+1$ data subcarriers corresponds to $\mathcal{G}_{k,\mathrm{br},q1} = \hat{h}_{k,\mathrm{br},q1}\Big/\sqrt{2}$ and $\mathcal{G}_{k+1,\mathrm{br},q1} = \hat{h}_{k+1,\mathrm{br},q1}\Big/\sqrt{2}$, respectively, for $q = 1,\ 2$.

Replacing Eq. (5.7) and Eq. (5.8) into Eq. (5.9) and Eq. (5.10) the following soft decision-variable is found

$$S_{k,\mathrm{br}} = \Gamma_{k,}s_k + \frac{\hat{h}^*_{\mathrm{br},11}}{\sqrt{2}} z^1_{k,\mathrm{br}} + \frac{\hat{h}_{\mathrm{br},21}}{\sqrt{2}} z^{*1}_{k+1,\mathrm{br}} \ . \tag{5.11}$$

$$S_{k+1,\mathrm{br}} = \Gamma_{k+1,}s_{k+1} + \frac{\hat{h}^*_{\mathrm{br},11}}{\sqrt{2}} z^1_{k+1,\mathrm{br}} - \frac{\hat{h}_{\mathrm{br},21}}{\sqrt{2}} z^{*1}_{k,\mathrm{br}} \ . \tag{5.12}$$

For $G = 1,\ 2$ the resulting soft-decision variables follow the expressions below. The summation is performed in order to combine the soft-decision variables related to each antenna element.

$$S_{k,\mathrm{br}} = \sum_{g=1}^{G} \left(y_{k,\mathrm{br},g}\mathcal{G}^*_{k,\mathrm{br},1g} + y^*_{k+1\mathrm{br},g}\mathcal{G}_{k+1,\mathrm{br},2g}\right) \ , \tag{5.13}$$

$$S_{k+1,\mathrm{br}} = \sum_{g=1}^{G} \left(-y^*_{k,\mathrm{br},g}\mathcal{G}_{k,\mathrm{br},2g} + y_{k+1,\mathrm{r},g}\mathcal{G}_{k+1,\mathrm{br},1g}\right) \ , \tag{5.14}$$

where the MRC equalisation coefficients for k and $k+1$ data subcarriers correspond to $\mathcal{G}_{k,\mathrm{br},qg} = \hat{h}_{k,\mathrm{br},qg}\Big/\sqrt{2}$ and $\mathcal{G}_{k+1,\mathrm{br},qg} = \hat{h}_{k+1,\mathrm{br},qg}\Big/\sqrt{2}$, respectively, for $q = 1,\ 2$ and $g = 1,\ 2$. After some mathematical manipulation, for $G = 2$ these soft-decision variables

may be expressed as:

$$S_{k,\mathrm{br}} = \Gamma_{k,} s_k + \frac{\hat{h}^*_{\mathrm{br},11}}{\sqrt{2}} z^1_{k,\mathrm{br}} + \frac{\hat{h}_{\mathrm{br},21}}{\sqrt{2}} z^{*1}_{k+1,\mathrm{br}} + \frac{\hat{h}^*_{\mathrm{br}12}}{\sqrt{2}} z^2_{k,\mathrm{br}} + \frac{\hat{h}_{k,\mathrm{br}22}}{\sqrt{2}} z^{*2}_{k+1,\mathrm{br}} \ , \tag{5.15}$$

$$S_{k+1,\mathrm{br}} = \Gamma_{k+1,} s_{k+1} + \frac{\hat{h}^*_{\mathrm{br}11}}{\sqrt{2}} z^1_{k+1,\mathrm{br}} - \frac{\hat{h}_{\mathrm{br}21}}{\sqrt{2}} z^{*1}_{k,\mathrm{br}} + \frac{\hat{h}^*_{\mathrm{br}12}}{\sqrt{2}} z^2_{k+1,\mathrm{br}} - \frac{\hat{h}_{\mathrm{br}22}}{\sqrt{2}} z^{*2}_{k,\mathrm{br}} \ , \tag{5.16}$$

where for k and k+1 data subcarriers $\Gamma_k = \frac{1}{2}\sum_{q=1}^{Q}\sum_{g=1}^{G}\left|\hat{h}_{k,\mathrm{br},qg}\right|^2$ and $\Gamma_{k+1} = \frac{1}{2}\sum_{q=1}^{Q}\sum_{g=1}^{G}\left|\hat{h}_{k+1,\mathrm{br},qg}\right|^2$, respectively, for $Q = 2$ and $G = 1,\ 2$.

For a generic k data subcarrier the variance of $S_{k,\mathrm{br}}$ can be written as $\sigma^2_{S_{\mathrm{br}}} = \Gamma^2_k + \Gamma_k\sigma^2_n$. Therefore, in order to transmit an unit power signal the RN normalises the expression in Eq. (5.9) - Eq. (5.10) and Eq. (5.15) - Eq. (5.16) according to the following factor

$$\alpha_k = \frac{1}{\sqrt{\Gamma^2_k + \Gamma_k\sigma^2_n}}. \tag{5.17}$$

According to Eq. (5.15) and Eq. (5.16) there are four noise components related to the SFBC de-mapping processing as follows

$$w_{k,\mathrm{br}} = \frac{\hat{h}^*_{\mathrm{br},11}}{\sqrt{2}} z^1_{k,\mathrm{br}} + \frac{\hat{h}_{\mathrm{br},21}}{\sqrt{2}} z^{*1}_{k+1,\mathrm{br}} + \frac{\hat{h}^*_{\mathrm{br},12}}{\sqrt{2}} z^2_{k,\mathrm{br}} + \frac{\hat{h}_{\mathrm{br},22}}{\sqrt{2}} z^{*2}_{k+1,\mathrm{br}} \ , \tag{5.18}$$

$$w_{k+1,\mathrm{br}} = \frac{\hat{h}^*_{\mathrm{br},11}}{\sqrt{2}} z^1_{k+1,\mathrm{br}} - \frac{\hat{h}_{\mathrm{br},21}}{\sqrt{2}} z^{*1}_{k,\mathrm{br}} + \frac{\hat{h}^*_{\mathrm{br}12}}{\sqrt{2}} z^2_{k+1,\mathrm{br}} - \frac{\hat{h}_{\mathrm{br},22}}{\sqrt{2}} z^{*2}_{k,\mathrm{br}} \ , \tag{5.19}$$

where $z^1_{k,\mathrm{br}}$ and $z^2_{k,\mathrm{br}}$ are the AWGN noise related to the receiver antenna at the RN. Therefore, considering that for each channel the index k is dropped, the following relation can be found

$$\begin{aligned}\mathbb{E}\left\{w_{k,\mathrm{br}} w_{k+1,\mathrm{br}}\right\} = \mathbb{E}\left\{\frac{-\hat{h}^*_{\mathrm{br},11}\hat{h}_{\mathrm{br}21}|z^{*1}_{k,\mathrm{br}}|^2}{\sqrt{2}}\right\} + \mathbb{E}\left\{\frac{\hat{h}^*_{\mathrm{br},11}\hat{h}_{\mathrm{br},21}|z^{*1}_{k+1,\mathrm{br}}|^2}{\sqrt{2}}\right\} + \\ \mathbb{E}\left\{\frac{-\hat{h}^*_{\mathrm{br},12}\hat{h}_{\mathrm{br},22}|z^{*2}_{k,\mathrm{br}}|^2}{\sqrt{2}}\right\} + \mathbb{E}\left\{\frac{\hat{h}^*_{\mathrm{br},12}\hat{h}_{\mathrm{br},22}|z^{*2}_{k+1,\mathrm{br}}|^2}{\sqrt{2}}\right\}.\end{aligned} \tag{5.20}$$

Equation (5.20) shows that $\mathbb{E}\left\{w_{k,\mathrm{br}} w_{k+1,\mathrm{br}}\right\} = 0$ is true only and if only

$$\mathbb{E}\left\{|z^{*1}_{k,\mathrm{br}}|^2\right\} = \mathbb{E}\left\{|z^{*1}_{k+1,\mathrm{br}}|^2\right\} = \mathbb{E}\left\{|z^{*2}_{k,\mathrm{br}}|^2\right\} = \mathbb{E}\left\{|z^{*2}_{k+1,\mathrm{br}}|^2\right\} \ = \ \sigma^2_n \ . \tag{5.21}$$

Therefore, Eq. (5.20) - Eq. (5.21) show that the noise components on subcarriers k and $k+1$ are uncorrelated and the noise terms at both antennas have equal variances. Such condition is exploit in the next section when the relation between the variance of the individual noises at the RN or UT and the variance of the overall received signal at the UT in Phase II are found.

5.4.2 Phase II

While the BS is idle the normalised soft-decision variable is sent to the destination. For $G = 1$, the signal received at the UT on k subcarrier is expressed according to

$$y_{k,\mathrm{ru}} = \alpha_k S_{k,\mathrm{br}} h_{k,\mathrm{ru}} + z^1_{k,\mathrm{ru}} \ . \tag{5.22}$$

where $z^1_{k,\mathrm{ru}}$ is the noise $\mathcal{CN}(0, \sigma_n^2)$. Replacing Eq. (5.11) into Eq. (5.22) on k data subcarrier, the received signal at UT for $G = 1$ is given by

$$y_{k,\mathrm{ru}} = \alpha_k \Gamma_{k,} h_{k,\mathrm{ru}} s_k + \alpha_k \frac{\hat{h}^*_{k,\mathrm{br},11}}{\sqrt{2}} z^1_{k,\mathrm{br}} h_{k,\mathrm{ru}} + \alpha_k \frac{\hat{h}_{k,\mathrm{br},21}}{\sqrt{2}} z^{*1}_{k+1,\mathrm{br}} h_{k,\mathrm{ru}} + z^1_{k,\mathrm{ru}} \ . \tag{5.23}$$

For $G = 2$, the signals received at the UT on k and $k + 1$ subcarriers are expressed by

$$y_{k,\mathrm{ru}} = \frac{1}{\sqrt{2}} \left(h_{k,\mathrm{ru},1} \alpha_k S_{k,\mathrm{br}} - h_{k+1,\mathrm{ru},2} \alpha^*_{k+1} S^*_{k+1,\mathrm{br}} \right) + z^1_{k,\mathrm{ru}} \ . \tag{5.24}$$

$$y_{k+1,\mathrm{ru}} = \frac{1}{\sqrt{2}} \left(h_{k,\mathrm{ru},2} \alpha^*_k S^*_{k,\mathrm{br}} + h_{k+1,\mathrm{ru},1} \alpha_{k+1} S_{k+1,\mathrm{br}} \right) + z^1_{k+1,\mathrm{ru}} \ . \tag{5.25}$$

Replacing Eq. (5.15) - Eq. (5.16) into Eq. (5.24) - Eq. (5.25) the received signal at the RN for $G = 2$ on k and $k + 1$ subcarriers can be expressed as

$$
\begin{aligned}
y_{k,\mathrm{ru}} = & \frac{1}{\sqrt{2}}\left(h_{k,\mathrm{ru},1}\alpha_k\Gamma_{k,}s_k\right) + \frac{1}{\sqrt{2}}\left(h_{k,\mathrm{ru}1}\alpha_k\frac{\hat{h}^*_{\mathrm{br},11}}{\sqrt{2}}z^1_{k,\mathrm{br}}\right) + \\
& \frac{1}{\sqrt{2}}\left(h_{k,\mathrm{ru},1}\alpha_k\frac{\hat{h}_{\mathrm{br},21}}{\sqrt{2}}z^{*1}_{k+1,\mathrm{br}}\right) + \frac{1}{\sqrt{2}}\left(h_{k,\mathrm{ru},1}\alpha_k\frac{\hat{h}^*_{\mathrm{br},12}}{\sqrt{2}}z^2_{k,\mathrm{br}}\right) + \\
& \frac{1}{\sqrt{2}}\left(h_{k,\mathrm{ru},1}\alpha_k\frac{\hat{h}_{\mathrm{br},22}}{\sqrt{2}}z^{*2}_{k+1,\mathrm{br}}\right) - \frac{1}{\sqrt{2}}\left(h_{k+1,\mathrm{ru},2}\alpha^*_{k+1}\Gamma^*_{k+1,}s^*_{k+1}\right) + \\
& \frac{1}{\sqrt{2}}\left(h_{k+1,\mathrm{ru},2}\alpha^*_{k+1}\frac{\hat{h}_{\mathrm{br},11}}{\sqrt{2}}z^{1*}_{k+1,\mathrm{br}}\right) - \frac{1}{\sqrt{2}}\left(h_{k+1,\mathrm{ru},2}\alpha^*_{k+1}\frac{\hat{h}^*_{\mathrm{br},21}}{\sqrt{2}}z^1_{k,\mathrm{br}}\right) + \\
& \frac{1}{\sqrt{2}}\left(h_{k+1,\mathrm{ru},2}\alpha^*_{k+1}\frac{\hat{h}_{\mathrm{br},12}}{\sqrt{2}}z^{2*}_{k+1,\mathrm{br}}\right) - \frac{1}{\sqrt{2}}\left(h_{k+1,\mathrm{ru},2}\alpha^*_{k+1}\frac{\hat{h}^*_{\mathrm{br},22}}{\sqrt{2}}z^2_{k,\mathrm{br}}\right) + z^1_{k,\mathrm{ru}}\ . \quad (5.26)
\end{aligned}
$$

$$
\begin{aligned}
y_{k+1,\mathrm{ru}} = & \frac{1}{\sqrt{2}}\left(h_{k,\mathrm{ru},2}\alpha^*_k\Gamma^*_{k,}s^*_k\right) + \frac{1}{\sqrt{2}}\left(h_{k,\mathrm{ru},2}\alpha^*_k\frac{\hat{h}_{\mathrm{br},11}}{\sqrt{2}}z^{1*}_{k,\mathrm{br}}\right) + \\
& \frac{1}{\sqrt{2}}\left(h_{k,\mathrm{ru},2}\alpha^*_k\frac{\hat{h}^*_{\mathrm{br},21}}{\sqrt{2}}z^1_{k+1,\mathrm{br}}\right) + \frac{1}{\sqrt{2}}\left(h_{k,\mathrm{ru},2}\alpha^*_k\frac{\hat{h}_{\mathrm{br},12}}{\sqrt{2}}z^{2*}_{k,\mathrm{br}}\right) - \\
& \frac{1}{\sqrt{2}}\left(h_{k,\mathrm{ru},2}\alpha^*_k\frac{\hat{h}^*_{k,\mathrm{br},22}}{\sqrt{2}}z^2_{k+1,\mathrm{br}}\right) + \frac{1}{\sqrt{2}}\left(h_{k+1,\mathrm{ru},1}\alpha_{k+1}\Gamma_{k+1,}s_{k+1}\right) + \\
& \frac{1}{\sqrt{2}}\left(h_{k+1,\mathrm{ru},1}\alpha_{k+1}\frac{\hat{h}^*_{\mathrm{br},11}}{\sqrt{2}}z^1_{k+1,\mathrm{br}}\right) - \frac{1}{\sqrt{2}}\left(h_{k+1,\mathrm{ru},1}\alpha_{k+1}\frac{\hat{h}_{\mathrm{br},21}}{\sqrt{2}}z^{*1}_{k,\mathrm{br}}\right) + \\
& \frac{1}{\sqrt{2}}\left(h_{k+1,\mathrm{ru},1}\alpha_{k+1}\frac{\hat{h}^*_{\mathrm{br},12}}{\sqrt{2}}z^2_{k+1,\mathrm{br}}\right) - \frac{1}{\sqrt{2}}\left(h_{k+1,\mathrm{ru},1}\alpha_{k+1}\frac{\hat{h}_{\mathrm{br},22}}{\sqrt{2}}z^{*2}_{k,\mathrm{br}}\right) + z^1_{k+1,\mathrm{ru}}\ .
\end{aligned} \quad (5.27)
$$

From Eq. (5.26) the following relation can be found

$$
\frac{\sigma^2_{y_{\mathrm{ru},k}}}{\sigma^2_n} = 1 + \frac{1}{2\sigma^2_n}|h_{k,\mathrm{ru},1}|^2\alpha^2_k\Gamma^2_k + \alpha^2_k\Gamma_k\Gamma_{k,\mathrm{ru}}. \quad (5.28)
$$

Equation (5.28) relates the variance of the individual noises at the RN or UT and the variance of the overall received signal at the UT in Phase II. As shown in Eq. (5.21) the noise terms at both antennas have equal variances. For SFBC decoding, the knowledge of the noise variance is strictly not needed, even if we consider the variance conditioned to the realisation of the BS-RN channels in the equalisation coefficients. However, if s_k and s_{k+1} or symbols

of the pairs of codewords were transmitted in different branches, then for optimal channel decoding the use of the different variances would be needed for soft decision. The variance of the overall noise conditioned to the channel realisation is given by

$$\sigma^2_{k,\mathrm{t}} = \alpha^2_k \Gamma_k \Gamma_{k,\mathrm{ru}} \sigma^2_n + \sigma^2_n \ , \text{where } \Gamma_{k,\mathrm{ru}} = \sum_{g=1}^{G} \left| \hat{h}_{k,\mathrm{ru}g} \right|^2 \frac{1}{G}, \text{for } G = 1,\ 2. \tag{5.29}$$

Since the terms $\alpha_k \Gamma_k$, as discussed in the next section, do not vary much it would be reasonable the consider of their average, as it is proposed and computed in the following section.

Concerning the estimation, it is clear that if different pilots are affected by noise terms with different variances this should have some impact in the estimation performance. However, for the same reasons pointed out above since the terms $\alpha_k \Gamma_k$ do not vary significantly (for most of the E_b/N_0 range of interest) it is reasonable to consider their average, as shown in Appendix A, for particular case of estimates corrupted by independent Gaussian noise with different variances.

The soft-decision variables related to Eq. (5.24) - Eq. (5.24) are expressed by

$$S_{k,\mathrm{ru}} = \mathcal{G}^*_{k,\mathrm{ru},1} y_{k,\mathrm{ru}} + \mathcal{G}_{k+1,\mathrm{ru},2} y^*_{k+1,\mathrm{ru}} \ , \tag{5.30}$$

$$S_{k+1,\mathrm{ru}} = -\mathcal{G}_{k,\mathrm{ru},2} y^*_{k,\mathrm{ru}} + \mathcal{G}^*_{k+1,\mathrm{ru},1} y_{k+1,\mathrm{ru}} \ , \tag{5.31}$$

where the MRC equalisation coefficients are given by $\mathcal{G}_{k,\mathrm{ru},g} = \alpha_k \Gamma_k \hat{h}_{k,\mathrm{ru}g}$, for $g = 1,\ 2$. Therefore, for $G = 2$ the soft-decision variable can expressed by

$$\begin{aligned} S_{k,\mathrm{ru}} = {} & \alpha_k \Gamma_k \Gamma_{k,\mathrm{ru}} s_k + \alpha_k \Gamma_{k,\mathrm{ru}} h^*_{\mathrm{br},11} z^1_{k,\mathrm{br}} + \alpha_k \Gamma_{k,\mathrm{ru}} h_{\mathrm{br},21} z^{1*}_{k+1,\mathrm{br}} + \\ & \alpha_k \Gamma_{k,\mathrm{ru}} h^*_{\mathrm{br},12} z^2_{k,\mathrm{br}} + \alpha_k \Gamma_{k,\mathrm{ru}} h_{\mathrm{br},22} z^{2*}_{k+1,\mathrm{br}} + h_{\mathrm{ru},1} z^1_{k,\mathrm{ru}} + h_{\mathrm{ru},2} z^{1*}_{k+1,\mathrm{ru}} \ . \end{aligned} \tag{5.32}$$

$$\begin{aligned} S_{k+1,\mathrm{ru}} = {} & \alpha_{k+1} \Gamma_{k+1} \Gamma_{k+1,\mathrm{ru}} s_{k+1} + \alpha_{k+1} \Gamma_{k+1,\mathrm{ru}} h^*_{\mathrm{br},11} z^1_{k+1,\mathrm{br}} - \alpha_{k+1} \Gamma_{k+1,\mathrm{ru}} h_{\mathrm{br},21} z^{1*}_{k,\mathrm{br}} + \\ & \alpha_{k+1} \Gamma_{k+1,\mathrm{ru}} h^*_{\mathrm{br},12} z^2_{k+1,\mathrm{br}} - \alpha_{k+1} \Gamma_{k+1,\mathrm{ru}} h_{\mathrm{br},22} z^{2*}_{k,\mathrm{br}} + h^*_{\mathrm{bu},1} z^1_{k+1,\mathrm{ru}} - h_{\mathrm{bu},2} z^{1*}_{k,\mathrm{ru}} \ . \end{aligned} \tag{5.33}$$

After performing the equalisation in Phase II, the UT combines the signals received from the RN and the BS. By performing this combining, the diversity of the relay path is exploited. This processing is conducted by taking into account $S_{k,\mathrm{bu}}$ and $S_{k,\mathrm{ru}}$ with ensure optimal

equalisation and MRC combining. The result corresponds to the variable to be hard-decoded.

5.5 Parameters and Channel Estimates

According to the aforementioned scenario, in Phase I the involved links BS-RN and BS-UT correspond to point-to-point links and therefore, can be estimated by conventional estimators either at the RN or UT. However, in Phase II for equalisation purpose at the UT, it is necessary to estimate the variance of the overall noise and for the RN-UT links it is necessary to know the characteristics of the channels BS-RN and the equivalent channel BS-RN-UT, i.e., $h_{k,\mathrm{e},g} = \alpha_k \Gamma_k h_{k,\mathrm{ru},g}$.

5.5.1 Computing the Variance of the Overall Noise

Considering that the UT can estimate the equivalent channels $h_{k,\mathrm{e},g} = \alpha_k \Gamma_k h_{k,\mathrm{ru},g}$ it cannot individually estimate the parameters α_k, Γ_k and $h_{k,\mathrm{br},qg}$ that are required in the computation of the variance of the overall noise, as presented in Eq. (5.29).

In order to overcome such a shortcoming, it is assumed that UT has knowledge of the second moment of the expected value of all channels and therefore, it is proposed the use of the noise variance unconditioned to the channel realisation, σ_{t}^2, instead of its instantaneous value $\sigma_{k,\mathrm{t}}^2$. Consequently, σ_{t}^2 is referred as the expectation value of the variance of the overall noise.

Considering that α_k is given by Eq. (5.17), for $Q = 2$ and $G = 1$, Eq. (5.29) can be expressed by

$$\sigma_{\mathrm{t}}^2 \approx \frac{1}{\mathbb{E}\left\{\Gamma_k^2\right\} + \mathbb{E}\left\{\Gamma_k\right\}\sigma_n^2} \mathbb{E}\left\{\Gamma_k\right\} \mathbb{E}\left\{\left|\hat{h}_{k,\mathrm{ru}}\right|^2\right\} \sigma_n^2 + \sigma_n^2 \tag{5.34}$$

$$\sigma_{\mathrm{t}}^2 \approx \frac{\mathbb{E}\left\{\frac{1}{2}\sum_{q=1}^{Q}\sum_{g=1}^{G}\left|\hat{h}_{k,\mathrm{br},qg}\right|^2\right\} \mathbb{E}\left\{\left|\hat{h}_{k,\mathrm{ru}}\right|^2\right\} \sigma_n^2}{\mathbb{E}\left\{\left(\frac{1}{2}\sum_{q=1}^{Q}\sum_{g=1}^{G}\left|\hat{h}_{k,\mathrm{br},qg}\right|^2\right)^2\right\} + \mathbb{E}\left\{\frac{1}{2}\sum_{q=1}^{Q}\sum_{g=1}^{G}\left|\hat{h}_{k,\mathrm{br},qg}\right|^2\right\}\sigma_n^2} + \sigma_n^2. \tag{5.35}$$

Correspondingly, for $Q = 2$ and $G = 2$, σ_{t}^2 is given by

$$\sigma_{\mathrm{t}}^2 \approx \frac{1}{\mathbb{E}\left\{\Gamma_k^2\right\} + \mathbb{E}\left\{\Gamma_k\right\}\sigma_n^2} \mathbb{E}\left\{\Gamma_k\right\} \mathbb{E}\left\{\Gamma_{k,\mathrm{ru}}\right\} \sigma_n^2 + \sigma_n^2 \tag{5.36}$$

$$\sigma_{\mathrm{t}}^2 \approx \frac{\mathbb{E}\left\{\frac{1}{2}\sum_{q=1}^{Q}\sum_{g=1}^{G}\left|\hat{h}_{k,\mathrm{br},qg}\right|^2\right\}\mathbb{E}\left\{\frac{1}{2}\sum_{g=1}^{G}\left|\hat{h}_{k,\mathrm{ru},g}\right|^2\right\}\sigma_n^2}{\mathbb{E}\left\{\left(\frac{1}{2}\sum_{q=1}^{Q}\sum_{g=1}^{G}\left|\hat{h}_{k,\mathrm{br},qg}\right|^2\right)^2\right\}+\mathbb{E}\left\{\frac{1}{2}\sum_{q=1}^{Q}\sum_{g=1}^{G}\left|\hat{h}_{k,\mathrm{br},qg}\right|^2\right\}\sigma_n^2}+\sigma_n^2. \tag{5.37}$$

For $Q=2$ and $G=1$, $\mathbb{E}\left\{\frac{1}{2}\sum_{q=1}^{Q}\sum_{g=1}^{G}\left|\hat{h}_{k,\mathrm{br},qg}\right|^2\right\}=1$ and $\mathbb{E}\left\{\left(\frac{1}{2}\sum_{q=1}^{Q}\sum_{g=1}^{G}\left|\hat{h}_{k,\mathrm{br},qg}\right|^2\right)^2\right\}=1.5$. Similarly for $Q=2$ and $G=2$, $\mathbb{E}\left\{\frac{1}{2}\sum_{q=1}^{Q}\sum_{g=1}^{G}\left|\hat{h}_{k,\mathrm{br},qg}\right|^2\right\}=2$ and $\mathbb{E}\left\{\frac{1}{2}\sum_{g=1}^{G}\left|\hat{h}_{k,\mathrm{ru},qg}\right|^2\right\}=1$ as well as $\mathbb{E}\left\{\left(\frac{1}{2}\sum_{q=1}^{Q}\sum_{g=1}^{G}\left|\hat{h}_{k,\mathrm{br},qg}\right|^2\right)^2\right\}=5$, assuming $\mathbb{E}\left\{|h_k|^2\right\}=1$. Hence, Eq. (5.35) and Eq. (5.37) follows the expressions below, respectively.

$$\sigma_{\mathrm{t}}^2 \approx \frac{\sigma_n^2}{1.5+\sigma_n^2}+\sigma_n^2, \text{ for G = 1.} \tag{5.38}$$

$$\sigma_{\mathrm{t}}^2 \approx \frac{2\sigma_n^2}{5+2\sigma_n^2}+\sigma_n^2, \text{ for G = 2.} \tag{5.39}$$

5.5.2 Estimating the Equivalent Channel

The UT is unable to estimate α_k and Γ_k as these factors depend on the channels $h_{k,\mathrm{br},qg}$ which the UT is unable to estimate as well, estimating the channels based on the unitary pilots transmitted by the RN does not provide the proper equivalent channel. Instead, it provide $h_{k,\mathrm{ru},g}$.

In order to estimate the equivalent channel it is proposed a transmission scheme that consists on transmitting the factor $\alpha_k\Gamma_k$ at the pilot subcarriers as depicted in Figure 5.6 for $N_f=4$, where the pilot subcarriers are represented in dark and light grey and $\hat{s}_k$ represents the soft-decision variable transmitted by the RN in k data subcarriers, for $k=1,\ 2,\ 3,\ 5,\ 6,\ 7,\cdots$. The parameters $\alpha_k\Gamma_k$ are not constant over the subcarriers and they depend on the channels $h_{k,\mathrm{br},qg}$ that are estimated at the RN. Consequently, in the signal transmitted by the RN ,the amplitude of the pilots are variable. According to [58]-[59] for the LS estimation the minimum MSE is obtained when the pilots in frequency domain are equispaced and equipowered and as

presented in Section 3.4.2 the MMSE filtering is performed after the LS estimation.

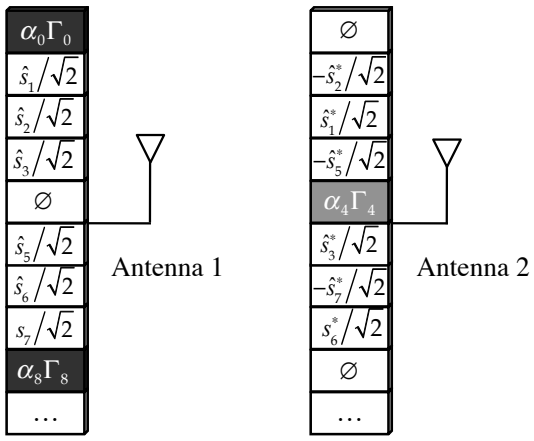

Figure 5.6: Symbols arrangement per antenna at the RN.

In a pilot-based transmission, equispaced and equipowered pilots are multiplexed within data symbols, such that the transmitted vector is devised to convey pilot and data in different sets of subcarriers. The pilots are arranged in the frequency domain such that the pilot separation in frequency dimension is N_f, as shown in Figure 5.7 a), where the sphere marks represent pilots whereas diamond marks represent data components. The corresponding vector in the time domain presents pilot and data symbols overlapped as well as the pilots separated by N_t where $N_t = K/N_f$, being K the number of subcarriers, as shown in Figure 5.7 b).

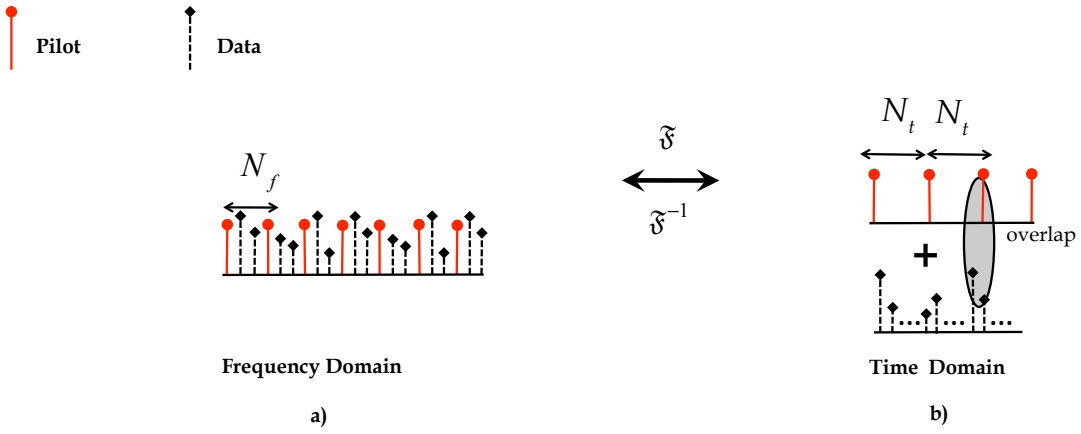

Figure 5.7: Equidistant and equipowered pilots.

The situation is different if equispaced and non-equipowered pilots are considered, according to the Figure 5.8 a). In such case, if in the frequency domain the pilot separation

in frequency dimension is N_f, the corresponding time domain vector presents extra samples among the pilots that are separated by N_t and overlapped data symbols, according to Figure 5.8 b).

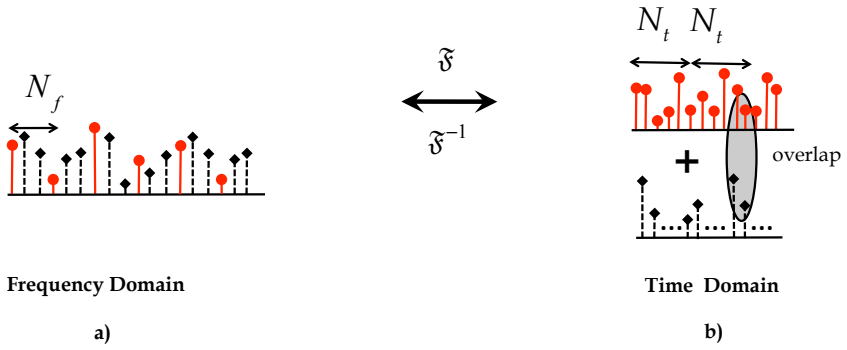

Figure 5.8: Equidistant and non-equipowered pilots.

According to the proposed transmission, $\alpha_k \Gamma_k$ corresponds to the equispaced and non-equipowered pilots. If the MMSE estimator is implemented in the time domain, the resulting estimation may present degradation stemmed from the new pilots, according to the Figure 5.9.

Figure 5.9 represents the receiver side where the received signal in the time domain presents undesired samples among the pilots that are separated by N_t and overlapped data symbols. In order to estimate the channel the received signal is convolved with the pilot signal, i.e., a pulse train with unitary amplitude. Such operation corresponds to multiply by 1 the subcarriers at frequencies N_f as by design these are the positions reserved to the pilots thus, the data component in the received signal vanishes. As result the replicas of the CIR are spread and that may compromise the conventional MMSE performance, since this estimator was designed assuming the pilots were equispaced and equipowered. Therefore, it is important to assess the impact of using $\alpha_k \Gamma_k$ as pilots.

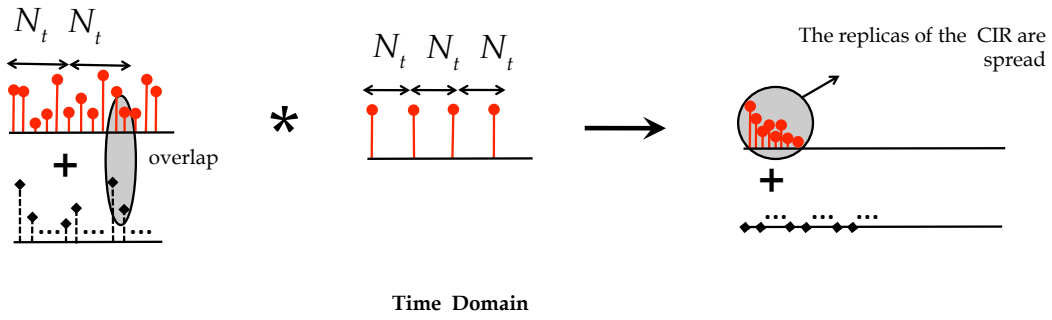

Figure 5.9: Equispaced and non-equipowered pilots and the corresponding CIR.

In order to understand how much can be the fluctuation in terms $\alpha_k\Gamma_k$, we compute it for different channels and schemes, $2 \times 1 \times 1$ and $2 \times 2 \times 1$, as shown in Figure 5.10 that presents the behaviour of $\alpha_k\Gamma_k$ per subcarrier.

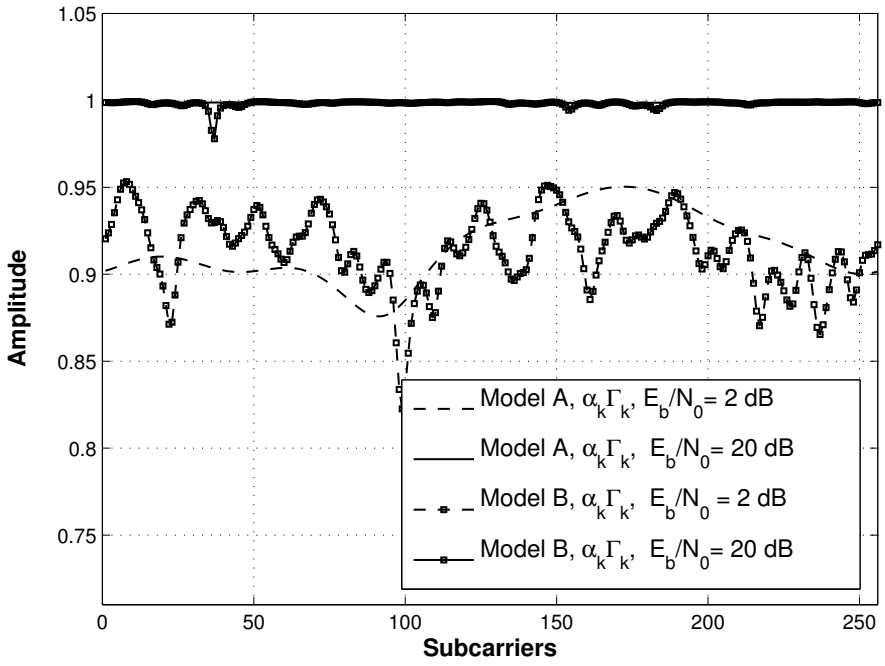

Figure 5.10: $\alpha_k\Gamma_k$ per subcarrier.

In Figure 5.10 the channels follow ITU Pedestrian Model A and B at 10 km/h, where continuous lines represent $E_b/N_0 = 20$ dB, dashed lines represent $E_b/N_0 = 2$ dB. The lines with no marks represent the Model A whereas the lines with square marks represent the Model B. In both cases, for the scheme $2 \times 2 \times 1$ at $E_b/N_0 = 20$ dB, the amplitudes of $\alpha_k\Gamma_k$ are close

to 1 with negligible fluctuation whereas at $E_b/N_0 = 2$ dB, the result is slightly different. Such factor also presents an amplitude close to 1 however, the fluctuation is more tangible. For the scheme $2 \times 1 \times 1$ at $E_b/N_0 = 20$ dB the fluctuation pattern is similar to the scheme $2 \times 2 \times 1$ at $E_b/N_0 = 20$ dB however, at $E_b/N_0 = 2$ dB the fluctuation is much more tangible. Figure 5.10 shows that using $\alpha_k\Gamma_k$ as pilot may have implications in the estimator performance.

The results in Figure 5.10 can be explained according to Eq. (5.40), α_k depends on the noise variance σ_n^2. Accordingly, $\alpha_k\Gamma_k$ tends to one as the noise decreases and it can be approximated by

$$\alpha_k\Gamma_k = \left(\frac{1}{\sqrt{\Gamma_k^2 + \Gamma_k\sigma_n^2}}\right)\Gamma_k \approx \frac{1}{\sqrt{\Gamma_k^2}}\Gamma_k = 1. \tag{5.40}$$

5.5.3 The Impact of Using $\alpha_k\Gamma_k$ as Pilot

The results in the above figure emphasise that using the factor $\alpha_k\Gamma_k$ as pilots may degrade the estimator performance and the degradation is likely to stem from:

- Pilots with some fluctuation in amplitude: The estimator is designed assuming that the amplitude of the pilots is constant. Therefore, if this condition is not verified the replicas are spread as shown in Figure 5.9;
- Decreasing the amplitude of the pilots: The SNR of the pilots is decreased as well;
- The MMSE filter depends on the statistics of the channel BS-RN;

Despite it is considered the MMSE estimator in the time domain in this analysis, the causes presented previously degrade the performance of any other estimator scheme as well. In order to quantify how these effects can degrade the estimator's performance, each effect is evaluated separately in a SISO system, since the BS-RN and RN-UT channels correspond to point-to-point links.

Firstly, it is evaluated the impact of the fluctuation of the pilot amplitude, i.e., the pilots per subcarrier assume random values. It is considered that the pilots (originally with unitary amplitude) have their amplitude disturbed by a noise with zero mean and variance equal to $\sigma_{\alpha\Gamma}^2 = \mathrm{E}\left\{|1 - \alpha_k\Gamma_k|^2\right\}$, where $\sigma_{\alpha\Gamma}^2$ quantifies how far $\alpha_k\Gamma_k$ would be from the pilots with unitary amplitude. It can be expressed $\sigma_{\alpha\Gamma}^2$ as:

$$\sigma_{\alpha\Gamma}^2 = 1 + \mathbb{E}\left\{|\alpha_k\Gamma_k|^2\right\} - 2\mathbb{E}\left\{|\alpha_k\Gamma_k|\right\}. \tag{5.41}$$

Therefore, the pilots have some fluctuation in amplitude that depend on $\alpha_k \Gamma_k$ and are equal to $p_{\alpha\Gamma} = 1 + z$, where z is noise $\mathcal{CN}(0, \sigma^2_{\alpha\Gamma})$. The performance of an OFDM SISO system whereby the pilots correspond to $p_{\alpha\Gamma}$ is shown in Figure 5.11 (dash line). For reference, it is also included the SISO performance for unitary pilots, p_1. Since this analysis focus on the degradation of the estimator performance, the results are presented in terms of the normalised MSE and both results consider the ITU Pedestrian Model A and B. Figure 5.11 shows that the variation in the pilot amplitude causes a penalty for low values of E_b/N_0. For $E_b/N_0 = 1$ dB, the difference in performance between the results is not significant and the results converge asymptotically.

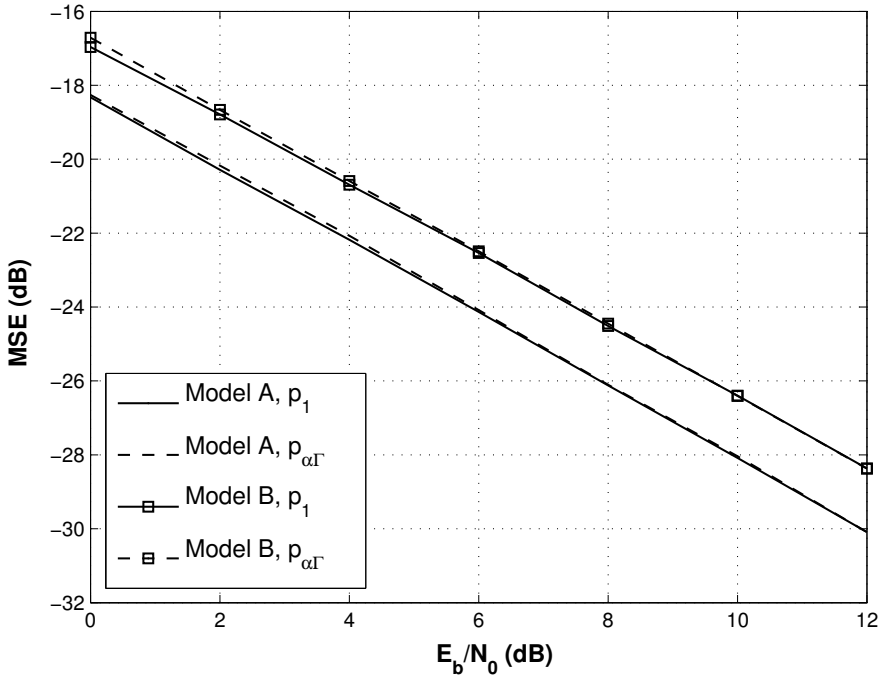

Figure 5.11: MSE performance: Pilots with fluctuation in amplitude.

Second, it is analysed the decreasing in the pilot amplitude. In order to evaluate such an effect it is also considered the ITU Pedestrian Model A and B and an OFDM SISO system where the transmitted pilots assume non-unitary yet constant values for all pilot subcarriers, p_c. The results assume a normalised MSE with regards to the pilot amplitude and are shown in Figure 5.12 and Figure 5.13, for Model A and B, respectively. For reference it is included the SISO performance for unitary pilots, p_1, as well. Both results show that the performances

present a constant shift in the MSE when the pilots are not unitary. The MSE decreases as SNR of the pilots decreases therefore, such shift stem from the normalisation in the MSE. Actually, assuming a MSE without the normalisation, with regards the pilot amplitude, the results are coincident hence, such effect does not impact the estimator performance. The difference in performances in Figure 5.12 and Figure 5.13 are related to selectivity of the channel Model B that is more severe than Model A.

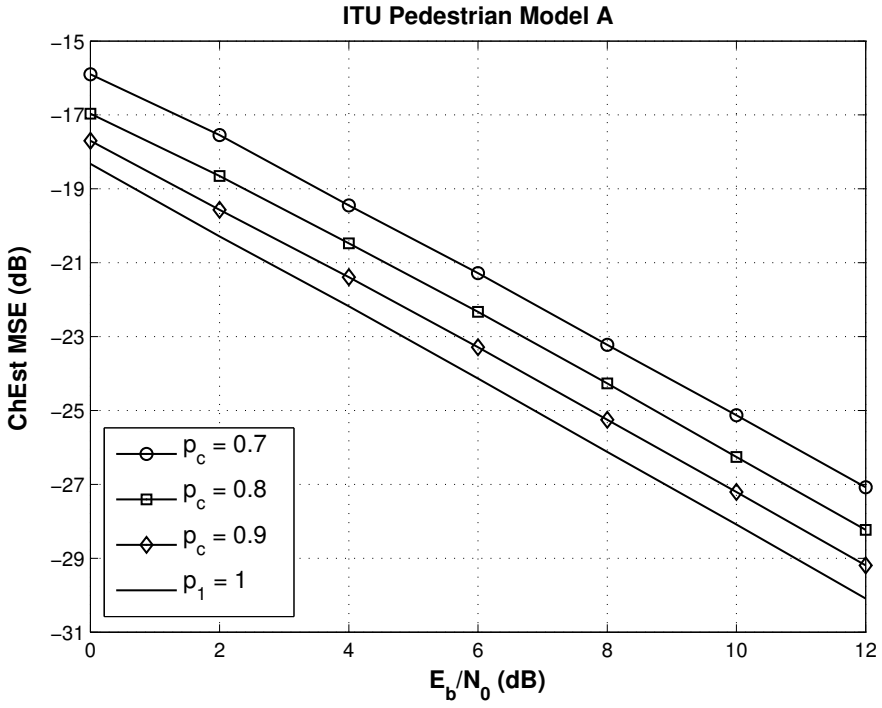

Figure 5.12: MSE performance: pilots with non-unitary yet constant values.

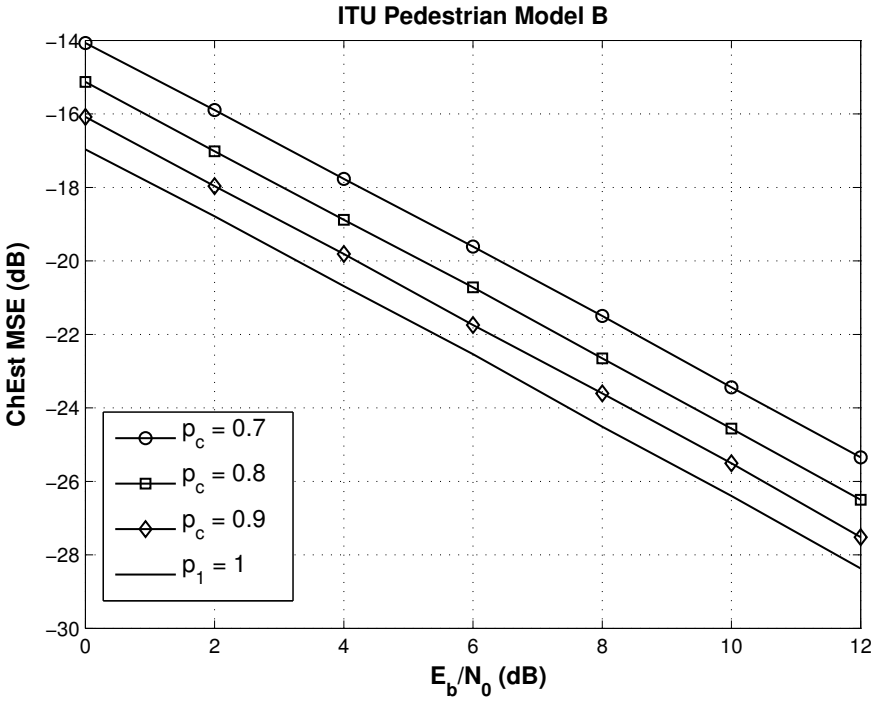

Figure 5.13: MSE performance: pilots with non-unitary yet constant values.

Thirdly, it is analysed the effect regarding the dependence of the MMSE filter on the link BS-RN. Hereafter, for simplicity the index g related to G is dropped as the channels RN-UT are estimated individually. Therefore, the individual equivalent channel is referred as $h_{k,\mathrm{e}} = \alpha_k \Gamma_k h_{k,\mathrm{ru}}$.

Let us recall the expressions the describe the MMSE implementation in the time domain that are

$$\widetilde{\mathbf{W}}_{\mathrm{mmse}} = \mathbf{R}_{\tilde{h}\hat{\tilde{h}}} \mathbf{R}^{-1}_{\hat{\tilde{h}}\hat{\tilde{h}}}, \tag{5.42}$$

where the autocorrelation matrix $N_t \times N_t$ is given by

$$\mathbf{R}_{\hat{\tilde{h}}\hat{\tilde{h}}} = \mathbb{E}\left\{\hat{\tilde{\mathbf{h}}}\hat{\tilde{\mathbf{h}}}^H\right\} = \mathbf{R}_{\tilde{h}\tilde{h}} + \frac{\sigma_n^2}{N_t}\mathbf{I}_{N_t}, \tag{5.43}$$

and the cross-correlation matrix $N_t \times N_t$ is expressed according to

$$\mathbf{R}_{\tilde{\hat{h}}\hat{\tilde{h}}} = \mathbb{E}\left\{\tilde{\mathbf{h}}\hat{\tilde{\mathbf{h}}}^H\right\} = \mathbf{R}_{\tilde{h}\tilde{h}}, \tag{5.44}$$

where the diagonal autocorrelation matrix $N_t \times N_t$ follows

$$\mathbf{R}_{\tilde{h}\tilde{h}} = \text{diag}\left(\sigma^2_{h,0} \;\; \sigma^2_{h,1} \;\; \cdots \;\; \sigma^2_{h,L-1} \;\; \cdots \;\; 0\right). \tag{5.45}$$

As the realisation of the channels BS-RN does not depend on the realisation of the channels RN-UT, the factor $\alpha_k\Gamma_k$ and the $h_{k,\text{ru}}$ are independent. For simplicity let us refer $\alpha_k\Gamma_k$ as ϑ_k hence, $h_{k,\text{e}} = \vartheta_k h_{k,\text{ru}}$ follows

$$\mathbb{E}\Big\{h_{k,\text{e}}h^H_{k+1,\text{e}}\Big\} = \mathbb{E}\Big\{(\vartheta_k h_{k,\text{ru}})(\vartheta_{k+1}h_{k+1,\text{ru}})^H\Big\} = \mathbb{E}\Big\{\vartheta_k\vartheta^H_{k+1}h_{k,\text{ru}}h^H_{k+1,\text{ru}}\Big\} \tag{5.46}$$

$$\mathbb{E}\Big\{h_{k,\text{e}}h^H_{k+1,\text{e}}\Big\} = \mathbb{E}\Big\{\vartheta_k\vartheta^H_{k+1}\Big\}\mathbb{E}\Big\{h_{k,\text{ru}}h^H_{k+1,\text{ru}}\Big\} = R_\vartheta R_{h_{\text{ru}}} = R_{h_{\text{e}}} \tag{5.47}$$

Correspondingly, $\mathbf{R}_{h_{\text{e}}} = \mathbf{R}_\vartheta\mathbf{R}_{h_{\text{ru}}}$ and therefore, in the time domain $\mathbf{R}_{h_{\text{e}}}$ corresponds to $\mathbf{R}_{\tilde{h}_{\text{e}}} = \mathbf{F}^{-1}\mathbf{R}_{h_{\text{e}}}\mathbf{F}$ such that, $\mathbf{R}_{\tilde{h}_{\text{e}}} = \mathbf{R}_{\tilde{\vartheta}}\mathbf{R}_{\tilde{h}_{\text{ru}}}$.

Therefore, the MMSE filter in Eq. (5.42) for the equivalent channel can be expressed according to

$$\widetilde{\mathbf{W}}_{\text{mmse,e}} = \mathbf{R}_{\tilde{h}_{\text{e}}\hat{\tilde{h}}_{\text{e}}}\mathbf{R}^{-1}_{\hat{\tilde{h}}_{\text{e}}\hat{\tilde{h}}_{\text{e}}}, \tag{5.48}$$

such that the corresponding cross-correlation matrix is given by

$$\mathbf{R}_{\hat{\tilde{h}}_{\text{e}}\hat{\tilde{h}}_{\text{e}}} = \mathbb{E}\left\{\hat{\tilde{\mathbf{h}}}_{\text{e}}\hat{\tilde{\mathbf{h}}}^H_{\text{e}}\right\} = \mathbf{R}_{\tilde{h}_{\text{e}}\tilde{h}_{\text{e}}} + \frac{\sigma^2_n}{N_t}\mathbf{I}_{N_t} \tag{5.49}$$

and the cross-correlation matrix is expressed according to

$$\mathbf{R}_{\tilde{h}_{\text{e}}\hat{\tilde{h}}_{\text{e}}} = \mathbb{E}\Big\{\tilde{\mathbf{h}}_{\text{e}}\hat{\tilde{\mathbf{h}}}^H_{\text{e}}\Big\} = \mathbf{R}_{\tilde{h}_{\text{e}}\tilde{h}_{\text{e}}}, \tag{5.50}$$

Therefore, MMSE filter for the equivalent channel may be express as

$$\widetilde{\mathbf{W}}_{\text{mmse,e}} = \mathbf{R}_{\hat{\tilde{\vartheta}}\hat{\tilde{\vartheta}}}\mathbf{R}_{\tilde{h}_{\text{ru}}\tilde{h}_{\text{ru}}}\left(\mathbf{R}_{\hat{\tilde{\vartheta}}\hat{\tilde{\vartheta}}}\mathbf{R}_{\tilde{h}_{\text{ru}}\tilde{h}_{\text{ru}}} + \frac{\sigma^2_n}{N_t}\mathbf{I}_{N_t}\right)^{-1}. \tag{5.51}$$

As previously presented in Eq. (5.40), the factor $\alpha_k\Gamma_k$ tends asymptotically to one. Examining the MMSE filter expressions, it is also expected that Eq. (5.51) tends asymptotically to Eq. (3.23) as it depends on $\alpha_k\Gamma_k$. As it is impractical to obtain $\mathbf{R}_{\hat{\tilde{\vartheta}}\hat{\tilde{\vartheta}}}$ analytically, several

simulation were performed taking into account such a matrix and the noise variance σ_n^2 considering the channels models ITU Pedestrian Model A and B. The results in Figure 5.14 show that $\mathbf{R}_{\hat{\vartheta}\hat{\vartheta}}$ is not diagonal and, for moderate σ_n^2, the maximum element off-diagonal are close to -40 dB which corresponds to negligible values. Therefore, implementing the MMSE filter according to Eq. (5.51) does not contribute to improve the estimator performance and increases the system complexity.

According to the results in Figure 5.11, Figure 5.12 and Figure 5.13 in terms of MSE, transmitting pilots with non-constant and non-unitary values brings minor penalties, for low values of E_b/N_0, without increasing the estimator complexity. The analyses of the aforementioned effects show that the MMSE can be use in the EF scenario without compromising its performance. The analysis can be applied to any other channel without loss of generality. However, in terms of the overall system performance, better results are expected for less selective channels.

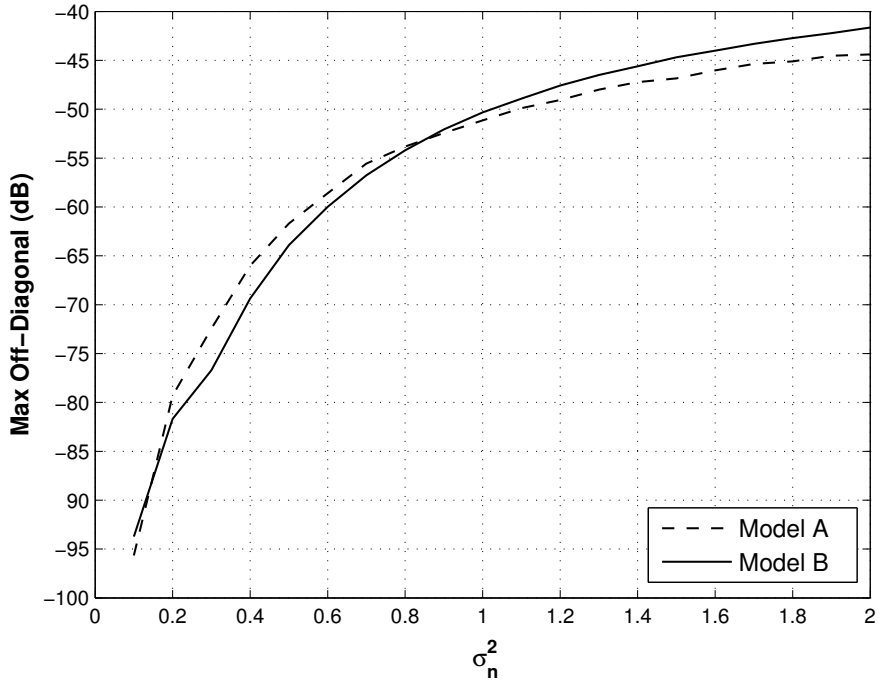

Figure 5.14: Maximum element off-diagonal of $\mathbf{R}_{\hat{\vartheta}\hat{\vartheta}}$.

5.6 Performance Assessment

5.6.1 System Parameters

In order to evaluate the performance of the presented relay assisted schemes it is considered a typical scenario and the simulation parameters are summarised in Table 5.2. The channel estimation performance is presented in terms of MSE and E_b/N_0.

There are considered the following pilot separations in frequency dimension $N_f = 4$ and $N_v = 1$. It is considered the channel model ITU Pedestrian B with the tap delays modified according to the sampling interval. Both the UT and the RN were considered as mobile terminals hence, the Doppler effect was considered in both links BS - RN and RN - UT.

Table 5.2: Simulation parameters

Modulation	QPSK
Carrier Frequency	2 GHz
Sampling Interval	89.3 ns
# **Subcarriers**	1024
OFDM frame	9 symbols
Channel Taps	6 taps
Channel Statistics	Identical
Velocity	10 km/h

This analysis focus on the $2 \times 1 \times 1$ and $2 \times 2 \times 1$ scenarios and in the simulations it is assumed that the channels are uncorrelated, the receiver is perfectly synchronised and the insertion of a long enough cyclic prefix in the transmitter ensures that the orthogonality of the subcarriers is maintained after transmission.

The normalised MSE performance of the cooperative channel is evaluated by averaging the MSE's of the direct, MSE_h, and the relaying channel, MSE_{h_e}. Since the direct channel corresponds to a MISO its MSE is obtained also by averaging the MSE of the B-U channels. The MSE of the relaying channel corresponds to the MSE of the equivalent channel which is calculated by averaging the individual channels MSE. Thus, the resulting MSE, i.e. the MSE

of the cooperative channel, is given by:

$$\text{MSE} = \frac{1}{2}\left(\frac{1}{2}\left(\text{MSE}_h\right) + \text{MSE}_{h_\text{e}}\right). \tag{5.52}$$

In order to assess the acquisition of the variance of the overall noise, it is depicted in Figure 5.15 the system BER performance assuming that the perfect channel estimation information is available at the receiver. For reference it is considered as well as the cases where the variance of the overall noise is the conditioned one and the average ones. According to the results, the performance penalty of using the averaged noise variance is less than 0.8 dB which is a tolerable penalty to pay in order to obtain the variance of the overall noise regarding the a low complexity implementation. Therefore, it is considered the use of σ_t in our schemes.

In order to validate the use of the proposed scheme, some channel estimation simulations were performed using the MMSE estimator in the time domain. Figure 5.16 depicts the BER attained with perfect CSI and the MMSE estimator when the RN was employing the proposed pilots. The difference of performance is minimal in both cases, specially for $2 \times 2 \times 1$, and in the $2 \times 1 \times 1$ scheme which is in the worst case this difference is 0.5 dB.

Figure 5.17 depicts the normalised MSE's performance of the $2 \times 1 \times 1$ scheme. These results show that the proposed pilot allocation, at the RN allows the estimator satisfactory estimate the required channel. When comparing the channel estimator for the link with relay against the one of the direct link, there is some penalty which accounts for the additional noise added at the relay. The relative penalty decreases as E_b/N_0 increases and can be verified to converge to 2.2 dB which is the factor of 3/5 that relates the overall and individual noises in the asymptotic case, according to Eq. (5.38). According to Figure 5.18, this penalty is smaller in the $2 \times 2 \times 1$ scheme, since the factor $\alpha_k \Gamma_k$ presents a flatter behaviour.

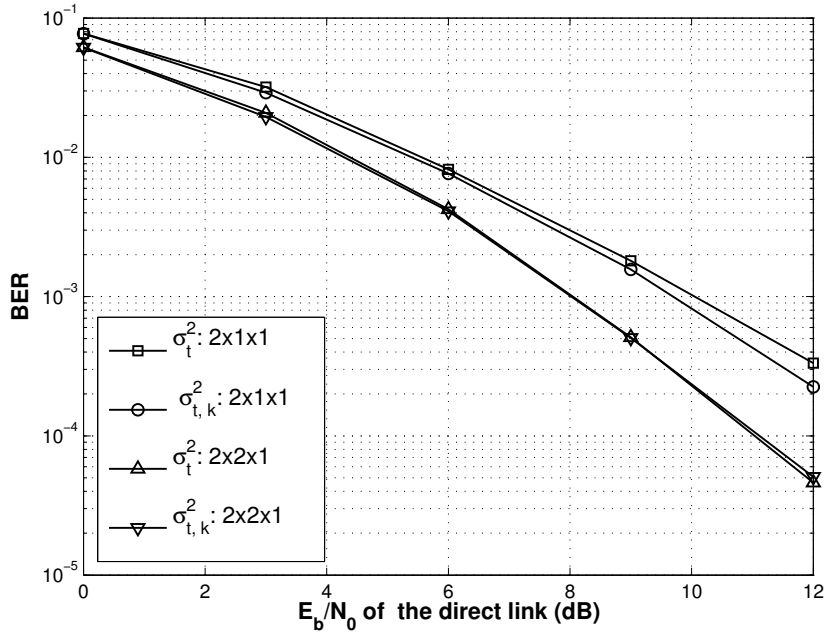

Figure 5.15: System BER performance: Impact of using σ_{t}^2 and $\sigma_{k,\mathrm{t}}^2$.

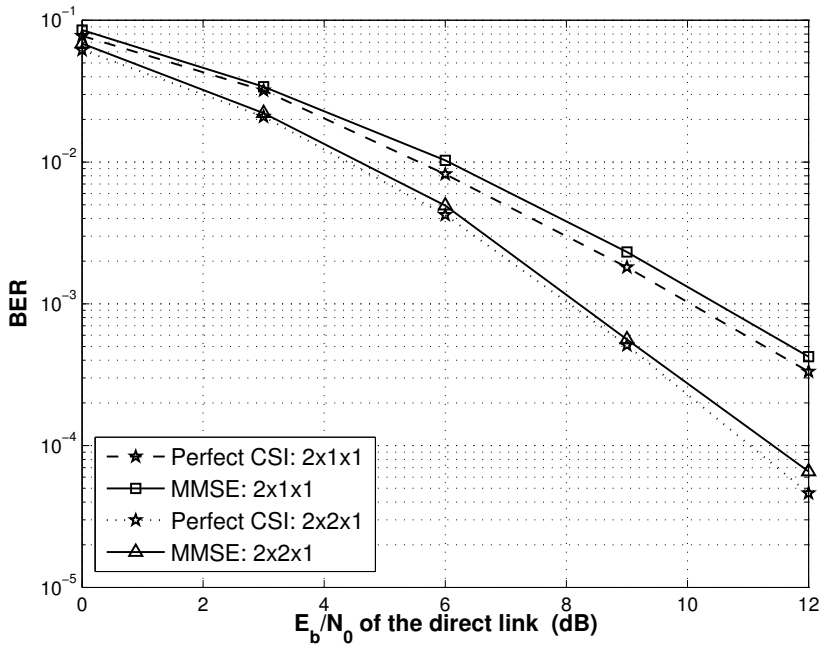

Figure 5.16: System BER performance: Perfect channel knowledge and channel estimates.

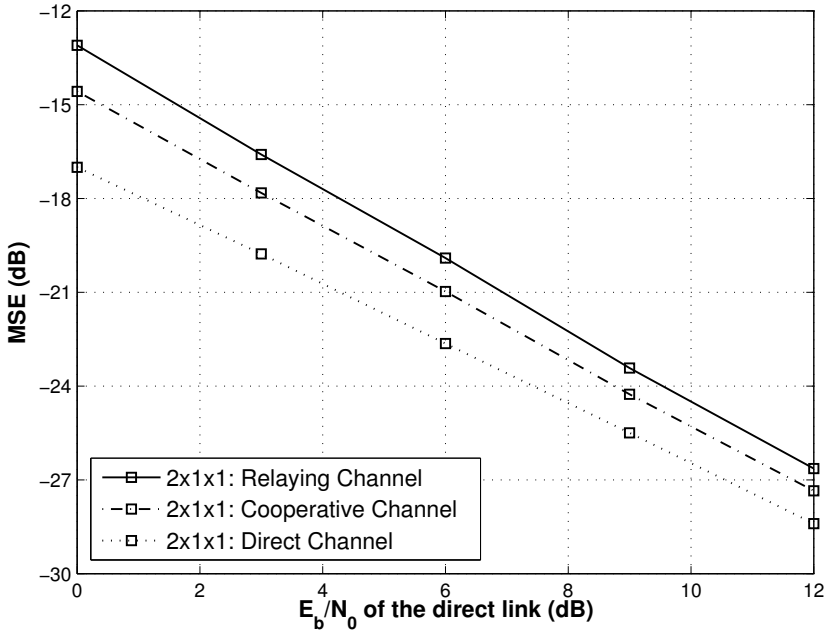

Figure 5.17: Channel estimation MSE performance: RA Scheme $2 \times 1 \times 1$.

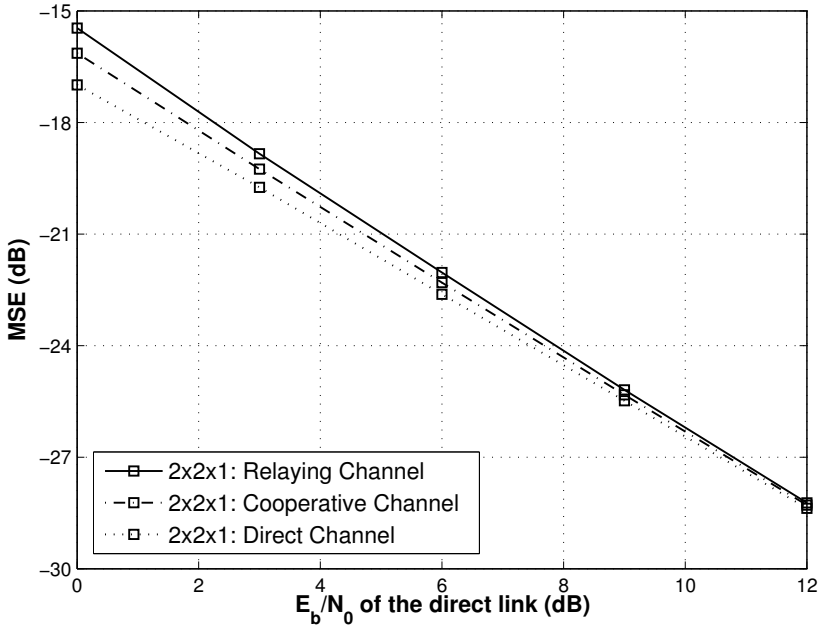

Figure 5.18: Channel estimation MSE performance: RA Scheme $2 \times 2 \times 1$.

5.7 Conclusion

In this chapter it was considered two problems of channel estimation in a scenario where spatial diversity provided by SFBC is complemented with the use of a half-duplex relay node employing the EF protocol. The channel estimation scheme was based on the MMSE and it was proposed a scheme where the estimates of the BS-RN links are inserted in the pilot positions in the RN-UT transmission. For the estimation of the equivalent channel, i.e. BS-RN-UT, at the destination it was analysed several simplifying options enabling the operation of channel estimation namely the use of average statistics for the overall noise and the impact of the fluctuations in the amplitude of the equivalent channel. In the RA $2 \times 1 \times 1$ scheme is shown that in the asymptotic case of high E_b/N_0, and equal noise statistics at the relay and destination the penalty in the estimation equivalent channel is 2.2 dB relatively to the case of a direct link using the same pilot density. This difference in performance is smaller in the RA $2 \times 2 \times 1$ scheme since the equivalent channel presents a flatter behaviour. The resulting estimation was assessed in terms of the BER of the overall link through simulation with channel representative of a real scenario and the results have shown its effectiveness despite a moderate complexity.

Chapter 6

A Data-Aided Channel Estimation Method for OFDM Relay-Assisted

6.1 Introduction

Point-to-point links can explore the information of a specific data in order to improve the channel estimates, such technique is known as data-aided channel estimation [103]-[105]. In some cases, no pilot symbols are sent and only data information is considered to estimate the channel. Such as the work in [103], where channel estimation is performed using pseudo noise sequence and the data obtained from Log-likelihood criterion. The authors in [104] proposed a technique based on cost reference particle filter for combined CIR estimation and phase noise tracking. In [105] was proposed a channel estimation method based on pilot and data information, where the data are estimated using direction of arrivals, direction of departures and path fading coefficients of propagation.

Concerning channel estimation for relay-assisted systems, most of research are based on pilots or training sequences. Nevertheless, the channels in a cooperative scenarios can also be estimated or aided using the energy of the transmitted data [106]-[109]. As such, in [106], a recursive channel estimation method based on the channel coder feedback information and linear interpolation is proposed. [107] proposed an estimator method that obtain initial estimation based on maximum likelihood and improve it via Expectation Maximisation (EM). In [108], the authors proposed an iterative channel estimator based on the EM algorithm to separately estimate the channels BS-RN and RN-UT, that on the initial phase uses a training sequence and after can use the regenerated data. Although not using directly the regenerated data, in [109] superposition of pilots and data was considered and based on the non-Gaussian

nature of the dual-hop relay link, the authors proposed a first-order autoregressive channel model and derived a Kalman filter-based estimator.

The works aforementioned consider single-antenna network elements (source, relay and destination). However, as referred in the previous chapters, in several scenarios namely in the downlink of cellular systems, it is both feasible and beneficial to consider the BS and the RN (if dedicated) with antenna arrays. The analysis presented in the previous chapter considered the EF protocol for RA scenarios. Such a protocol is an alternative to achieve higher diversity in MIMO cooperative schemes. We have shown that, with appropriate pilot-based transmission at the RN, the equivalent channel BS-RN-UT can be estimated at the UT and the optimal equalisation can be performed as well. Nevertheless, relatively to point-to-point link case, the estimates performance present some degradation. The EF MIMO cooperative schemes comply with such demands and the results presented in the previous chapter have motivated further investigation regarding channel estimation. In contrast to the AF cooperative schemes, for which several proposals have been published, channel estimation schemes to improve the EF equivalent channel estimates have not been reported in the literature.

This chapter addresses such a channel and proposes a pilot-data based channel estimation scheme for the EF RA scenario discussed in Chapter 5. The estimation method at the UT consists of two iterations; in the first one, only pilots are used to estimate the channels and the results are used to perform a first decision on the data symbol. Then, in the next iteration, these symbols are used as virtual pilots to improve the channel estimates to be used in the final symbol decision. The MMSE criterion is used in the design of the estimator for both the pilot-based and data-aided. We show that even with the first iteration being inaccurate still there is potential for improving the channel estimates using data.

The remaining of this chapter is organised as follows. In Section 6.2 the system model is recalled and for consistency reasons the key aspects of the studied system are restated as well. Section 6.3 presents the proposed pilot-data aided estimator. The system performance is evaluated in Section 6.4. Finally, some concluding remarks are presented in Section 6.5.

6.2 EF Relay-Assisted System Model

We consider an OFDM transmission and the channel model as described in Section 5.3 and summarised in the following. The power transmitted by the BS and the RN is equally allocated between the two antennas and the data symbol s_k follows the Alamouti mapping rule as described in Table 5.1.

As pilot and data symbols are conveyed in different sets of subcarriers, at the BS and the RN the pilot separations N_v and N_f follow the pattern depicted in Figure 5.2 and the symbols are arranged according to Figure 5.3.

For consistency reasons, the key aspects of the system discussed in Chapter 5 are restated below.

The scenario, shown in Figure 6.1, is referred as $Q \times G \times 1$ where it is considered that $Q = G = 2$. Therefore, the involved links are $h_{\mathrm{br},qg}$, $h_{\mathrm{bu},q}$ and $h_{\mathrm{ru},g}$, for $q = g = 1,\ 2$.

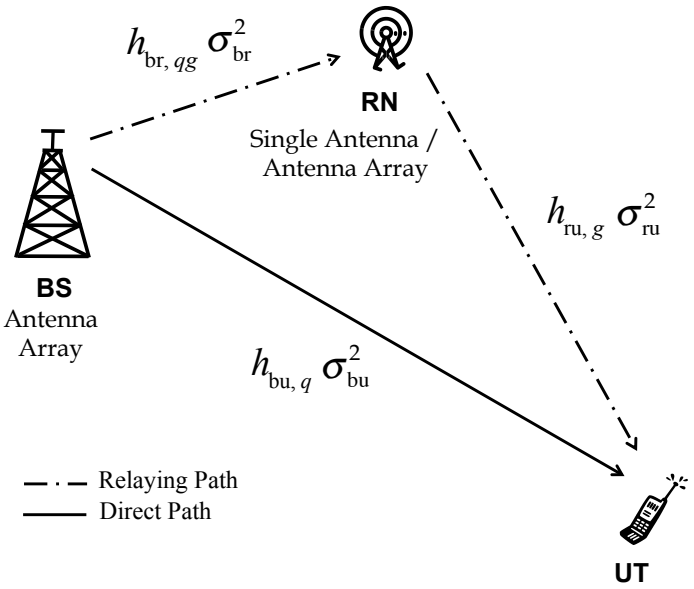

Figure 6.1: EF RA scenario.

It is assumed that the noise components on subcarriers k and $k + 1$ are uncorrelated and the noise terms at a pair of antennas, between two terminals, have equal variances.

Throughout this analysis the subscripts *br*, *bu* and *ru* are related to the links BS-RN, BS-UT and RN-UT, respectively.

Figure 6.2 shows the corresponding block diagram of the studied scenario where the EF half-duplex relaying protocol is employed. The continuous line represents the Phase I whereas the dashed line corresponds to the Phase II. The key variables related to the each phase are shown in the block diagram as well. s and p are the data symbols and the pilots transmitted in the broadcast phase whereas S_{br} and S_{bu} are the soft decision variables related to this phase. The normalisation factor is represented by α and $\alpha\Gamma$ corresponds to the information that is conveyed in the pilots subcarriers in Phase II and S_{bu} is the soft-decision variable that is de-mapped in this phase. The expressions related to each variable are presented in the following sections, according to the phase of the protocol.

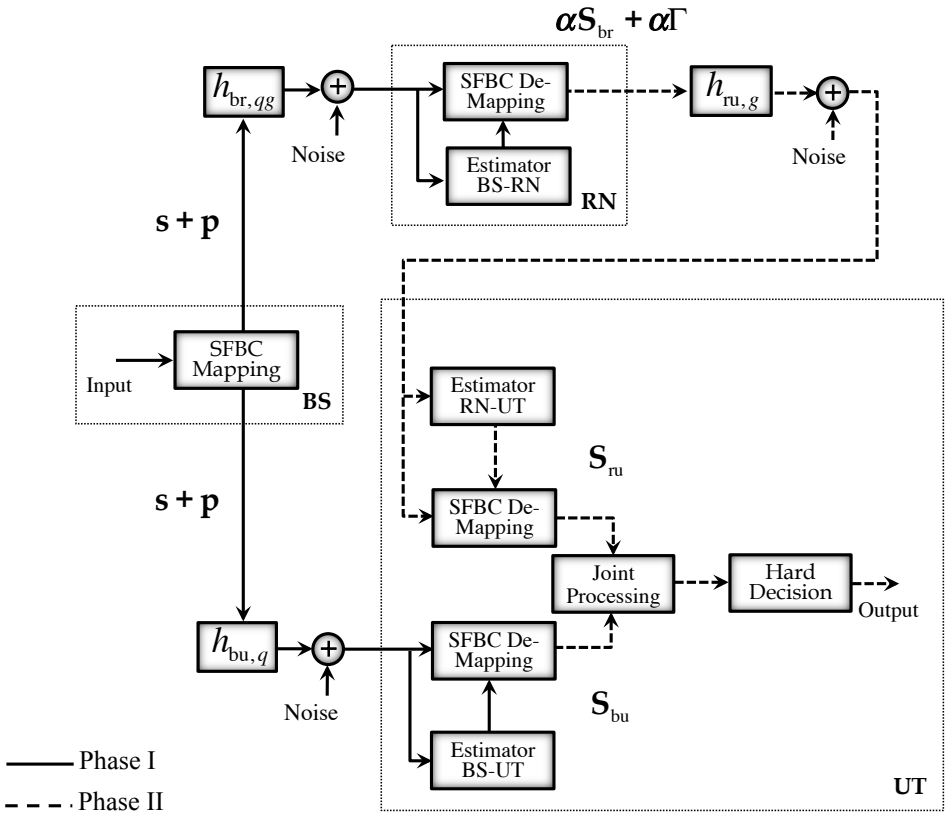

Figure 6.2: EF RA system: Block diagram.

6.2.1 Phase I

- **At the UT**

In Phase I the soft-decision variables de-mapped at the UT on data subcarriers k and $k+1$ are given by

$$S_{k,\mathrm{bu}} = \Gamma_{k,\mathrm{bu}} s_k + \frac{\hat{h}^*_{\mathrm{bu},1}}{\sqrt{2}} z^1_{k,\mathrm{bu}} + \frac{\hat{h}_{\mathrm{bu},2}}{\sqrt{2}} z^{*1}_{k+1,\mathrm{bu}} \ , \tag{6.1}$$

$$S_{k+1,\mathrm{bu}} = \Gamma_{k+1,\mathrm{bu}} s_{k+1} + \frac{\hat{h}^*_{\mathrm{bu},1}}{\sqrt{2}} z^1_{k+1,\mathrm{bu}} - \frac{\hat{h}_{\mathrm{bu},2}}{\sqrt{2}} z^{*1}_{k,\mathrm{bu}} \ , \tag{6.2}$$

where $z^1_{k,\mathrm{bu}}$ is the noise $\mathcal{CN}(0, \sigma^2_{\mathrm{bu}})$ and for k and $k+1$ data subcarriers $\Gamma_{k,\mathrm{bu}} = \frac{1}{2} \sum_{q=1}^{Q} \left| \hat{h}_{k,\mathrm{bu},q} \right|^2$ and $\Gamma_{k+1,\mathrm{bu}} = \frac{1}{2} \sum_{q=1}^{Q} \left| \hat{h}_{k+1,\mathrm{bu},q} \right|^2$, respectively.

- **At the RN**

Similarly, the soft-decision variable de-mapped at the RN per g antenna on data subcarriers k and $k+1$ are

$$S_{k,\mathrm{br}} = \Gamma_k s_k + \frac{\hat{h}^*_{\mathrm{br},11}}{\sqrt{2}} z^1_{k,\mathrm{br}} + \frac{\hat{h}_{\mathrm{br},21}}{\sqrt{2}} z^{*1}_{k+1,\mathrm{br}} + \frac{\hat{h}^*_{\mathrm{br}12}}{\sqrt{2}} z^2_{k,\mathrm{br}} + \frac{\hat{h}_{k,\mathrm{br}22}}{\sqrt{2}} z^{*2}_{k+1,\mathrm{br}} \ , \tag{6.3}$$

$$S_{k+1,\mathrm{br}} = \Gamma_{k+1} s_{k+1} + \frac{\hat{h}^*_{\mathrm{br}11}}{\sqrt{2}} z^1_{k+1,\mathrm{br}} - \frac{\hat{h}_{\mathrm{br}21}}{\sqrt{2}} z^{*1}_{k,\mathrm{br}} + \frac{\hat{h}^*_{\mathrm{br}12}}{\sqrt{2}} z^2_{k+1,\mathrm{br}} - \frac{\hat{h}_{\mathrm{br}22}}{\sqrt{2}} z^{*2}_{k,\mathrm{br}} \ , \tag{6.4}$$

where $z^1_{k,\mathrm{br}}$ and $z^2_{k,\mathrm{br}}$ are the noises $\mathcal{CN}(0, \sigma^2_{\mathrm{br}})$ related to each antenna at the RN and for k and $k+1$ data subcarriers $\Gamma_k = \frac{1}{2} \sum_{q=1}^{Q} \sum_{g=1}^{G} \left| \hat{h}_{k,\mathrm{br},qg} \right|^2$ and $\Gamma_{k+1} = \frac{1}{2} \sum_{q=1}^{Q} \sum_{g=1}^{G} \left| \hat{h}_{k+1,\mathrm{br},qg} \right|^2$, respectively.

As for generic k data subcarrier, the variance of S_{br} is given by $\sigma^2_{S_{\mathrm{br}}} = \Gamma^2_k + \Gamma_k \sigma^2_n$, the factor that normalises the signal transmitted by the RN, S_{br}, is $\alpha_k = \left(\sqrt{\Gamma^2_k + \Gamma_k \sigma^2_{\mathrm{br}}} \right)^{-1}$.

6.2.2 Phase II

At the UT the soft-decision variable de-mapped is expressed as

$$S_{k,\mathrm{ru}} = \alpha_k \Gamma_k \Gamma_{k,\mathrm{ru}} s_k + \alpha_k \Gamma_{k,\mathrm{ru}} h^*_{\mathrm{br},11} z^1_{k,\mathrm{br}} + \alpha_k \Gamma_{k,\mathrm{ru}} h_{\mathrm{br},21} z^{1*}_{k+1,\mathrm{br}} + \alpha_k \Gamma_{k,\mathrm{ru}} h^*_{\mathrm{br},12} z^2_{k,\mathrm{br}} + \alpha_k \Gamma_{k,\mathrm{ru}} h_{\mathrm{br},22} z^{2*}_{k+1,\mathrm{br}} + h_{\mathrm{ru},1} z^1_{k,\mathrm{ru}} + h_{\mathrm{ru},2} z^{1*}_{k+1,\mathrm{ru}} \ . \quad (6.5)$$

$$S_{k+1,\mathrm{ru}} = \alpha_{k+1} \Gamma_{k+1} \Gamma_{k+1,\mathrm{ru}} s_{k+1} + \alpha_{k+1} \Gamma_{k+1,\mathrm{ru}} h^*_{\mathrm{br},11} z^1_{k+1,\mathrm{br}} - \alpha_{k+1} \Gamma_{k+1,\mathrm{ru}} h_{\mathrm{br},21} z^{1*}_{k,\mathrm{br}} + \alpha_{k+1} \Gamma_{k+1,\mathrm{ru}} h^*_{\mathrm{br},12} z^2_{k+1,\mathrm{br}} - \alpha_{k+1} \Gamma_{k+1,\mathrm{ru}} h_{\mathrm{br},22} z^{2*}_{k,\mathrm{br}} + h^*_{\mathrm{bu},1} z^1_{k+1,\mathrm{ru}} - h_{\mathrm{bu},2} z^{1*}_{k,\mathrm{ru}} \ . \quad (6.6)$$

where $z^1_{k,\mathrm{ru}}$ is the noise $\mathcal{CN}(0, \sigma^2_{\mathrm{ru}})$ and for k and $k+1$ data subcarriers $\Gamma_{k,\mathrm{ru}} = \sum_{g=1}^{G} \left|\hat{h}_{k,\mathrm{ru}g}\right|^2 \frac{1}{G}$ and $\Gamma_{k+1,\mathrm{ru}} = \sum_{g=1}^{G} \left|\hat{h}_{k+1,\mathrm{ru}g}\right|^2 \frac{1}{G}$.

The variance of the overall noise, obtained from the expressions that represent signal received at the UT in Phase II in Eq. (5.24) and Eq. (5.25), is expressed by

$$\sigma^2_{k,\mathrm{t}} = \alpha^2_k \Gamma_k \Gamma_{k,\mathrm{ru}} \sigma^2_{\mathrm{br}} + \sigma^2_{\mathrm{ru}} \ . \quad (6.7)$$

In order to obtain $\sigma^2_{k,\mathrm{t}}$ it is necessary to acquire at the UT the parameters that are obtained at the RN, i.e., α_k and Γ_k. As discussed in the previous chapter, since the terms $\alpha_k \Gamma_k$ do not vary much it is reasonable the use of their average that is given by

$$\sigma^2_{\mathrm{t}} \approx \frac{2\sigma^2_{\mathrm{br}}}{5 + 2\sigma^2_{\mathrm{br}}} + \sigma^2_{\mathrm{ru}}. \quad (6.8)$$

As shown in Figure 6.2, at the UT, the soft-decision variables $S_{k,\mathrm{bu}}$ and $S_{k,\mathrm{ru}}$ are combined in the Joint Processing block in order to be hard-decoded.

6.3 Improving the Relay Channel Estimates

For the links BS-UT and BS-RN the estimator at the UT and the RN, in Phase I, can estimate the channels by making use of classical point-to-point link estimators. Nevertheless, for the links RN-UT the estimator at the UT, in Phase II, has to estimate the equivalent channel, $h_{k,\mathrm{e}g} = \alpha_k \Gamma_k h_{k,\mathrm{ru},g}$. As discussed in Section 5.5.2, allocating unitary pilots at pilot subcarriers is an approach that provides estimates in case of point-to-point links. For the

relaying links in the EF RA system the pilot subcarriers should convey the factor $\alpha_k \Gamma_k$, during the RN transmission, in order to provide accurate equivalent channels estimated at the UT. As shown in the results, despite to obtain accurate channel estimates the additional sources of noise inherent to the EF MIMO scheme present some penalty relatively to the point-to-point MSE performance. In order to overcome such degradation, an estimator for the relaying links is studied.

6.3.1 Proposed Pilot-Data Aided Channel Estimator Scheme

This section focus on Phase II where only the relay channels are estimated at the UT. The following block diagram is slightly different from the one presented in Figure 6.2. Such a diagram highlights (shaded area) the actions that are taken in the proposed pilot-data aided channel estimation scheme.

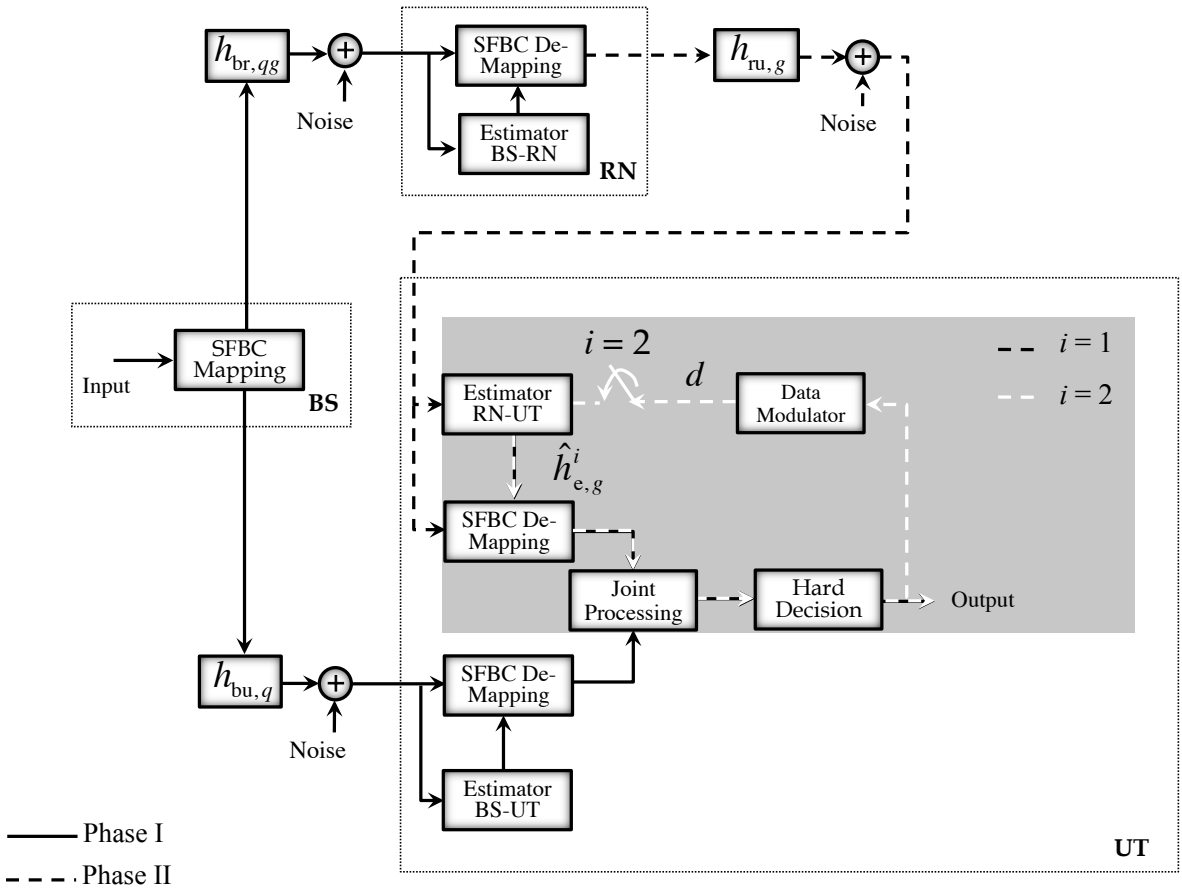

Figure 6.3: Pilot-Data aided Estimation: Block diagram.

According to the diagram the superscript i indicates in which iteration the estimate is acquired and d represents the regenerated data-symbol that are obtained after the Data-Modulator block. For the iteration $i = 1$, represented by the black dashed line, the initial estimates, $\hat{h}^1_{\mathrm{e},g}$, are obtained using only pilot symbols whereas for $i = 2$, represented by the white dashed line, the data symbol regenerated in $i = 1$ are used to improved the initial estimates and obtain the pilot-data based channel estimates $\hat{h}^2_{\mathrm{e},g}$.

6.3.1.1 The Data-based Channel Estimation

According to the EF RA system, one OFDM symbol is made up K subcarriers such that the subcarriers carrying pilot symbols are spaced by N_f therefore, the set of pilot subcarriers corresponds to $\mathfrak{P} = \{0, N_f, 2N_f, \ \cdots, K - N_f\}$. Since in the studied scenario the BS and the RN terminals are equipped with two antennas, the pilot subcarriers are arranged such that each antenna has different sub-sets of subcarriers, i.e., $\mathfrak{P}_1 = \{0, 2N_f, \cdots, K - 2N_f\}$ and $\mathfrak{P}_2 = \{N_f, 3N_f, \cdots, K - N_f\}$. Correspondingly, the set of data subcarriers corresponds to $\mathfrak{J} = \{1, 2, \cdots, J\}$, where J is the size of the data subcarrier set, where according to our system model $J = K - N_t$, for $N_t \in \mathbb{N}$

Let us represent the subcarriers that carry pilot and the data symbols by the vectors $\mathbf{s}$ and $\mathbf{p}$, respectively. If pilot symbols are multiplexed with data symbols in different subcarriers then $\mathbf{s}$ and $\mathbf{p}$ contain non-zero elements in different positions. The pilot array for one OFDM symbol is represented by $\mathbf{p} = [\mathbf{p}_1 \ \ \mathbf{p}_2]$ and similarly, the data symbol array is given by $\mathbf{s} = [\mathbf{s}_1 \ \ \mathbf{s}_2]$ where $\mathbf{p}_1$, $\mathbf{p}_2$, $\mathbf{s}_1$ and $\mathbf{s}_2$ are $1 \times K$. If the SFBC is applied, the non-zero elements of $\mathbf{s}_1$ and $\mathbf{s}_2$ correspond to SFBC mapped symbols.

In frequency domain the received signal at the destination corresponds to $\mathbf{y} = (\mathbf{s}+\mathbf{p})\mathbf{h}+\mathbf{z}$, where $\mathbf{h}$ is the vector representing the diagonal of the channel matrix. In the studied case cooperative system $Q \times G \times 1$, throughout the phase II $\mathbf{y}$ follows Eq. (5.24) - Eq. (5.25) and $\mathbf{h}$ can be expressed by $\mathbf{h}_{\mathrm{e}} = [\mathbf{h}_{\mathrm{e}1} \ \ \mathbf{h}_{\mathrm{e}2}]$, where $\mathbf{h}_{\mathrm{e}1}$ and $\mathbf{h}_{\mathrm{e}2}$ are the diagonals of the $K \times K$ matrix that represent the CFR of the channels between the RN and the UT.

According to Eq. (6.5) - Eq. (6.6), the additional source of noise imply that the channel estimates present some penalties relatively to the case of a point-to-point link. As discussed in Section 3.3.1, a pilot pattern can be described as a matrix that acquires samples of the channel. Hence, the pattern should have enough pilot density in order to track the channel

variations. The distortion stemmed from insufficiently high sampling causes aliasing that is an irrevocable distortion. Therefore, the pilot separation both in time and frequency dimensions should be selected according to the channel characteristics. The performance of the channel estimation can be improved by increasing the pilot density. Increasing such a density by a factor of 1/2 can improve the channel estimation performance in 3 dB. Nevertheless, such an approach reduce the number of subcarrires used to convey data information thus, it decreases the spectral efficiency of the system. In order cope with the degradation imposed by the EF relaying link characteristics, the performance of the relaying channel estimates can be improved by performing data-based channel estimation. This approach uses the data symbols as virtual pilots such that the spectral efficiency of the system is not compromised. Figure 6.4 shows the flow chart related to pilot-data-aided estimation. The blocks Virtual Pilot Selection and Estimation Combining and MMSE Filtering are detailed in Section 6.3.2. In our specific implementation the pilot-data-aided estimation is restricted to one data iteration however, it can be easily generalised to perform more than one. In our work, for all cases evaluated, it did not bring significant gain therefore, it was not considered.

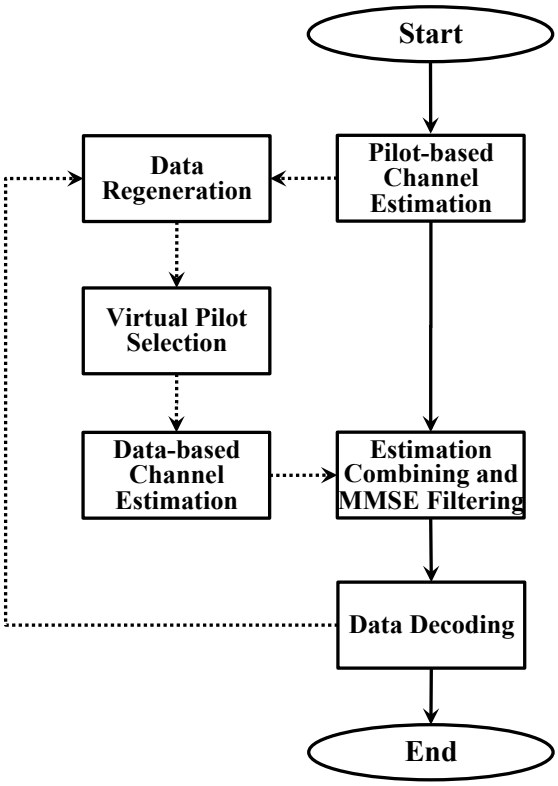

Figure 6.4: Pilot-Data-aided estimation: Flow chart.

In the first iteration only pilots are used to estimate the channels and the data-aided estimation takes place after the regeneration of the data symbol that are used in the LS estimation, considering only data subcarriers. As Alamouti is used at the RN, the LS estimation based on the data symbol information requires a matrix inversion. Considering that two data symbols are encoded in subcarriers j and $j+1$, the LS estimate for the equivalent channels is given by

$$\hat{\mathbf{h}}_{\mathrm{ls}}^{\mathrm{d}} = \sqrt{2}\Big(\mathbf{D}^{-1}\mathbf{y}_{\mathrm{ru}}\Big), \tag{6.9}$$

where $\hat{\mathbf{h}}_{\mathrm{ls}}^{\mathrm{d}} = \begin{bmatrix}\hat{\mathbf{h}}_{\mathrm{e1}} & \hat{\mathbf{h}}_{\mathrm{e2}}\end{bmatrix}^T$, $\mathbf{y}_{\mathrm{ru}} = \begin{bmatrix}\mathbf{y}_{\mathrm{ru},j} & \mathbf{y}_{\mathrm{ru},j+1}\end{bmatrix}^T$ and $\mathbf{D}$ corresponds to the regenerated data symbol matrix that follows Eq. (6.13) for j and $j+1$ data subcarriers.

$$\mathbf{D} = \begin{pmatrix} d_j & -d_{j+1}^* \\ d_{j+1} & d_j^* \end{pmatrix},\ j \in \mathfrak{J}. \tag{6.10}$$

The MSE of the estimates in Eq. (6.9) is given by:

$$\mathbb{E}\left\{|e|^2\right\} = \frac{1}{J}\left(\sum_{j\in\mathfrak{J}} \mathbb{E}\left\{\left|h_j - \hat{h}_j\right|^2\right\}\right). \tag{6.11}$$

For QPSK with unit power, it is derived in Appendix B, for SISO and MISO channels, an approximate relation between the MSE data-aided estimation and the error probability P_b. Under the assumption that the correlation involving the data and noise are negligible it follows

$$\mathbb{E}\left\{|e|^2\right\} \approx \begin{cases} \sigma_n^2\left(1 + 2P_b\mathrm{SNR}\right) & ,\ \text{for SISO channels} \\ \dfrac{1}{2}\sigma_n^2\left(1 + P_b\mathrm{SNR}\right) & ,\ \text{for MISO channels} \end{cases}, \tag{6.12}$$

where the SNR is such that the noise power per subcarrier is σ_n^2 and the average received signal power (including pilots) is normalised to 1, i.e., $\mathrm{SNR} = 1/\sigma_{\mathrm{n}}^2$.

According to the error expression in Eq. (6.12), for a moderate error probability (e.g., 0.01), the increase in the error is not significant. Therefore, as a large number of subcarriers are considered in the data-aided estimation, even with first data iteration being very inaccurate, there is potential to improve the channel estimates as the output of this estimation is combined with the pilot-based one and the MMSE filter is applied.

As the RN is equipped with two antennas, the use of Alamouti coding leads to some issues

when considering the regenerated data as virtual pilots.

In order to illustrate the problem let us consider the subcarriers j and $j+1$ where the data sent over these subcarriers is represented by the matrix $\mathbf{S}$, according to

$$\mathbf{S} = \begin{pmatrix} s_j & -s_{j+1}^* \\ s_{j+1} & s_j^* \end{pmatrix}, \; j \in \mathfrak{J}. \tag{6.13}$$

At the UT in subcarrier j and $j+1$ we get

$$y_{j,\mathrm{ru}} = \frac{1}{\sqrt{2}}\Big(s_j w_{j,\mathrm{ru},1} - s_{k+1}^* w_{j+1,\mathrm{ru},2}\Big) + z'_{j,\mathrm{ru}} \; , \tag{6.14}$$

$$y_{j+1,\mathrm{ru}} = \frac{1}{\sqrt{2}}\Big(s_j^* w_{j,\mathrm{ru},2} + s_{j+1} w_{j+1,\mathrm{ru},1}\Big) + z'_{j+1,\mathrm{ru}} \; , \tag{6.15}$$

where $w_{j,\mathrm{ru},1}$ and $w_{j,\mathrm{ru},2}$ refer to the equivalent channels $\alpha_j \Gamma_j h_{j,\mathrm{ru},1}$ and $\alpha_j \Gamma_j h_{j,\mathrm{ru},2}$ between the RN and the UT whereas $z'_{j,\mathrm{ru}}$ refers to the noise components at the UT in Phase II.

In the Alamouti decoding it is assumed that the channels for adjacent subcarriers are similar and then we have

$$y_{j,\mathrm{ru}} = \frac{1}{\sqrt{2}}\Big(s_j w_{\mathrm{ru},1} - s_{k+1}^* w_{\mathrm{ru},2}\Big) + z'_{j,\mathrm{ru}} \; , \tag{6.16}$$

$$y_{j+1,\mathrm{ru}} = \frac{1}{\sqrt{2}}\Big(s_j^* w_{\mathrm{ru},2} + s_{j+1} w_{\mathrm{ru},1}\Big) + z'_{j+1,\mathrm{ru}} \; , \tag{6.17}$$

where the subscript j was dropped in the channels representation.

This allows us to obtain the LS data-aided estimation according to Eq. (6.9). Such an estimation is performed assuming that $w_{j,\mathrm{ru},1} = w_{j+1,\mathrm{ru},1}$ and $w_{j,\mathrm{ru},2} = w_{j+1,\mathrm{ru},2}$ which is only an approximation as there will be some change from subcarrier j to $j+1$ (even minor) according the channel characteristics. In fact what is obtained, in the absence of noise, for each channel is

$$\hat{w}_j = \frac{w_j + w_{j+1}}{2}. \tag{6.18}$$

Such a data-based estimate merges the LS estimation as well as the Alamouti decoding and does not recover the true channel instead, for each pair of adjacent data subcarrier we obtain an average of the true values. This implies that in case of Alamouti coding even if we use J

data subcarriers we only obtain $J/2$ estimates which each one corresponds to an average. This occurs even without the presence of noise and therefore, an error floor is expected in terms of MSE performance of any channel estimation that takes as starting point the LS estimates obtained from the Alamouti decoded data. This is illustrated in Figure 6.5 that corresponds to the performance of the channel estimates, considering pilot and data contributions with similar weighs, for a MISO system considering the channel model ITU Pedestrian Model A and B. The data-aided estimation performances for channels that do not present subcarriers highly correlated, i.e., selective channels, are expected to present more noticeable error floor as it is presented in Figure 6.5, where the error floor in the performance of Model B is more severe relatively to Model A. Such a performance is due to fact that the subcarriers in Model A are more correlated than in Model A as Model B, with 6 distant taps, is more dispersive than Model A, with 4 taps apart.

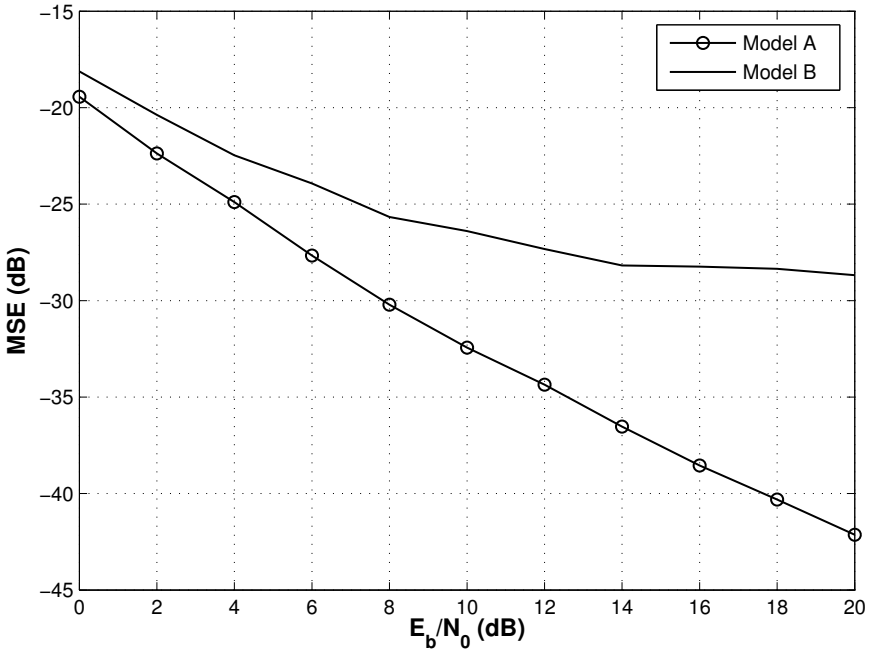

Figure 6.5: Pilot-Data channel estimation: MISO case.

As the majority of the involved data subcarriers are adjacent, the degradations inherent to LS data-base estimation and the proposed solution to reduced them are addressed in the following section.

6.3.2 Adjacent Virtual Pilot Subcarriers

As aforementioned in Section 3.3.1 for the LS estimation the minimum MSE is obtained when the pilots in frequency domain are equispaced and equipowered [58]-[59]. In Eq. (6.9) it is considered that the data subcarriers used in the SFBC coding are adjacent. In fact, when designing the transmitted frame, pilots are inserted and therefore not all pairs of subcarriers corresponding to one SFBC codeword will be adjacent. For example, lets consider a pilot spacing of 4, i.e. $N_f = 4$, there will be pilots at subcarriers 0, 4, 8, $\cdots$ and the first SFBC codeword will be transported at the adjacent subcarriers 1 and 2, but the second codeword will be transported at the subcarriers 3 and 5. In addition, according to [110] when adjacent subcarriers carry pilots, the involved FFT matrix approximates to an ill-conditioned matrix and a small inaccuracy in the observed elements may cause a large degradation in the estimation therefore, there is the noise enhancement effect as the estimate is likely to be vulnerable to the noise.

The degradation related to the nonequispaced virtual pilots can be prevent by selecting subsets of equidistant virtual pilots before performing the LS estimation. The number of subsets, $\mathfrak{j}_\mathfrak{n}$, depend on the pilot separation, N_f, such that, $n = 1, 2, 3, \cdots, N_f - 1$. The selection processing is depicted in Figure 6.6, where $N_f = 4$ and each subset is represented by a different pattern.

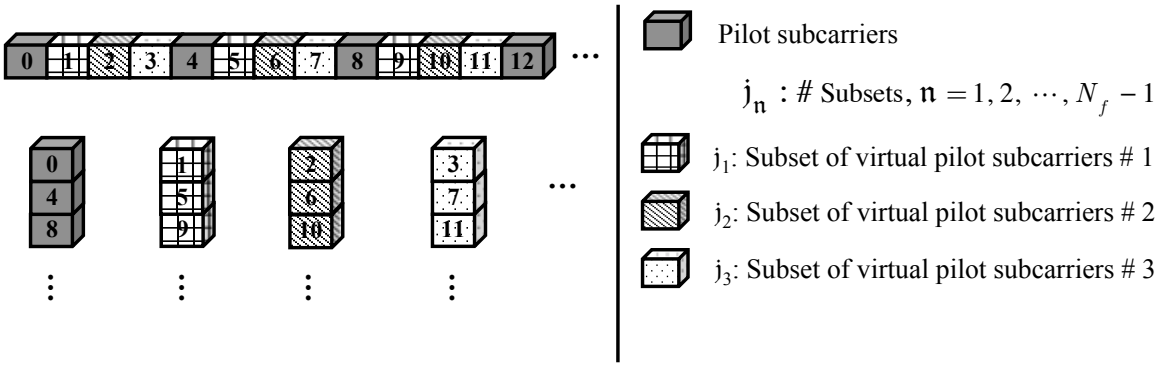

Figure 6.6: Virtual pilots - Selection Processing.

In such a case, the subsets correspond to $\mathfrak{j}_1 = \{1, \cdots, n(N_f - 1), \cdots, J/(N_f - 1)\}$, $\mathfrak{j}_2 = \{2, \cdots, n(N_f - 1), \cdots, J/(N_f - 1)\}$ and $\mathfrak{j}_3 = \{3, \cdots, n(N_f - 1), \cdots, J/(N_f - 1)\}$. Such an operation leads to $\mathfrak{j}_\mathfrak{n} = N_f - 1$ subsets of virtual pilots that are used to perform the

LS data-aided estimation, leading to $\hat{\tilde{\mathbf{h}}}_{\mathrm{j_n}}$ estimates of size $1 \times J/(N_f - 1)$.

In order to obtain the CIR estimates of size $K \times 1$, each estimate $\hat{\tilde{\mathbf{h}}}_{\mathrm{j_n}}$ is zero-padded, as follows in Eq. (6.19), where $\mathbf{0}_{\mathrm{j_n}N_t}$ corresponds to a vector of size $1 \times \mathrm{j_n}N_t$ with null samples. Such an operation is similar to applying an ideal low-pass window with a cut-off frequency $J(N_f - 1)^{-1} - 1$.

$$\hat{\tilde{\mathbf{h}}}_{\mathrm{ls}}^{\mathrm{dj_n}} = \left[\hat{\tilde{\mathbf{h}}}_{\mathrm{j_n}} \quad \mathbf{0}_{\mathrm{j_n}N_t}\right]^T . \tag{6.19}$$

The pilot-data-aided CIRs estimates are combined according to Eq. (6.20). An averaging factor guarantees that the resulting power is normalised to 1 and by design this factor results in $\mathrm{j_n} + 1$. After combining the CIRs, the MMSE filtering is applied to enhance the estimate. The final CIR estimate is expressed by

$$\hat{\tilde{\mathbf{h}}}_{\mathrm{e}} = \left\{ \mathrm{diag}\left(\widetilde{\mathbf{W}}_{\mathrm{mmse}}\right) \circ \left[\left(\sum_{\mathrm{j}} \hat{\tilde{\mathbf{h}}}_{\mathrm{ls}}^{\mathrm{dj_n}} + \hat{\tilde{\mathbf{h}}}_{\mathrm{ls}}^{\mathrm{p}} \right) \Big/ \mathrm{j_n} + 1 \right] \right\} . \tag{6.20}$$

where $\hat{\tilde{\mathbf{h}}}_{\mathrm{ls}}^{\mathrm{p}}$ corresponds to the LS estimation implemented in the time domain considering only pilots. The corresponding block diagram of the pilot-data-aided estimation scheme is depicted in Figure 6.7.

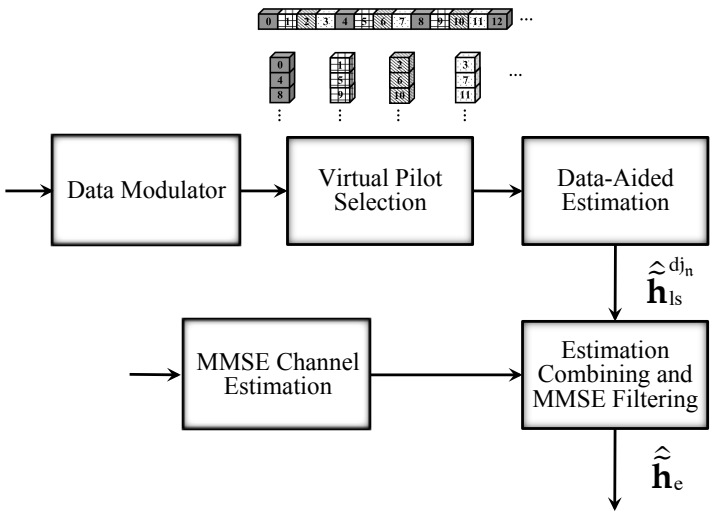

Figure 6.7: Pilot-Data-aided estimation: Block-diagram.

6.4 Performance Assessment

6.4.1 System Parameters

In order to evaluate the performance of the presented channel estimation scheme it is considered a typical scenario and the simulation parameters are summarised in Table 6.1. The channel estimation performance is presented in terms of MSE and E_b/N_0 of the direct link. The following pilot separations are considered $N_f = 4, 8, 16$ and $N_v = 1$. The ITU Pedestrian A and B are considered as channel models with the tap delays modified according to the sampling interval. Both the UT and the RN are assumed as mobile terminals hence, the Doppler effect is considered in both links BS-RN and RN-UT.

It is assumed that the channels are uncorrelated, the receiver is perfectly synchronised and the insertion of a long enough cyclic prefix in the transmitter ensures that the orthogonality of the subcarriers is maintained after transmission.

Since BS and RN are both equipped with an antenna array the resulting MSE of the direct channels BS-UT (DL) and the relay channels RN-UT (RL) are obtained by averaging the individuals MSEs.

Table 6.1: Simulation parameters

Modulation	QPSK
Carrier Frequency	2 GHz
Sampling Interval	89.3 ns
# Subcarriers	1024
OFDM frame	9 symbols
Channel Taps	4 taps (Model A) and 6 taps (Model B)
Velocity	10 km/h

The estimator performance is assessed in three scenarios which are referred in Table 6.2 as: #1: all links have the same statistics; #2 the links BS-RN are 3 dB better than the links BS-UT and RN-UT; #10: the overall relay links are 10 dB better than the direct ones.

Table 6.2: Assessed links statistics

Scenario #	Link Statistics
1	$E_b/N_0^{\mathrm{BS-RN}} = E_b/N_0^{\mathrm{RN-UT}} = E_b/N_0^{\mathrm{BS-UT}}$
2	$E_b/N_0^{\mathrm{BS-RN}} = E_b/N_0^{\mathrm{BS-UT}} + 10$ dB
3	$E_b/N_0^{\mathrm{BS-RN}} = E_b/N_0^{\mathrm{RN-UT}} = E_b/N_0^{\mathrm{BS-UT}} + 10$ dB

Figure 6.8 shows the MSE of the CFR estimate of the relay and the direct links employing the pilot and the pilot-data estimators, considering the Scenario #1 and considering the channel Model A. It shows that the pilot-based estimates of the RL present a penalty over the DL that accounts for the extra source of noise aforementioned. It also shows that the pilot-data based estimation method can significantly overcome such penalisation and provides a performance better than the DL for all N_f considered. For high values of E_b/N_0 as N_f increases the relative gain provided by the data-aided estimator increases as well. The results show that for $E_b/N_0 = 6$ dB, the pilot-data based performance provide 3 dB and 5 dB gain over the estimator using only pilots for $N_f = 4$ and $N_f = 16$, respectively. For low values of E_b/N_0 the gain is smaller however, even for E_b/N_0 as low as 0.5 dB the gain approximately 2 dB over the pilot-based estimator, for $N_f = 4$. The gain reduction as E_b/N_0 decreases is expected since the probability of error in the first iteration increases and therefore several virtual pilots used for the second iteration are erroneous. Moreover, inspection of the curves of Figure 6.8, shows that the MSE of the pilot-data based estimator for a given N_f is always below of the one achieved considering the pilot-based estimator with pilot separation of $N_f/2$. This means that the total number of pilots can be halved leading to an improved spectral efficiency. In Figure 6.8 it is also presented, in green line, the performance of the pilot-data estimator for $N_f = 4$ when perfect decoded data is used instead of regenerated one. Such a results means that considering several iterations in this algorithm, the gain expected would be smaller than 0.77 dB, which is the difference in performance of the pilot-data based estimator when perfect and regenerated data, green and black lines, respectively, are employed. According to our results, with only one data iteration the proposed estimator provides significant gains over the pilot-based estimator, black and red results.

In Figure 6.9 similar results are presented however, considering the channel Model B.

Such a channel has much lower coherence bandwidth than Model A and as it can be noticed for $N_f = 16$ the pilot-data based starts presenting an error floor for high values of E_b/N_0. Such behaviour is expected as in Alamouti coding it is obtained the average channel of two subcarriers, actually. With Model A the channels for two adjacent subcarriers are strongly correlated and averaging introduces no remarkable error, but for Model B the correlation is lower than Model A and averaging effect starts to be significant for high values of E_b/N_0. This error floor effect occurs for all the values of N_f but the larger the pilot separation the faster (in terms of E_b/N_0) it starts to be pronounced. Such an effect can be reduced by using different weight for the data and pilot contributions in Eq. (6.20). Also in Figure 6.9 it is depicted, in green line, the performance of the pilot-data estimator for $N_f = 4$ when perfect decoded data is used instead of regenerated one. Similarly to the previous results, considering several iterations in this algorithm, the gain expected would be smaller than 0.4 dB, which is the difference in performance of the pilot-data based estimator when perfect and regenerated data, green and black lines, respectively, are employed. The proposed estimator provides significant gains over the pilot-based estimator, black and red results, with only one data iteration.

Figure 6.10 - Figure 6.13 present the estimators MSE performance considering the Scenarios # 2 and # 3. The choice for such scenarios for downlink derives from the fact that, in most real circumstances, the relaying links have higher transmission quality conditions than the direct link. The results presented in Figures 6.10 - Figure 6.13 emphasise the benefits of cooperation in terms of MSE and the improvements that are achieved using the proposed pilot-data scheme as well.

Figure 6.10 - Figure 6.11 show the results relative to Scenario # 2, for channel Models A and B, respectively. In both cases the pilot-based estimates of the RL and DL present approximately the same performance. Such performances are due to the fact that in the case that the links between BS and RN are highly reliable, most of the data information is successfully detected at the RN, which has a positive impact on the relaying links. It can be noticed that the proposed pilot-data estimator for $N_f = 16$ achieves approximately the same performance of the pilot-based one for $N_f = 4$, therefore requiring only 1/4 of the pilot subcarriers used by the pilot-based method.

Figure 6.12 - Figure 6.13 depict the results relative to Scenario # 3 for channel Models A

and B, respectively. Such results show that in these scenarios both links BS-RN and RN-UT have higher quality conditions over the direct ones. In such a case the noise variances have a minor impact on the pilot-based estimates and due that the RL performance outperforms the DL one. Nevertheless, the proposed scheme can improve the RL performance. For $N_f = 8$ the proposed estimator presents a performance close to the pilot-data performance considering only 1/2 of the pilots used by the pilot-based estimator, i.e. $N_f = 4$. In such a scenario, the MSE of the pilot-data based estimator for a given N_f is quite close to the one achieved considering the pilot-based estimator with pilot separation of $N_f = 4$.

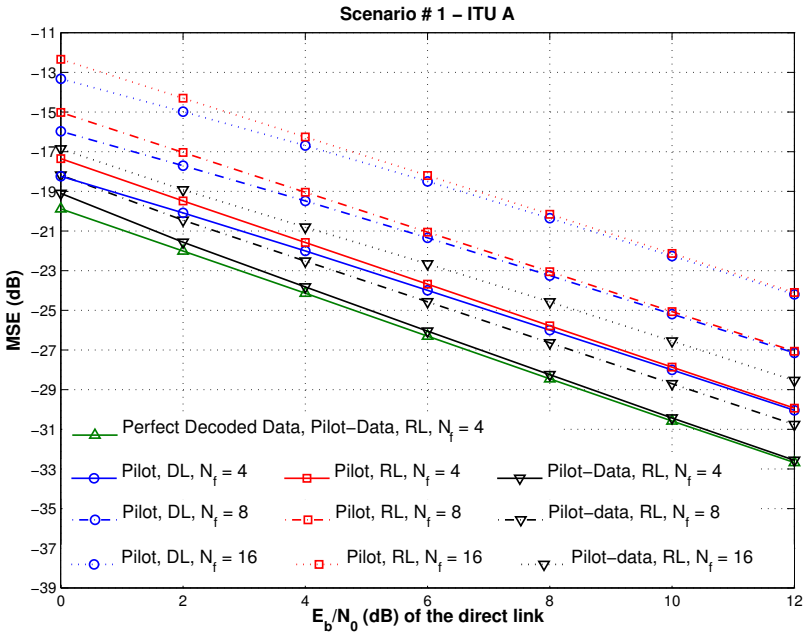

Figure 6.8: MSE performance: Scenario #1 and ITU Pedestrian Model A.

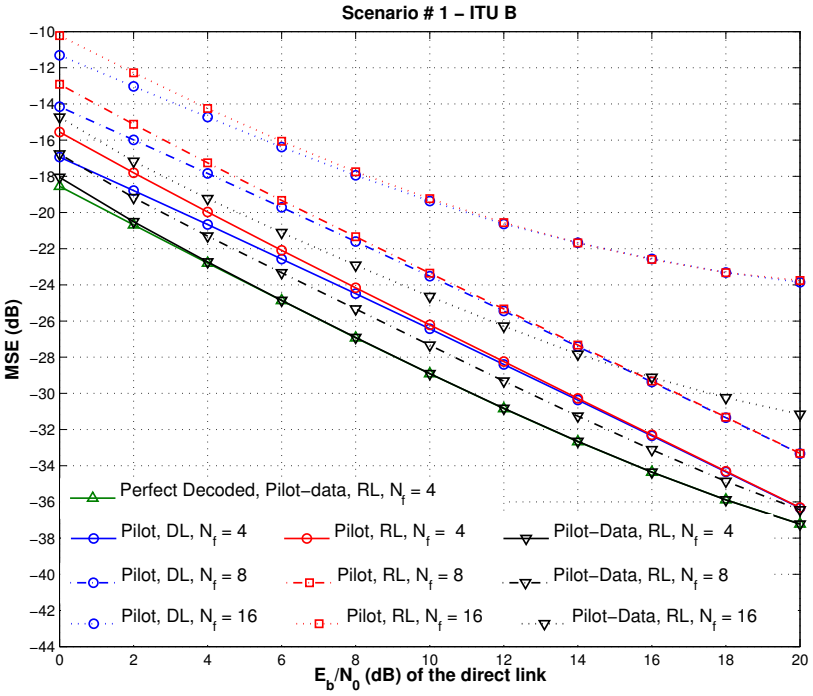

Figure 6.9: MSE performance: Scenario #1 and ITU Pedestrian Model B.

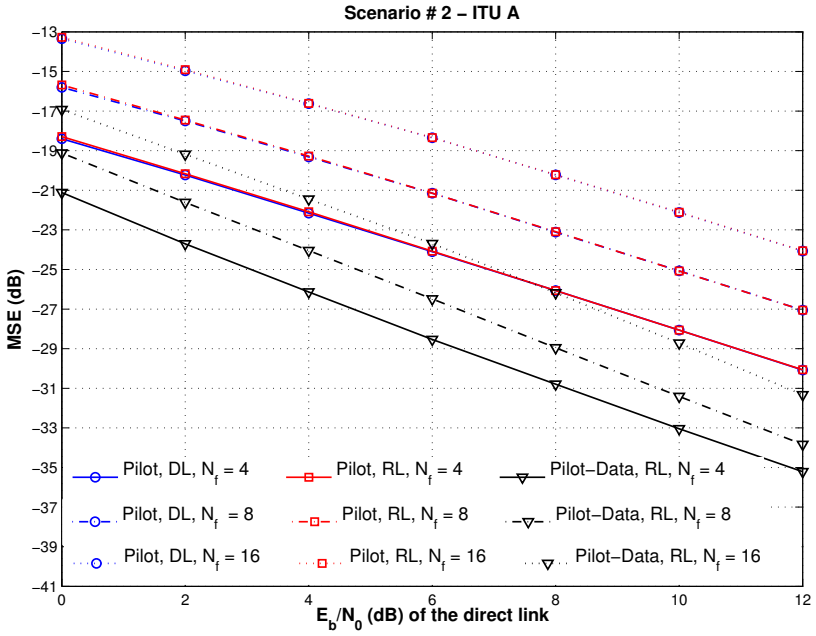

Figure 6.10: MSE performance: Scenario #2 and ITU Pedestrian Model A.

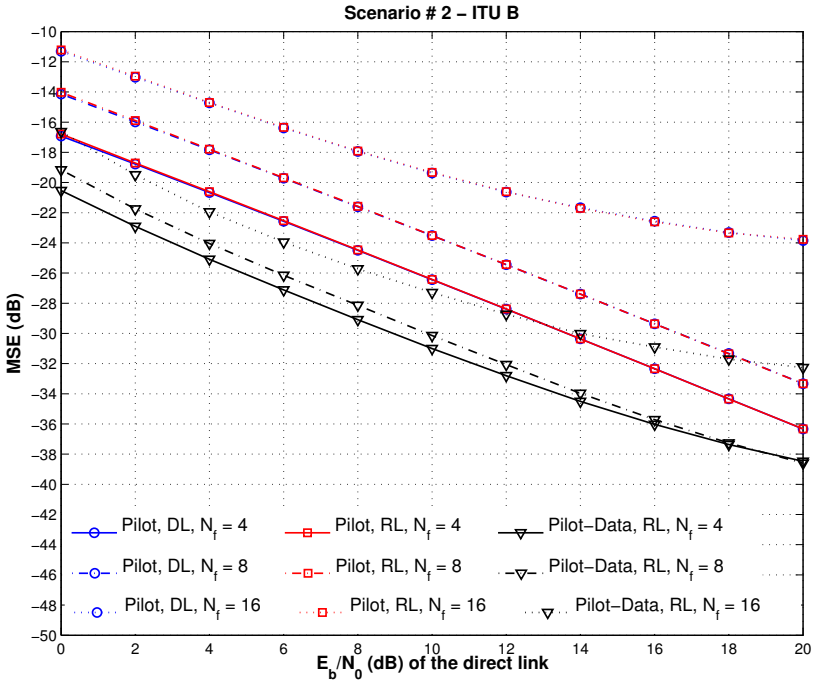

Figure 6.11: MSE performance: Scenario #2 and ITU Pedestrian Model B.

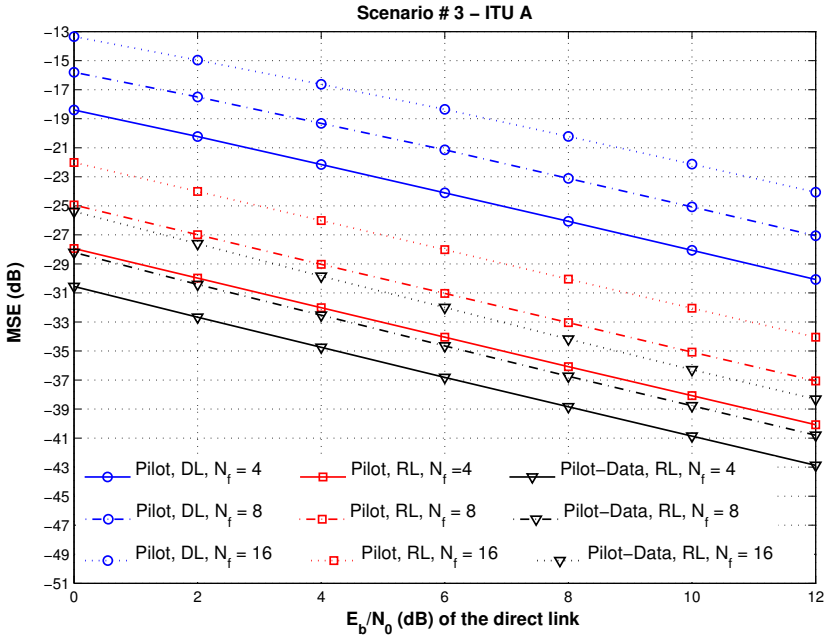

Figure 6.12: MSE performance: Scenario #3 and ITU Pedestrian Model A.

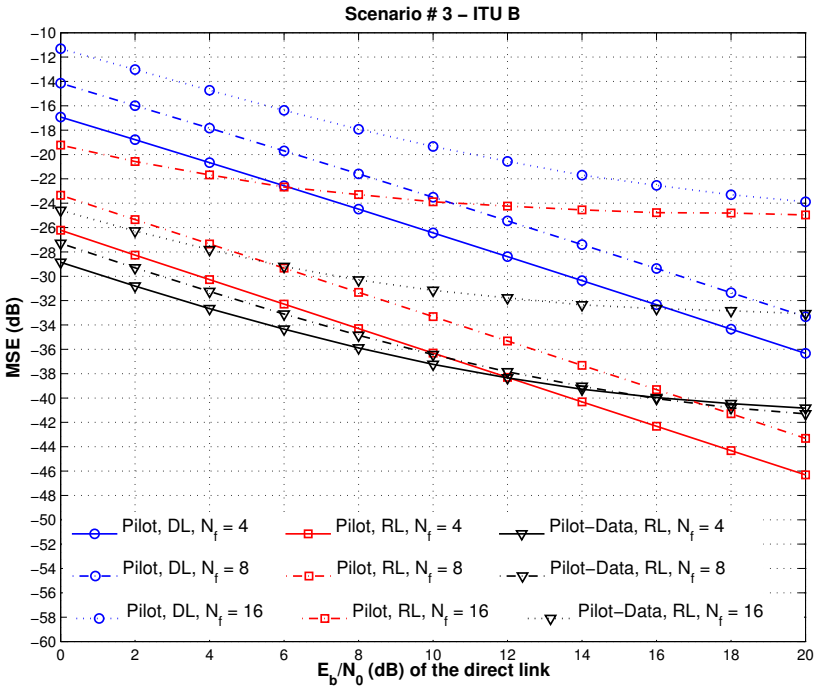

Figure 6.13: MSE performance: Scenario #3 and ITU Pedestrian Model B.

6.5 Conclusion

A pilot-data based estimation algorithm was proposed for an EF MIMO cooperative scenario where the spatial diversity provided by Alamouti is complemented with the use a relaying node. The proposed estimation method consists of two iterations and uses the MMSE criterion to design the estimator for both pilot-based and data-aided iterations. The data-aided estimation component is carried out using the regenerated data symbols as virtual pilots. In different scenarios, the results have shown that for the same pilot density the MSE is reduced approximately by 3 dB or alternatively requires half of pilot density to achieve the same performance therefore improving the overall system spectral efficiency with only one data iteration.

Chapter 7

Conclusions and Future Works

7.1 Summary and Concluding Remarks

The growing demands for high data rate in cellular systems requires innovative approaches in the design of the upcoming cellular generations. The recent interest in RA cooperative communication brought a new perspective to cellular networks, as the connection between the BS and UT may involve dedicated RN's or other users acting as RN's. Therefore, efficient channel estimation techniques for RA cooperative system are required.

This thesis addressed the channel estimation problem in the context of mobile cooperative communications. The investigated schemes considered transparent and non-transparent relaying protocols in realistic environments and included the multicarrier signal processing technique OFDM. The contributions were evaluated with standardised specifications and the ITU multipath channel models.

After an introduction regarding the evolution of the communication systems as well as the demand for high data rate cellular systems and the scope of this thesis, Chapter 2 presented the principles and propagation mechanisms related to wireless environment and systems as well as the cooperative communications and the relaying approaches were introduced. Chapter 3 discussed the issues related to the channel estimation processing in the context of OFDM-based systems as well as their impacting factors such as the pilot density and pilot pattern.

As part of the study, Chapter 4 focused on the relay channel statistics regarding the AF relaying protocol, considering a two-hop relay channel for the downlink and single antenna nodes. This chapter allowed to identify the main issues, in channels estimation, brought by

the use of relays, namely:

- The impact of the additional noise introduced in the compound path. Such an aspect limits the average SNR received at the UT;
- The effect of the delay spread caused by the fact that the relay path is a compound channel. This aspect limits the maximum distance, N_f, considered in the pilot pattern and therefore, demands for a high density of pilots;
- These observations and their respective quantification led to the design of a modified MMSE estimator in oder to cope with these additional disturbances;

In a cooperative scenario employing the AF relaying protocol and multiple antennas at the BS and the RN for each data symbol the compound channel from the source to one antenna element of the RN corresponds to a sum of two complex Gaussian random variables. In such a scenario even if we use multiple antennas at the RN we will achieve the same diversity of a $2 \times 1 \times 1$ system. In order to obtain the benefits provided by the use of multiple antennas, at the RN we need to equalise and combine the received signals and then re-encode it using Alamouti coding. In Chapter 5 the main points and conclusions found:

- The mathematical link characterisation for RA scenarios employing the EF relaying protocol;
- It was verified that the solo information about the equivalent channel it is not enough to perform an equalisation that maximises the SNR, which requires the knowledge of the noise variance introduced at the RN;
- A channel estimation scheme was proposed with some simplification in order to cope with the impossibility of accessing the instantaneous noise variance added at the RN. Despite this simplification the scheme did not present significant degradation relatively to the case where it was assumed that all parameters were available. However, there was some penalty comparatively to the single hop case;

The results presented in Chapter 5 motivated further investigation considering the studied scenario $2 \times 2 \times 1$ as well as the proposed pilot transmission scheme. Theretofore, only pilot-based estimator had been considered in the previous chapters, in Chapter 6 it was proposed a

two stage iterative pilot and data aided estimator designed to estimate the relay channel with aid of the regenerated data-symbol, as virtual pilots. According to the analytical study and results, the following findings were highlighted:

- It was shown that even with moderate probability of symbol error, in the first data iteration, there was potential to improve the channel estimates using the regenerated data symbols;
- It was verified that two specific aspects lead to an error floor on the estimate performance, namely: the fact that the Alamouti coding implied that for each pair of subcarriers, what was effectively estimated was the average and because of the insertion of pilots data subcarriers may not be adjacent; a second fact that adjacent subcarriers would be used as virtual pilots;
- A channel estimation scheme was proposed such that it eliminated the impairments that compensates the use of data subcarriers;
- The results showed that with a single data iteration this scheme allowed, for the same performance objective, the use of half of the pilot density;

The contributions presented in this thesis have relevant interest for application in next generation of cellular networks for which cooperative scenarios and approaches are regarded.

7.2 Directions for Future Works

The research area addressed in this thesis demand for continuous investigation. Regarding channel estimation for the cooperative cellular network there are some topics that are still open and can be addressed.

- In order to reduce the complexity of the pilot-data-aided estimator some adaptive mechanisms, based on the statistics of the channel, can be implemented in order to use the data-aided estimation when needed;
- Also regarding the pilot and data aided estimator, another point of interest can be the design of an adaptive pilot matrix with appropriate density, based on the long term

statistics of channel. Such that, the spectral efficiency of the system can be increased without compromising the estimation performance;

- In this thesis the estimators processed an estimate per OFDM sysmbol such that, in a given OFDM frame $N_t = 1$. Nevertheless, in each OFDM symbol its channel estimate can be improved by using the estimates of the previous symbols. Such an estimation can consider recursive approaches or filters in order to explore the long term statistics of the channel;

- The studied cooperative scenarios considered the use of one RN, either equipped with one or two antennas. Nonetheless, a higher diversity can be achieved in more complex scenarios where multiple RN's are considered;

- This thesis considered pilot-based estimator, as it is standardised in order to guarantee an acceptable performance. Nevertheless, from the theoretical perspective, implementations considering blind estimations would be interesting. An estimator that considers a blind estimation merged with data-aided one can improve the spectral efficiency of the system;

- Software Defined Radio (SDR) platforms could be implemented in order to assess the real-time performance of the pilot-data-aided estimation scheme.

References

[1] M. Palma, A. Lamperez, T. K. Sarkar, and D. L. Sengupta. The Father of Radio: A Brief Chronology of the Origin and Development of Wireless Communications. *IEEE Antennas and Propagation Magazine*, 53(6):83–114, December 2011.

[2] S. Jeszenszky. From Electric Oscillations to Marconi's Wireless Telegraph. *IEEE Antennas and Propagation Magazine*, 53(2):221–228, April 2011.

[3] A. Silva. *Pré-Filtragem no Espaço-Frequência para o Sistema MC-CDMA*. PhD thesis, University of Aveiro, 2007.

[4] E. Dahlman, S. Parkvall, J. Skold, and P. Beming. *3G Evolution: HSPA and LTE for Mobile Broadband*. Academic Press - Elsevier, New York, 2007.

[5] H. Holma and A. Toskala. *WCDMA for UMTS – HSPA Evolution and LTE*. Wiley, West Sussex, 4th edition, 2007.

[6] M. Bhalla and A. Bhalla. Generations of Mobile Wireless Technology: A Survey. *International Journal of Computer Applications*, 5(4):26–32, August 2010.

[7] M. Schwartz. *Mobile Wireless Communications*. Cambridge University Press, New York, 2004.

[8] Rysavy Research and 4G Americas. Mobile Broadband Explosion - The 3GPP Wireless Evolution. *White Papers*, August, 2012.

[9] U. Varshney. 4G Wireless Networks. *IT Professional*, 14(5):34–39, September 2012.

[10] D. Pareit, B. Lannoo, I. Moerman, and P. Demeester. The History of WiMAX: A Complete Survey of the Evolution in Certification and Standardization for IEEE 802.16 and WiMAX. *IEEE Communications Surveys & Tutorials*, 14(4):1183–1211, January 2012.

[11] UMTS Forum. Spectrum for Future Development of IMT-2000 and IMT-Advanced. *White Papers*, (January), 2012.

[12] ITU - Broadband Comission and UNESCO. The state of the Broadband 2012: Achieving Digital Inclusion for All. Technical Report September, 2012.

[13] Ericsson. Traffic and Market Data Report: On the Pulse of the Networked Society. Technical report, 2012.

[14] Cisco. Cisco Visual Networking Index : Global Mobile Data Traffic Forecast Update, 2011 – 2016. *White Papers*, (February):1–29, 2012.

[15] P. Bhat, S. Nagata, L. Campoy, I. Berberana, T. Derham, Guangyi Liu, X. Shen, P. Zong, and J. Yang. LTE-Advanced: An Operator Perspective. *IEEE Communications Magazine*, 50(2):104–114, February 2012.

[16] P. Marsch, B. Raaf, A. Szufarska, P. Mogensen, H. Guan, M. Farber, S. Redana, K. Pedersen, and T. Kolding. Future Mobile Communication Networks: Challenges in the Design and Operation. *IEEE Vehicular Technology Magazine*, 7(1):16–23, March 2012.

[17] Z. Shen, A. Papasakellariou, J. Montojo, D. Gerstenberger, and F. Xu. Overview of 3GPP LTE-Advanced Carrier Aggregation for 4G Wireless Communications. *IEEE Communications Magazine*, 50(2):122–130, February 2012.

[18] E. Pateromichelakis, M. Shariat, A. Quddus, and R. Tafazolli. On the Evolution of Multi-Cell Scheduling in 3GPP LTE / LTE-A. *IEEE Communications Surveys & Tutorials*, PP(99):1–17, 2012.

[19] F Capozzi, G. Piro, L. A. Grieco, G. Boggia, and P. Camarda. Downlink Packet Scheduling in LTE Cellular Networks: Key Design Issues and a Survey. *IEEE Communications Surveys & Tutorials*, PP(99):1–23, 2012.

[20] C. Kosta, B. Hunt, A. Quddus, and R. Tafazolli. On Interference Avoidance through Inter-Cell Interference Coordination (ICIC) Based on OFDMA Mobile Systems. *IEEE Communications Surveys & Tutorials*, PP(99):1–23, 2012.

[21] Y. Kishiyama, A. Benjebbour, H. Ishii, and T. Nakamura. Evolution Concept and Candidate Technologies for Future Steps of LTE-A. In *2012 IEEE International Conference on Communication Systems (ICCS)*, pages 473–477. IEEE, November 2012.

[22] H. T. Friis. Simple Transmission Formula. In *Proceedings of the I.R.E. and Waves and Electrons*, number 1, pages 254–256, 1946.

[23] M. Dohler and Y. Li. *Cooperative Communications: Hardware, Channel & PHY*. Wiley, Chippenham, 2010.

[24] C. Ribeiro. *Channel and Frequency Offset Estimation Schemes for Multcarrier Systems*. PhD thesis, University of Aveiro, 2010.

[25] P. Marques. *Estimação do Canal Ráadio-Móvel para Sistemas Celulares 3G e B3G*. PhD thesis, University of Aveiro, 2007.

[26] T. Chiueh and P. Tsai. *OFDM Baseband Receiver Design for Wireless Communications*. Wiley, Singapure, 2007.

[27] J. G. Proakis. *Digital Communications*. McGraw-Hill, New York, 4th edition, 2001.

[28] K. J. R. Liu, A. K. Sadek, W. Su, and A. Kwasinski. *Cooperative Communications and Networking*. Cambridge University Press, Cambridge, 2009.

[29] E. C. van der Meulen. Three-Terminal Communication Channels. *Advances in Applied Probability*, 3:120–154, 1971.

[30] T. M. Cover and A. A. E. Gamal. Capacity Theorems for the Relay Channel. *IEEE Transsactions on Information Theory*, 25(5):572–584, 1979.

[31] A. Sendonaris, E. Erkip, and B. Aazhang. Increasing Uplink Capacity via User Cooperation Diversity. In *1998 IEEE International Symposium on Information Theory*, pages 156–156. IEEE, 1998.

[32] A. Sendonaris, E. Erkip, and B. Aazhang. User Cooperation Diversity - Part I: System Description. *IEEE Transactions on Communications*, 51(11):1927–1938, November 2003.

[33] A. Sendonaris, E. Erkip, and B. Aazhang. User cooperation Diversity - Part II: Implementation Aspects and Performance Analysis. *IEEE Transactions on Communications*, 51(11):1939–1948, 2003.

[34] IEEE. IEEE Standard for Local and Metropolitan Area Networks Part 16: Air Interface for Broadband Wireless Access Systems Amendment 1: Multiple Relay Specification. Technical Report June, IEEE, 2009.

[35] 3GPP. TR 36.913, Requirements for Further Advancements for Evolved Universal Terrestrial Radio Access (E-UTRA) (LTE-Advanced). Technical report, 3GPP, 2011.

[36] IEEE. IEEE Standard for Local and Metropolitan Area Networks Part 16: Air Interface for Broadband Wireless Access Systems Amendment 3: Advanced Air Interface. Technical Report May, IEEE, 2011.

[37] F. H. P. Fitzek and M. D. Katz. *Cooperation in Wireless Networks: Principles and Applications*. Springer, 2006.

[38] T. Riihonen, R. Wichman, and S. Werner. Evaluation of OFDM(A) Relaying Protocols: Capacity Analysis in Infrastructure Framework. *IEEE Transactions on Vehicular Technology*, 61(1):360–374, January 2012.

[39] Z. Chen, H. Liu, and W. Wang. Optimal Transmit Strategy of a Two-Hop Decode-and-Forward MIMO Relay System with Mean and Covariance Feedback. *IEEE Communications Letters*, 14(6):530–532, June 2010.

[40] D. Lee and J. H. Lee. Outage Probability of Decode-and-Forward Opportunistic Relaying in a Multicell Environment. *IEEE Transactions on Vehicular Technology*, 60(4):1925–1930, May 2011.

[41] H. H. Sneessens, L. Vandendorpe, and J. N. Laneman. Adaptive Compress-and-Forward Relaying in Fading Environments with or without Wyner-Ziv Coding. In *2009 IEEE International Conference on Communications*, pages 1–5. IEEE, June 2009.

[42] J. Jiang, S. T. John, and M. G. Peter. Design and Analysis of Compress-and-Forward Cooperation in a Virtual-MIMO Detection System. In *2010 IEEE Globecom Workshops*, volume 1, pages 126–130. IEEE, December 2010.

[43] S. Teodoro. *Distributed Coding for Systems with Cooperative Diversity*. PhD thesis, University of Aveiro, 2011.

[44] Y. Zhangs and H. Chen, editors. *Mobile WiMAX: Toward Broadband Wireless Metropolitan Area Networks*. Auerbach Publications, New York, 2007.

[45] Y. Li, Q. Yin, W. Xu, and H. Wang. On the Design of Relay Selection Strategies in Regenerative Cooperative Networks with Outdated CSI. *IEEE Transactions on Wireless Communications*, 10(9):3086–3097, 2011.

[46] S. Zhang and V. K. N. Lau. Multi-Relay Selection Design and Analysis for Multi-Stream Cooperative Communications. *IEEE Transactions on Wireless Communications*, 10(4):1082–1089, 2011.

[47] A. Ikhlef, D. S. Michalopoulos, and R. Schober. Max-Max Relay Selection for Relays with Buffers. *IEEE Transactions on Wireless Communications*, 11(3):1124–1135, March 2012.

[48] CODIV. FP7-ICT-2007-215477 CODIV Initial Scenarios Definition and Top Level Technical Requirements. Technical report, CODIV, 2008.

[49] R. Vaze and R. W. Heath. On the Capacity and Diversity-Multiplexing Tradeoff of the Two-Way Relay Channel. *IEEE Transactions on Information Theory*, 57(7):4219–4234, July 2011.

[50] G. Amarasuriya, C. Tellambura, and M. Ardakani. Two-Way Amplify-and-Forward Multiple-Input Multiple-Output Relay Networks with Antenna Selection. *IEEE Journal on Selected Areas in Communications*, 30(8):1513–1529, September 2012.

[51] M. Ozdemir and H. Arslan. Channel Estimation for Wireless OFDM Systems. *IEEE Communications Surveys & Tutorials*, 9(2):18–48, 2007.

[52] H. Zamiri-Jafarian and S. Pasupathy. Robust and Improved Channel Estimation Algorithm for MIMO-OFDM Systems. *IEEE Transactions on Wireless Communications*, 6(6):2106–2113, June 2007.

[53] C. Shin, R. W. Jr., and E. J. Powers. Blind Channel Estimation for MIMO-OFDM Systems. *IEEE Transactions on Vehicular Technology*, 56(2):670–685, March 2007.

[54] A. Tomasoni, S. Bellini, M. Ferrari, D. Gatti, and M. Siti. Efficient OFDM Channel Estimation via an Information Criterion. In *2012 IEEE International Conference on Communications (ICC)*, pages 3936–3941. IEEE, June 2012.

[55] WINNER. IST-2003-507581 WINNER Identification of Radio-Link Technologies. Technical Report 223, WINNER, 2004.

[56] S. Kaiser. *Multi-Carrier CDMA Mobile Radio Systems - Analysis and Optimization of Detection , Decoding , and Channel Estimation*. PhD thesis, VDI-Verlag, 1998.

[57] Y. G. Li. Pilot-Symbol-Aided Channel Estimation for OFDM in Wireless Systems. *IEEE Transactions on Vehicular Technology*, 49(4):1207–1215, July 2000.

[58] J. Choi and Y. Lee. Optimum Pilot Pattern for Channel Estimation in OFDM Systems. *IEEE Transactions on Wireless Communications*, 4(5):2083–2088, September 2005.

[59] M. J. Fernandez-Getino G., S. Zazo, and J. M. Paez-Borrallo. Pilot Patterns for Channel Estimation in OFDM. *Electronics Letters*, 36(12):1049, 2000.

[60] S. Boyd and L. Vandenberghe. *Convex Optimization*. Cambridge University Press, Cambridge, 2004.

[61] H. V. Poor. *An Introduction to Signal Detection and Estimation*. Springer-Verlag, New York, 2nd edition, 1994.

[62] C. Ribeiro and A. Gameiro. Direct Time-Domain Channel Impulse Response Estimation for OFDM-Based Systems. In *2007 IEEE 66th Vehicular Technology Conference*, pages 1082–1086. IEEE, September 2007.

[63] O. Edfors, M. Sandell, J. van de Beek, S. K. Wilson, and P. Borjesson. OFDM Channel Estimation by Singular Value Decomposition. In *IEEE 46th Proceedings of Vehicular Technology Conference - VTC*, volume 2, pages 923–927. IEEE, 1996.

[64] O. Edfors, M. Sandell, and S. K. Wilson. OFDM Channel Estimation by by Singular Value Decomposition. *IEEE Transactions on Communications*, 46(7):931–939, 1998.

[65] K.B. Letaief. Analysis of Low-Complexity Windowed DFT-Based MMSE Channel Estimator for OFDM Systems. *IEEE Transactions on Communications*, 49(11):1977–1987, 2001.

[66] Y. Hara, A. Taira, L. Brunel, and T. Salzer. Frequency-Averaged MMSE Channel Estimator for Multicarrier Transmission Schemes. In *IEEE 60th Vehicular Technology Conference - Fall*, volume 1, pages 378–384. IEEE, 2004.

[67] X. Chen, H. Wang, and H. Hu. A Low Complexity Pilot-Aided Channel Estimation Resisting Residual Timing Errors for OFDM Systems. In *IEEE 18th International Symposium on Personal, Indoor and Mobile Radio Communications*, pages 1–5. IEEE, 2007.

[68] O. Cetin, B. Karakaya, and H. A. Cirpan. Low Complexity Channel Estimation for 3GPP LTE Downlink MIMO OFDM Systems. In *7th International Wireless Communications and Mobile Computing Conference*, number 1, pages 1441–1444. IEEE, July 2011.

[69] P. Hoeher, S. Kaiser, and P. Robertson. Two-Dimensional Pilot-Symbol-Aided Channel Estimation by Wiener Filtering. In IEEE, editor, *IEEE International Conference on Acoustics, Speech, and Signal Processing*, volume 3, pages 1845–1848. IEEE, 1997.

[70] C. Ribeiro and A. Gameiro. An OFDM Symbol Design for Reduced Complexity MMSE Channel Estimation. *Journal of Communication*, 3(4):26–33, 2008.

[71] D. J. C. MacKay. *Information Theory, Inference, and Learning Algorithms*. Cambridge University Press, Cambridge, 4th edition, 2003.

[72] Y. Li. Distributed Coding for Cooperative Wireless Networks: An Overview and Recent Advances. *IEEE Communications Magazine*, 47(8):71–77, August 2009.

[73] T. Wang, Y. Yao, and G. Giannakis. Non-Coherent Distributed Space-Time Processing for Multiuser Cooperative Transmissions. *IEEE Transactions on Wireless Communications*, 5(12):3339–3343, December 2006.

[74] F. Oggier and B. Hassibi. A Coding Scheme for Wireless Networks with Multiple Antenna Nodes and No Channel Information. In *2007 IEEE International Conference on Acoustics, Speech and Signal Processing - ICASSP '07*, number 2, pages 413 – 416. IEEE, 2007.

[75] L. Wang and L. Hanzo. Dispensing with Channel Estimation: Differentially Modulated Cooperative Wireless Communications. *IEEE Communications Surveys & Tutorials*, 14(3):836–857, 2011.

[76] S. Sugiura, S. Chen, H. Haas, P. M. Grant, and L. Hanzo. Coherent versus Non-Coherent Decode-and-Forward Relaying Aided Cooperative Space-Time Shift Keying. *IEEE Transactions on Communications*, 59(6):1707–1719, June 2011.

[77] J.N. Laneman, D.N.C. Tse, and G.W. Wornell. Cooperative Diversity in Wireless Networks: Efficient Protocols and Outage Behavior. *IEEE Transactions on Information Theory*, 50(12):3062–3080, December 2004.

[78] R.U. Nabar, H. Bolcskei, and F.W. Kneubuhler. Fading Relay Channels: Performance Limits and Space–Time Signal Design. *IEEE Journal on Selected Areas in Communications*, 22(6):1099–1109, August 2004.

[79] T. Wang, A. Cano, G. B. Giannakis, and J. N. Laneman. High-Performance Cooperative Demodulation With Decode-and-Forward Relays. *IEEE Transactions on Communications*, 55(7):1427–1438, July 2007.

[80] F. Gao, T. Cui, and A. Nallanathan. On channel estimation and optimal training design for amplify and forward relay networks. *IEEE Transactions on Wireless Communications*, 7(5):1907–1916, May 2008.

[81] B. Gedik and M. Uysal. Two Channel Estimation Methods for Amplify-and-Forward Relay Networks. In *2008 Canadian Conference on Electrical and Computer Engineering*, pages 615–618. IEEE, May 2008.

[82] M. Liu, J. Zhang, Y. Zhang, and Y. Liu. A Channel Estimation Scheme for Amplify-and-Forward OFDM Relay Networks. In *2009 IEEE 70th Vehicular Technology Conference Fall*, pages 1–5. IEEE, September 2009.

[83] P. Lioliou, M. Viberg, and M. Coldrey. Performance Analysis of Relay Channel Estimation. In *2009 Conference Record of the Forty-Third Asilomar Conference on Signals, Systems and Computers*, pages 1533–1537. IEEE, 2009.

[84] O. Amin, B. Gedik, and M. Uysal. Channel estimation for Amplify-and-Forward Relaying: Cascaded Against Disintegrated Estimators. *IET Communications*, 4(10):1207–1216, 2010.

[85] S. Bharadwaj and N. B. Mehta. Performance Analysis of Fixed Gain Amplify-and-Forward Relaying with Time-Efficient Cascaded Channel Estimation. In *2011 IEEE*

Global Telecommunications Conference - GLOBECOM 2011, pages 1–5. IEEE, December 2011.

[86] G. Huang, Y. Wang, and J. Coon. Performance of Multihop Decode-and-Forward and Amplify-and-Forward Relay Networks with Channel Estimation. In *Proceedings of 2011 IEEE Pacific Rim Conference on Communications, Computers and Signal Processing*, pages 352–357. IEEE, August 2011.

[87] T. Kong and Y. Hua. Optimal Design of Source and Relay Pilots for MIMO Relay Channel Estimation. *IEEE Transactions on Signal Processing*, 59(9):4438–4446, September 2011.

[88] D. Neves, C. Ribeiro, A. Silva, and A. Gameiro. An Iterative Pilot-Data Aided Estimator for OFDM-Based Relay-Assisted Systems. In *IEEE Third Latin-American Conference on Communications*, pages 1–6. IEEE, October 2011.

[89] I. Avram, N. Aerts, H. Bruneel, and M. Moeneclaey. Quantize and Forward Cooperative Communication: Channel Parameter Estimation. *IEEE Transactions on Wireless Communications*, 11(3):1167–1179, March 2012.

[90] G. Gui, W. Peng, A. Mehbodniya, and F. Adachi. Compressed Channel Estimation for Sparse Multipath Non-Orthogonal Amplify-and-Forward Cooperative Networks. In *2012 IEEE 75th Vehicular Technology Conference - VTC Spring*, number 2, pages 1–5. IEEE, May 2012.

[91] W. Hou and M. Jiang. Channel Estimation for AF-Type Cooperative OFDM Systems with Low Pilot Overhead. *IEEE Signal Processing Letters*, 19(10):651–654, October 2012.

[92] S. Jo, J. Choi, J. Baek, and J. Seo. Channel Estimation with Optimal Power Controls in Amplify-and-Forward Relay Networks. *IEEE Wireless Communications Letters*, PP(99):1–4, 2012.

[93] L. Rugini and P. Banelli. Pilot-Aided Estimation of Carrier Frequency Offsets and Channel Impulse Responses for OFDM Cooperative Communications. In *2012 IEEE 13th International Workshop on Signal Processing Advances in Wireless Communications - SPAWC*, pages 550–554. IEEE, June 2012.

[94] D. Neves, C. Ribeiro, A. Silva, and A. Gameiro. Channel Estimation Schemes for OFDM Relay-Assisted Systems. In *IEEE 69th Vehicular Technology Conference - Spring*, pages 1–5. IEEE, April 2009.

[95] Y. Jing and X. Yu. ML-Based Channel Estimations for Non-Regenerative Relay Networks with Multiple Transmit and Receive Antennas. *IEEE Journal on Selected Areas in Communications*, 30(8):1428–1439, September 2012.

[96] J. Ma, P. Orlik, J. Zhang, and G.Y. Li. Pilot Matrix Design for Estimating Cascaded Channels in Two-Hop MIMO Amplify-and-Forward Relay Systems. *IEEE Transactions on Wireless Communications*, 10(6):1956–1965, June 2011.

[97] P. Lioliou, M. Viberg, and M. Coldrey. Efficient Channel Estimation Techniques for Amplify-and-Forward Relaying Systems. *IEEE Transactions on Communications*, PP(99):1–6, 2012.

[98] O. Longoria and R. Parra. Estimation of Correlated MIMO Channels using Partial Channel State Information and DPSS. *IEEE Transactions on Wireless Communications*, 10(11):3711–3719, November 2011.

[99] C. Chiang and C. C. Fung. Robust Training Sequence Design for Spatially Correlated MIMO Channel Estimation. *IEEE Transactions on Vehicular Technology*, 60(7):2882–2894, September 2011.

[100] R. Arablouei and K. Dogganccay. Modified RLS Algorithm with Enhanced Tracking Capability for MIMO Channel Estimation. *Electronics Letters*, 47(19):1101, 2011.

[101] A. Moco, S. Teodoro, A. Silva, H. Lima, and A. Gameiro. Single and multiple antenna, relay-assisted techniques for uplink and downlink OFDM systems. *IARIA International Journal on Advances in Systems and Measurements*, 3(1&2):1–13, 2010.

[102] S. Teodoro, A. Silva, J. M. Gil, and A. Gameiro. Distributed Space-Frequency Block Coding for a 2-Antenna Relay in Downlink OFDM Systems. In *2009 9th International Symposium on Communications and Information Technology*, pages 853–858. IEEE, September 2009.

[103] M. Liu, M. Crussiere, and J. F. Helard. A Novel Data-Aided Channel Estimation With Reduced Complexity for TDS-OFDM Systems. *IEEE Transactions on Broadcasting*, 58(2):247–260, June 2012.

[104] S. Negusse and P. Zetterberg. Cost Reference Particle Filter in Data Aided Channel Estimation and Phase Noise Tracking for OFDM Systems. In *2012 IEEE International Conference on Acoustics, Speech and Signal Processing (ICASSP)*, pages 3153–3156. IEEE, March 2012.

[105] M. Jin and Y. Li. Pilot and Data Aided Channel Estimation for Correlated Flat MIMO Systems Based on Multipath Structure. In *2011 International Conference on Electronics, Communications and Control (ICECC)*, pages 953–956. IEEE, September 2011.

[106] M. Song, D. Kim, and G. Im. Recursive Channel Estimation Method for OFDM-Based Cooperative Systems. *IEEE Communications Letters*, 14(11):1029–1031, November 2010.

[107] N. Aerts, I. Avram, D. Duyck, and M. Moeneclaey. EM Based Channel Estimation in an Amplify-and-Forward Relaying Network. In *21st Annual IEEE International Symposium on Personal, Indoor and Mobile Radio Communications*, pages 724–729. IEEE, September 2010.

[108] J. S. Sheu and W. H. Sheen. An EM Algorithm-Based Channel Estimation for OFDM Amplify-And-Forward Relaying Systems. In *2010 IEEE International Conference on Communications*, pages 1–5. IEEE, May 2010.

[109] X. Zhou, T. A. Lamahewa, and P. Sadeghi. Kalman Filter-Based Channel Estimation for Amplify and Forward Relay Communications. In *2009 Conference Record of the Forty-Third Asilomar Conference on Signals, Systems and Computers*, pages 1498–1502. IEEE, 2009.

[110] R. Negi and J. Cioffi. Pilot Tone Selection for Channel Estimation in a Mobile OFDM system. *IEEE Transactions on Consumer Electronics*, 44(3):1122–1128, 1998.

Appendix A

Estimates Corrupted by Noise Terms with Different Variances

A.1. Introduction

The objective of the presented Appendix is to show that, in estimation cases where the observed elements are corrupted by noises, with different variances, the average value of the elements may provide a fitting approximation. This Appendix validates the assumption of approximating the harmonic mean by the arithmetic one, an approximation considered in Section 5.4.2.

A.2. Estimation in the Presence of Noise Terms with Different Variances

Firstly, let us consider the estimation of a parameter y based on n observations, $n = 1, \cdots N-1$, where the different samples are corrupted by zero mean Gaussian noise terms but with possibly different variances as shown below.

$$\begin{aligned} y_0 &= h + n_0 \\ y_1 &= h + n_1 \\ &\vdots \\ y_{N-1} &= h + n_{N-1}. \end{aligned} \tag{A1.1}$$

The noise variance of each estimate is given by σ_n^2 and the MSE estimate is given by

$$\hat{h} = \alpha \sum_n \frac{y_n}{\sigma_n^2}. \tag{A1.2}$$

where α is adjusted to ensure that the estimate is centric, i.e.,

$$\alpha = \sum_n \frac{1}{1/\sigma_n^2}. \tag{A1.3}$$

The variance of the error is given by

$$E\left[\left(h - \hat{h}\right)^2\right] = \alpha = \sum_n \frac{1}{1/\sigma_n^2}. \tag{A1.4}$$

It can be noted that, for N observations, α is N times the harmonic mean. It is known that the difference between the harmonic (H) and the arithmetic (A) mean is bounded by

$$A - H \le \frac{\left(M - m\right)s^2}{m\left(M - m\right) + s^2}, \tag{A1.5}$$

where m and M are the minimum and the maximum terms of the sequence and s^2 is its variance.

If the terms $\alpha_k \Gamma_k \Gamma_{\mathrm{ru},k}$ have small fluctuation, then $M - m$ is low and s^2 should be low as well. Therefore, $H \simeq A$ validates the assumption of approximating the harmonic mean by the arithmetic one. As such the use of the average terms in Eq. (5.38) – Eq. (5.39) is considered.

Appendix B

MSE Data-Aided Estimation and the Error Probability

A.1. Introduction

The objective of the presented Appendix is to derive, for SISO and MISO channels, an approximate relation between the MSE data-aided estimation and the error probability, considering that only data-symbols are used as virtual pilots.

Under the assumption that the correlation involving the data and noise are negligible, throughout this Annex the following definitions are considered.

- The received power is given by

$$\sum_{j\in\mathfrak{J}}\left|h_j\right|^2\mathbb{E}\left\{\left|s_j\right|^2\right\}=\sigma_j^2\sum_{j\in\mathfrak{J}}\left|h_j\right|^2, \text{where } \mathfrak{J} \text{ is the set of data subcarriers.}$$

- The power at the pilot subcarriers is

$$\sum_{p\in\mathfrak{P}}\left|h_p\right|^2 1=\sum_{p\in\mathfrak{P}}\left|h_p\right|^2, \text{where } \mathfrak{P} \text{ is the set of pilot subcarriers.}$$

- The noise variance per subcarriers is represented by σ_n^2 and therefore the total power is given by $K\sigma_n^2$, where K is the number of subcarries .

- If there is any distinction among pilot and data subcarriers the signal-to-noise ratio (SNR) is

$$\text{SNR}=\frac{\sigma_j^2\mathbb{E}\left\{\sum_k\left|h_k\right|^2\right\}}{K\sigma_n^2}.$$

- If $\sigma_j^2=1$, $\mathbb{E}\left\{\left|h_k\right|^2\right\}=1$ and $\mathbb{E}\left\{\sum_k\left|h_k\right|^2\right\}=K$ the SNR is given by $\text{SNR}=1/\sigma_n^2$.

A.2. Data-Aided Estimation - SISO Channel

According to the LS estimation in a SISO channel, the error in the channel estimates is

$$e=h_k-\hat{h}_k=h_k\left(1-d_k\hat{d}_k^*\right)+z_k\hat{d}_k^*, \tag{A2.1}$$

where d_k and $\hat{d}_k$ are the transmitted and the regenerated data symbol, respectively and for QPSK $\left|d_k\right|^2 = 1$ and $d_k^* = 1/d_k$, for $k \in \mathfrak{J}$.

The squared norm of the error vector is given by:

$$\begin{aligned} \left|e\right|^2 &= \left|h_k\right|^2 \left|1 - d_k \hat{d}_k^*\right|^2 + \left|w_k\right|^2 + 2\left|h_k\right|\left|1 - d_k \hat{d}_k^*\right|\left|z_k \hat{d}_k^*\right| \\ \mathbb{E}\left\{\left|e\right|^2\right\} &= \mathrm{E}\left\{\left|h_k\right|^2\right\}\mathrm{E}\left\{\left|1 - d_k \hat{d}_k^*\right|^2\right\} + \sigma_n^2 + \mathrm{E}\left\{2\left|h_k\right|\left|1 - d_k \hat{d}_k^*\right|\left|z_k \hat{d}_k^*\right|\right\}. \end{aligned} \tag{A2.2}$$

Since that $\left|1 - d_k \hat{d}_k^*\right|^2 = \left|1 - d_k / \hat{d}_k\right|^2 = \left|\hat{d}_k - d_k\right|^2 / \left|\hat{d}_k\right|^2 = \left|\varepsilon\right|^2$. For QPSK $d_k = \left(1 + \imath\right)/\sqrt{2}$ and therefore:

Table A.1 – Square Norm of the Error: SISO Channel Estimation

$\hat{d}_k$	ε	$\left\|\varepsilon\right\|^2$	Error Probability
$\left(1+\imath\right)/\sqrt{2}$	0	0	$1 - P_b$
$\left(-1+\imath\right)/\sqrt{2}$	$-2/\sqrt{2}$	2	$\sim P_b/2$
$\left(-1-\imath\right)/\sqrt{2}$	$-2\left(1+\imath\right)/\sqrt{2}$	4	~ 0
$\left(1-\imath\right)/\sqrt{2}$	$2\imath/\sqrt{2}$	2	$\sim P_b/2$

According to Table A.1 the expected value of the error is given by:

$$\begin{aligned} \mathbb{E}\left\{\left|e\right|^2\right\} &= \mathbb{E}\left\{\left|h_k\right|^2\right\}\mathbb{E}\left\{\left|\varepsilon\right|^2\right\} + \sigma_n^2 \\ \mathbb{E}\left\{\left|e\right|^2\right\} &= \mathbb{E}\left\{\left|h_k\right|^2\right\}\left(2P_b/2 + 2P_b/2\right) + \sigma_n^2 = 2\mathbb{E}\left\{\left|h_k\right|^2\right\}P_b + \sigma_n^2. \end{aligned} \tag{A2.3}$$

Since we assume $\mathbb{E}\left\{\left|h_k\right|^2\right\} = 1$ and $\sigma_n^2 = 1/\mathrm{SNR}$

$$\begin{aligned} \mathbb{E}\left\{\left|e\right|^2\right\} &\approx 2P_b + \sigma_n^2 \\ \mathbb{E}\left\{\left|e\right|^2\right\} &\approx \sigma_n^2\left(1 + 2P_b\mathrm{SNR}\right). \end{aligned} \tag{A2.4}$$

A.2. Data-Aided Estimation - MISO Channel

Since our scenario is a cooperative $2\times2\times1$ and the LS data estimation is used to estimate the channels RN–UT which is 2×1, we need provide expression for the squared norm of the error in this case as well.

In a MISO system the signal to be hard-decoded at the destination is given by:

$$\begin{cases} \hat{d}_k = g_1^* y_k + g_2 y_{k+1}^*, \quad g_1 = h_{1,k} \Big/ \left(\sqrt{2}\sigma_n^2\right) \\ \hat{d}_{k+1} = -g_2 y_k^* + g_1^* y_{k+1}, \quad g_2 = h_{2,k} \Big/ \left(\sqrt{2}\sigma_n^2\right) \end{cases}, \tag{A2.5}$$

where $h_{1,k}$ and $h_{2,k}$ are the channels per subcarriers k between the transmitter and the receiver, the received signal corresponds to y_k , in Eq. (A. 6), and $g_{1,2}$ are the equalisation constant.

$$\begin{cases} y_k = \dfrac{1}{\sqrt{2}}\left(h_{1,k} d_k - h_{2,k+1} d_{k+1}^*\right) + n_k \\ y_{k+1} = \dfrac{1}{\sqrt{2}}\left(h_{2,k+1} d_k^* + h_{1,k+1} d_{k+1}\right) + n_{k+1} \end{cases}. \tag{A2.6}$$

The LS estimation in a MISO system, for $k \in \mathfrak{J}$ is given by:

$$\mathbf{H} = \sqrt{2}\left(\mathbf{D}^{-1}\mathbf{Y}\right),$$

$$\text{for } \mathbf{D} = \begin{pmatrix} \hat{d}_k & -\hat{d}_{k+1}^* \\ \hat{d}_{k+1} & \hat{d}_k^* \end{pmatrix} \Rightarrow \mathbf{D}^{-1} = \frac{1}{\hat{d}_k\hat{d}_k^* + \hat{d}_{k+1}\hat{d}_{k+1}^*} \begin{pmatrix} \hat{d}_k & -\hat{d}_{k+1}^* \\ \hat{d}_{k+1} & \hat{d}_k^* \end{pmatrix}.$$

$$\mathbf{H} = \begin{pmatrix} h_{1,k} \\ h_2, k \end{pmatrix}, \text{ where } \begin{cases} \hat{h}_{1,k} = \dfrac{\sqrt{2}}{\hat{d}_k\hat{d}_k^* + \hat{d}_{k+1}\hat{d}_{k+1}^*}\left(\hat{d}_k^* y_k + \hat{d}_{k+1}^* y_{k+1}\right) + n_k \\ \hat{h}_{2,k} = \dfrac{\sqrt{2}}{\hat{d}_k\hat{d}_k^* + \hat{d}_{k+1}\hat{d}_{k+1}^*}\left(-\hat{d}_{k+1} y_k + \hat{d}_k y_{k+1}\right) + n_{k+1} \end{cases} \tag{A2.7}$$

Assuming $h_k \approx h_{k+1}$

$$\begin{cases} \hat{h}_{1,k} = \dfrac{h_{1,k}\left(\hat{d}_k^* d_k + \hat{d}_{k+1}^* d_{k+1}\right)}{\hat{d}_k\hat{d}_k^* + \hat{d}_{k+1}\hat{d}_{k+1}^*} + \dfrac{\hat{d}_k^* z_k}{\hat{d}_k\hat{d}_k^* + \hat{d}_{k+1}\hat{d}_{k+1}^*} + \dfrac{\hat{d}_{k+1}^* z_{k+1}}{\hat{d}_k\hat{d}_k^* + \hat{d}_{k+1}\hat{d}_{k+1}^*} \\ \hat{h}_{2,k} = \dfrac{h_{2,k}\left(d_k^*\hat{d}_k + d_{k+1}^*\hat{d}_{k+1}\right)}{\hat{d}_k\hat{d}_k^* + \hat{d}_{k+1}\hat{d}_{k+1}^*} + \dfrac{\hat{d}_k z_{k+1}}{\hat{d}_k\hat{d}_k^* + \hat{d}_{k+1}\hat{d}_{k+1}^*} + \dfrac{-\hat{d}_{k+1} z_k}{\hat{d}_k\hat{d}_k^* + \hat{d}_{k+1}\hat{d}_{k+1}^*} \end{cases}. \tag{A2.8}$$

The error in Eq. (A.8) is given by the following expression:

$$\begin{cases} e_1 = h_{1,k} - \hat{h}_{1,k} \\ e_2 = h_{2,k} - \hat{h}_{2,k} \end{cases}. \tag{A2.9}$$

By replacing Eq. (A.8) in Eq. (A.9) we may obtain

$$\begin{cases} e_1 = h_{1,k}\left(1 - \dfrac{\left(\hat{d}_k^* d_k + \hat{d}_{k+1}^* d_{k+1}\right)}{\hat{d}_k \hat{d}_k^* + \hat{d}_{k+1}\hat{d}_{k+1}^*}\right) + \dfrac{1}{\hat{d}_k \hat{d}_k^* + \hat{d}_{k+1}\hat{d}_{k+1}^*}\left(\hat{d}_k^* z_k + \hat{d}_{k+1}^* z_{k+1}\right) \\ e_2 = h_{2,k}\left(1 - \dfrac{\left(d_k^* \hat{d}_k + d_{k+1}^* \hat{d}_{k+1}\right)}{\hat{d}_k \hat{d}_k^* + \hat{d}_{k+1}\hat{d}_{k+1}^*}\right) + \dfrac{1}{\hat{d}_k \hat{d}_k^* + \hat{d}_{k+1}\hat{d}_{k+1}^*}\left(\hat{d}_k z_{k+1} - \hat{d}_{k+1} z_k\right) \end{cases}. \tag{A2.10}$$

The error vector is given by:

$$\begin{cases} \left|e_1\right| = \dfrac{1}{\left|\Psi\right|}\left[\left|h_{1,k}\right|\left|\Psi - \left(\hat{d}_k^* d_k + \hat{d}_{k+1}^* d_{k+1}\right)\right| + \left|\hat{d}_k^* n_k\right| + \left|\hat{d}_{k+1}^* n_{k+1}\right|\right] \\ \left|e_2\right| = \dfrac{1}{\left|\Psi\right|}\left[\left|h_{2,k}\right|\left|\Psi - \left(d_k^* \hat{d}_k + d_{k+1}^* \hat{d}_{k+1}\right)\right| + \left|\hat{d}_k z_{k+1}\right| + \left|-\hat{d}_{k+1} n_k\right|\right] \end{cases}, \quad \Psi = \hat{d}_k \hat{d}_k^* + \hat{d}_{k+1}\hat{d}_{k+1}^*. \tag{A2.11}$$

We assume that $d_k d_k^* = \left|d_k\right|$ and for QPSK $\left|d_k\right| = 1$, therefore $\Psi = 2$ and the expected value of the squared error is:

$$\begin{cases} \mathbb{E}\left\{\left|e_1\right|^2\right\} = \dfrac{1}{4}\left[\mathrm{E}\left\{\left|h_{1,k}\right|^2\right\}\mathbb{E}\left\{\left|2 - \left(\hat{d}_k^* d_k + \hat{d}_{k+1}^* d_{k+1}\right)\right|^2\right\} + \sigma_{n,k}^2 + \sigma_{n,k+1}^2\right] \\ \mathbb{E}\left\{\left|e_2\right|^2\right\} = \dfrac{1}{4}\left[\mathrm{E}\left\{\left|h_{2,k}\right|^2\right\}\mathbb{E}\left\{\left|2 - \left(d_k^* \hat{d}_k + d_{k+1}^* \hat{d}_{k+1}\right)\right|^2\right\} + \sigma_{n,k+1}^2 + \sigma_{n,k}^2\right] \end{cases}. \tag{A2.12}$$

Since $\left|2 - \left(\hat{d}_k^* d_k + \hat{d}_{k+1}^* d_{k+1}\right)\right|^2 = \left|2 - \left(d_k / \hat{d}_k + d_{k+1} / \hat{d}_{k+1}\right)\right|^2 = \left|\varepsilon\right|^2$, for QPSK $d_k = \left(1 + \imath\right)/\sqrt{2}$ and therefore, the following table follows.

Table A.2 – Square Norm of the Error: MISO Channel Estimation

$\hat{d}_k$	$\hat{d}_{k+1}$	ε	$\lvert\varepsilon\rvert^2$	Error Probability
$(1+\imath)/\sqrt{2}$	$(1+\imath)/\sqrt{2}$	0	0	$1-P_b$
$(-1+\imath)/\sqrt{2}$	$(1+\imath)/\sqrt{2}$	$-1-\imath$	2	$\sim P_b/4$
$(-1-\imath)/\sqrt{2}$	$(1+\imath)/\sqrt{2}$	$2\imath$	4	~ 0
$(1-\imath)/\sqrt{2}$	$(1+\imath)/\sqrt{2}$	$1-\imath$	2	$\sim P_b/4$
$(1+\imath)/\sqrt{2}$	$(-1+\imath)/\sqrt{2}$	$-1-\imath$	2	$\sim P_b/4$
$(1+\imath)/\sqrt{2}$	$(-1-\imath)/\sqrt{2}$	$-2\imath$	4	~ 0
$(1+\imath)/\sqrt{2}$	$(1-\imath)/\sqrt{2}$	$1-\imath$	2	$\sim P_b/4$
$(-1-\imath)/\sqrt{2}$	$(-1-\imath)/\sqrt{2}$	$4\imath$	16	~ 0

According to Table A.2 the expected value of the error square is given by:

$$\begin{aligned}\mathbb{E}\left\{\left|e_1\right|^2\right\} &= \frac{1}{4}\mathbb{E}\left\{\left|h_{1,k}\right|^2\right\}\mathbb{E}\left\{\left|\varepsilon\right|^2\right\}+2\sigma_n^2 \\ \mathbb{E}\left\{\left|e_1\right|^2\right\} &= \frac{1}{4}\mathbb{E}\left\{\left|h_{1,k}\right|^2\right\}\left(2P_b/4+2P_b/4+2P_b/4+2P_b/4\right)+2\sigma_n^2.\end{aligned} \tag{A2.13}$$

Since we assume $\mathbb{E}\left\{\left|h_k\right|^2\right\}=1$ and $\sigma_n^2=1/\mathrm{SNR}$

$$\begin{aligned}\mathbb{E}\left\{\left|e_1\right|^2\right\} &\approx \frac{1}{4}\mathrm{E}\left\{\left|h_{1,k}\right|^2\right\}2P_b+2\sigma_n^2 \\ \mathbb{E}\left\{\left|e_1\right|^2\right\} &\approx \frac{1}{2}\sigma_n^2\left(1+P_b\mathrm{SNR}\right).\end{aligned} \tag{A2.14}$$